

Master's Thesis

NNLO Contributions to Jet Production in Deep Inelastic Scattering

Thomas Biekötter

July 14, 2015

Supervisor & first examiner: Prof. Dr. Michael Klasen

Institute for theoretical Physics, Münster

Second examiner: Prof. Dr. Gernot Münster

Institute for theoretical Physics, Münster



"Men and women are not content to comfort themselves with tales of gods and giants, or to confine their thoughts to the daily affairs of life; they also build telescopes and satellites and accelerators, and sit at their desks for endless hours working out the meaning of the data they gather. The effort to understand the universe is one of the very few things which lifts human life a little above the level of farce and gives it some of the grace of tragedy."

– Steven Weinberg, *The First Three Minutes*

Abstract

In this thesis, the effects of next-to-next-to-leading order (NNLO) contributions to inclusive jet production in deep inelastic scattering (DIS) were investigated. The evaluated NNLO master formula is predicted by a unified threshold resummation formalism in the framework of quantum chromodynamics. The leading coefficients of the NNLO master formula were identified analytically by comparison to the already existing full next-to-leading order (NLO) calculation. It was shown that there is excellent agreement between the resummation approach and the purely perturbative NLO formulas. After adding the NNLO contributions to the NLO calculation, the cross section predictions were significantly modified. An analysis of jet-production data from the H1 collaboration at DESY was done to NNLO accuracy, resulting in a better description of cross section data differentially in the jet transverse momentum. A tendency to decrease the theoretical predictions in the observed kinematical phase space manifests itself in the determination of the strong coupling constant α_s , which got shifted to higher values when NNLO contributions were taken into account.

Contents

1. Introduction	1
2. Quantum Chromodynamics	3
2.1. Pertubative Quantum Chromodynamics	5
2.2. Ultraviolet divergences	7
2.2.1. Renormalization	10
2.2.2. Running coupling	12
2.3. Mass singularities	14
2.3.1. Phase Space Slicing	18
2.4. Factorization	21
2.5. Parton Distribution Functions	23
2.6. Resummation	25
3. Deep Inelastic Scattering	28
3.1. The Parton Model	29
3.2. LO cross section	33
3.3. NLO cross section	37
3.4. The program JetViP	42
3.4.1. The jet algorithm	43
3.5. Reproduction of H1-Analysis	44
3.5.1. The Breit frame	46
3.5.2. Corrections to perturbative calculation	47
3.5.3. Results	47
4. From NLO to NNLO	54
4.1. Threshold resummation	55
4.2. The master formula	60
4.3. Matching coefficients to NLO	64
4.4. NNLO contributions	69
4.4.1. Results	70
4.4.2. Determination of the strong coupling constant	74
5. Conclusion and outlook	76
A. Conventions	78
B. Feynman rules for QCD	79

C. Hadronic ep cross section	82
D. NNLO coefficients	86
E. Details on the implementation	88
F. Further plots	91
References	98

1. Introduction

Since the discovery of the standard model of particle physics, today's physics is faced with a completely new situation. The original challenge for science to find a model that explains the phenomena of a certain environment is already fulfilled, but to figure out what the theory is telling us, or rather what its precise predictions are, is a highly complex and calculation intensive exercise. It was only through the method of perturbation theory and Feynman's genius idea of using certain types of graphical tools to provide a more intuitive way of understanding calculations that made it possible to determine the predictions in good approximation.

However, this is not always the case. In a manner of speaking, quantum chromodynamics (QCD), the theory of the strong interaction, is the gadfly of the standard model. Particularly two aspects of QCD make calculations even more elaborate. Firstly, color-charged particles, which we call quarks and gluons, do not exist as free particles in nature at least in the conditions we observe in the universe, but only in color-neutral compound states. The fundamental nature of these particles is therefore hidden under normal circumstances. Secondly, QCD describes an interaction with a high coupling constant α_s . The calculation of experimentally accessible observables with perturbative methods relies on an expansion with respect to α_s and the assumption that α_s is so small that terms of higher order in α_s contribute less and can be neglected at a certain amount of precision. In quantum electrodynamics (QED) and the electroweak theory respectively, this is true, but in QCD it is just under appropriate circumstances.

It is due to a peculiar feature of QCD as a non-Abelian gauge theory that despite the problems mentioned above a perturbative approach (pQCD) is effective. This is the so-called *running coupling*. At high energies, or in other words when the particles come close to each other in scattering processes, the coupling constant α_s becomes small. This thesis is on deep inelastic scattering of electrons on protons (DIS), where this fact implies that the components of the proton (called *partons* for part of hadrons) are quasi-free. The actual interaction of the electron with those partons happens decoupled from the strong interactions between the partons in the proton before the scattering and the strong hadronization effects of free partons leaving the proton after the scattering. The process factorizes into a long-range, process-independent part and a short-range part, containing the actual scattering process. The short-range effects can be calculated perturbatively with the help of Feynman diagrams. Nevertheless the coupling constant α_s is still so big that higher orders than the first leading order (LO) are significant and have to be taken into account. Today, calculations of inclusive jet cross sections in DIS experiments are available up to next-to-leading order (NLO).

The experimental data analyzed in this thesis were measured at the Hadron Electron Ring Accelerator (HERA) in Hamburg and published by the H1 collaboration. The electron beam had an energy of 27.6 GeV and the proton beam an energy of 920 GeV

[1]. The cross sections were measured double differentially. An analysis of the data in NLO was already made. With a global fit to experimental inclusive jet cross section data, it was found a value of $\alpha_s(M_Z) = 0.1185 \pm 0.0017$, in good agreement with the world average value [1].

In this thesis the analysis will be extended to next-to-next-to-leading order (NNLO) contributions based on the re-expansion of resummation formulas [2]. This rather technical topic is not just an intellectual exercise. At the moment, the experimental data has smaller errors than the theoretical NLO analysis. The scale variation in NLO gives rise to error estimations between 5% and 15% [1]. This is an unsatisfactory status, and especially an NNLO calculation will improve the errors of the estimation of α_s . In the current world average value of α_s , only values that are determined by at least NNLO accuracy are considered. A more precise value for α_s will effect any calculation involving strong interactions and is therefore essential in proving QCD. To be more precise, when the quark masses are fixed, α_s is the only free parameter of QCD. This is effectively important today, since we are in the age of the large hadron collider at Cern.

The outline of this thesis is as follows. Firstly, the basic concepts of QCD are depicted. Subsequently, the role of DIS in the formulation of QCD is described and the common kinematic variables are introduced. An already existing program for calculating inclusive di- and trijet cross sections in DIS is used to reproduce the NLO analysis of the H1 collaboration. In the following chapters, the mathematical techniques used for calculating NNLO contributions, obtained from a unified threshold resummation formalism, are explained briefly. After that, the implementation of the NNLO contributions into the NLO program is described. This provides us with the ability to extend the analysis of the H1 data to NNLO accuracy. As a conclusion, the results of this work are discussed and a quick outlook to possible future enhancements in this field is stated.

2. Quantum Chromodynamics

Quantum chromodynamics is the theory for describing the strong interaction. The discovery of the strong force is highly connected to atomic and nuclear physics. After it was found out that the atomic nucleus consists of protons and neutrons, an additional force was postulated to explain, why the nucleus is stable although the positively charged protons repel each other by the electromagnetic interaction. As it turned out, the nuclear force binding the nucleons together is merely a residual of the actual strong force that acts between the constituents of the nucleons, which in fact are not elementary particles, but hadrons, i.e., built out of so-called *quarks*. Only little was known about the properties of the strong force between those quarks. Collider experiments showed that through the scattering of strongly interacting particles many unidentified particles are produced. This commonly named *particle zoo* seemed to have a pattern. One could find a way to classify the hadronic matter in baryons and mesons, consisting of three quarks and a quark and an antiquark respectively. Additionally, it was postulated that there are different flavored quarks like in the lepton sector. Gell-Mann postulated a mechanism for a systematic classification of hadrons called *The Eightfold Way* [3].

Still there was a problem, especially with some baryons predicted by the eightfold way like the Ω^- or the Δ^{++} . Their properties (electric charge, flavor, weak isospin, spin) contradicted the Pauli principle, because they could only be the result of a quark configuration, where the quarks have completely equal quantum numbers. The Pauli principle was and still is indisputable. Just one explanation could fix the problem and that was to postulate an additional quantum number for the quarks: The color. The question of how many colors there are was addressed in experiments where the creation or annihilation of quarks is involved. To get the correct branching ratios between leptonic and hadronic processes a color multiplicity of three for the quarks has to be included [4].

Naturally, the next problem emerged: Why did we not see the new degree of freedom directly in other experiments? The answer to that is rather simple while its explanation is not. It seems to be a fundamental law of nature that quarks are bound together to color-neutral objects and cannot exist as free particles, at least under the circumstances being observed. That is why baryons are made up out of three quarks with different color and mesons out of a quark and antiquark with definite color and its anti-color. In fact, that was the first motivation to postulate a degree of freedom with multiplicity three [3]. In this historical overview DIS was not mentioned, even though it is not less important. The reason for that is that its implications will be discussed separately in section 3.1 about the parton model.

The aim of theorists was now to formulate a quantized field theory for the strong interaction like it was done before in quantum electrodynamics or later in the electroweak theory for the electromagnetic and weak interaction. This sector of the standard model

was well described by a spontaneously broken $U_Y(1) \times SU_L(2)$ gauge symmetry. In this spirit, the step to construct a Lagrangian respecting $SU(3)_C$ symmetry was not too astonishing. In the following, based on reference [5], the main aspects of this theory, which today goes under the name of quantum chromodynamics, are presented. The starting point is the QCD Lagrangian (for simplicity for one quark flavor)

$$\mathcal{L} = \mathcal{L}_G + \mathcal{L}_{GF} + \mathcal{L}_{FP} + \mathcal{L}_F, \quad (2.1)$$

separated into the gauge, gauge fixing, Faddeev-Popov and fermion part. The gauge term \mathcal{L}_G is the kinetic term of the gauge fields A_μ^a ,

$$\mathcal{L}_G = -\frac{1}{4} F_{\mu\nu}^a F^{a\mu\nu}, \quad (2.2)$$

where the field strength tensor $F_{\mu\nu}^a$ is defined by

$$F_{\mu\nu}^a = \partial_\mu A_\nu^a - \partial_\nu A_\mu^a + g f^{abc} A_\mu^b A_\nu^c. \quad (2.3)$$

The fields A_μ^a are vector fields in the adjoint representation of the symmetry group $SU(3)_C$. They are counted by $a = 1, \dots, 8$ and represent the eight gluons mediating the interaction. f^{abc} are the structure constants of $SU(3)_C$ defined by the commutation relation of its generators T^a through

$$[T^a, T^b] = i f^{abc} T^c. \quad (2.4)$$

The parameter g is a measure for the coupling strength of strong interactions. The fermion part

$$\mathcal{L}_F = \bar{\psi}^i \left(i \gamma^\mu D_\mu^{ij} - m \right) \psi^j, \quad (2.5)$$

and \mathcal{L}_G together constitute the classical Lagrangian. Here, ψ^j is a fermionic Dirac field in the fundamental representation of $SU(3)_C$ and γ^μ are the Dirac matrices (see appendix A). The index $i = 1, 2, 3$ might be called color-index and is standing for the new degree of freedom in QCD. So ψ represents a quark with any flavor. $\bar{\psi}^i$ is the adjoint spinor field $\bar{\psi}^i = \psi^\dagger \gamma_0$, and m is the mass of the fermion. D_μ^{ij} is the covariant derivative in the fundamental representation

$$D_\mu^{ij} = \delta^{ij} \partial_\mu - i g T_{ij}^a A_\mu^a. \quad (2.6)$$

The two remaining parts of \mathcal{L} are necessary for quantizing the theory and to remove unphysical longitudinal gluon states. For the latter the term

$$\mathcal{L}_{FP} = (\partial^\mu \chi^{a*}) D_\mu^{ab} \chi^b \quad (2.7)$$

is added, where the *Faddeev-Popov ghost* field χ^a was introduced. The corresponding particle is called a ghost, because it is a bosonic scalar particle fulfilling fermionic commutation relations, and can therefore not be seen as a real particle. Finally, the gauge fixing term

$$\mathcal{L}_{GF} = -\frac{1}{2\xi} \left(\partial^\mu A_\mu^a \right)^2 \quad (2.8)$$

is necessary for a meaningful quantization of the QCD Lagrangian.¹ In particular, it provides the possibility to define a consistent gluon propagator. The price to pay is the existence of a new parameter ξ called gauge fixing parameter. While calculating any observable this parameter has to cancel out in the end, because an observable may not depend on the gauge you choose.²

The Lagrangian \mathcal{L} can be written as a sum

$$\mathcal{L} = \mathcal{L}_0 + \mathcal{L}_1, \quad (2.9)$$

where \mathcal{L}_0 is the free part and \mathcal{L}_1 is the interaction part of the Lagrangian. The free part consists of terms corresponding to each particle

$$\begin{aligned} \mathcal{L}_0 = & -\frac{1}{4}(\partial_\mu A_\nu^a - \partial_\nu A_\mu^a)(\partial^\mu A^{a\nu} - \partial^\nu A^{a\mu}) - \frac{1}{2\xi}(\partial^\mu A_\mu^a)^2 \\ & + (\partial^\mu \chi^{a*})(\partial_\mu \chi^a) + \bar{\psi}^i(i\gamma^\mu \partial_\mu - m)\psi^i, \end{aligned} \quad (2.10)$$

namely the gluons in the first line, the ghost in the first term of the second line and the quark in the last term. The remaining terms of \mathcal{L} are collected in the interaction part

$$\begin{aligned} \mathcal{L}_1 = & -\frac{g}{2}f^{abc}(\partial_\mu A_\nu^a - \partial_\nu A_\mu^a)A^{b\mu}A^{c\nu} - \frac{g^2}{4}f^{abe}f^{cde}A_\mu^a A_\nu^b A^{c\mu}A^{d\nu} \\ & - g f^{abc}(\partial^\mu \chi^{a*})\chi^b A_\mu^c + g\bar{\psi}^i T_{ij}^a \gamma^\mu \psi^j A_\mu^a. \end{aligned} \quad (2.11)$$

The expressions 2.10 and 2.11 will be the starting point for the study of QCD by perturbative methods (pQCD) in the following section.

2.1. Perturbative Quantum Chromodynamics

At this stage the careful reader will doubt that perturbation theory is a reasonable approach to QCD. A perturbative expansion of any physical quantity σ through

$$\sigma = \sum_n c_n \alpha_s^n + R_n \quad (2.12)$$

inescapably has to comply with some conditions [6]. First of all, the expansion parameter $\alpha_s = g^2/(4\pi)$ has to be small. Since the interaction is strong, this is generally not the case. Just under circumstances discussed in section 2.2.2 it is. A second condition is that we demand that the coefficients c_n do not spoil the expansion. In the field theoretical context this means that you have to deal with divergences in these coefficients properly (see section 2.2.1 and 2.3). Finally, even though we have removed the divergences, we still cannot assure that the remainder R_n will be small enough beyond a certain order n so that it can be neglected. In QCD this problem arises in certain regions of the phase space. This problem is tackled by resummation (see section 2.6). At this stage, we will trust in the usefulness of pQCD and describe the main consequences. Later on, the

¹There are plenty of ways to fix the gauge. The term in equation 2.8 is one example.

²Note that the gauge fixing term explicitly breaks the gauge symmetry, yet the important thing is that an observable is not influenced by the choice of the gauge fixing.



Figure 2.1.: Self-interaction of the gluon via the 3-gluon and 4-gluon vertex.

approaches that will guarantee the correctness of the expansion 2.12 will be presented briefly.

After the separation of \mathcal{L} one can deduce the propagators of the particles from the free part \mathcal{L}_0 and the vertices from \mathcal{L}_1 . These rules are summarized in appendix B. From there you go the usual way by constructing all possible Feynman diagrams at a certain order of α_s and deduce the corresponding Feynman amplitudes, which allow you to calculate an observable σ , that in our case is the cross section. QCD has a fundamental difference to quantum electrodynamics due to its non-Abelian nature. One gets additional vertices, because the gluon as the mediator of the force is color-charged itself, while the photon carries no electric charge. Therefore, one encounters vertices where only gluons are present. Figure 2.1 shows the 3-gluon vertex stemming from the first term and the 4-gluon vertex stemming from the second term of equation 2.11. They are a fundamental feature of the theory and their implications will be important in the context of vertex corrections. Another difference to QED is the existence of an additional ghost particle. This fact increases the number of diagrams to be considered for a given process. Any internal quark loop can be exchanged by a ghost loop. Furthermore, you will have to consider external ghosts for canceling the longitudinal degrees of freedom of external gluons, when you want to stick to the total polarization sum

$$\sum_{\text{Pol.}} \varepsilon_\mu(p) \varepsilon_\nu^*(p) = -g_{\mu\nu}, \quad (2.13)$$

where $\varepsilon_\mu(p)$ is the polarization vector for a gluon with momentum p . Alternatively, you could sum solely over the transverse polarization vectors of the gluon

$$\sum_{\text{T. Pol.}} \varepsilon_\mu^T(p) \varepsilon_\nu^{T,*}(p) = -g_{\mu\nu} + \frac{n_\mu p_\nu + n_\nu p_\mu}{n \cdot p} - \frac{n^2 p_\mu p_\nu}{(n \cdot p)^2}, \quad (2.14)$$

where $n_\nu \neq p_\mu$ is an arbitrary four-vector [7].

On tree-level the evaluation of Feynman diagrams in QCD is a straightforward exercise. Problems arise when you want to calculate higher order corrections. In NLO and above you will have to deal with two kinds of divergences. In virtual corrections, you are faced with ultraviolet (UV), infrared (IR) and collinear divergences, the latter arising from integration over undefined momenta.³ In real corrections, where you have

³We will regard all particles to be massless in our calculation. This is a good approximation when the top-quark contributions are not considered. In this case, it is unavoidable that collinear divergences will pop up.

additional particles in the final state, you will encounter soft and collinear divergences in the integration over the additional degrees of freedom in the phase space. The next sections are about how to deal with the divergences and how they cancel each other. To do that, one has to define a method for isolating the divergences, or to say it metaphorically, to make their degree of divergence visible. Such methods are called *regularization schemes*. The most suitable scheme for gauge theories and the most commonly used in QCD is *dimensional regularization* [8]. In this scheme the integration over loop momenta or the phase space integration is carried out in $D = 4 - 2\varepsilon$ dimensions. For UV-divergences ε will be chosen bigger than zero while it will be chosen smaller than zero for IR- and collinear divergences. The integration will lead to a result depending on D and is analytically continued to regions where D and the corresponding loop momentum are complex. The divergences will then appear as poles in ε . The main reason to choose dimensional regularization is because it preserves Lorentz invariance, gauge invariance and unitarity of the theory. To maintain the coupling parameter g to be massless, a mass scale μ is introduced. The coupling is then defined by

$$g = g_0 \mu^\varepsilon, \quad (2.15)$$

where g_0 is the new dimensionless coupling constant.

2.2. Ultraviolet divergences

The first type of divergence we want to deal with are the ultraviolet (UV) divergences. As already mentioned, they arise because of divergent integrals over undefined momentum during the calculation of Feynman amplitudes of diagrams containing a closed loop. This is why on tree-level there are no UV divergences. They appear in virtual higher order corrections. The outline of this section is the following. Firstly, we will follow reference [5] in the regularization and renormalization of a specific example of a UV divergence, the one-loop quark self-energy. Later on, the renormalization procedure will be applied to the whole theory and we will encounter a new renormalized QCD Lagrangian in subsection 2.2.1. Finally, we will focus on a special aspect of virtual corrections, making the coupling strength to a function of a newly introduced scale parameter in subsection 2.2.2.

The full quark propagator includes so-called radiative corrections in higher order of QCD. The propagator $S_{ij}(p)$ for a quark with mass m and momentum p is

$$S_{ij}(p) = \frac{\delta_{ij}}{m - \not{p} - \Sigma(p)}, \quad (2.16)$$

where $\Sigma(p)$ is called the *self-energy part* containing all radiative corrections stemming from one-particle irreducible diagrams. The propagator can be expanded with respect to the self-energy,

$$S_{ij}(p) = \delta_{ij} [S_0(p) + S_0(p)\Sigma(p)S_0(p) + S_0(p)\Sigma(p)S_0(p)\Sigma(p)S_0(p) + \dots], \quad (2.17)$$

where

$$\delta_{ij}S_0(p) = \delta_{ij} \frac{1}{m - \not{p}} \quad (2.18)$$

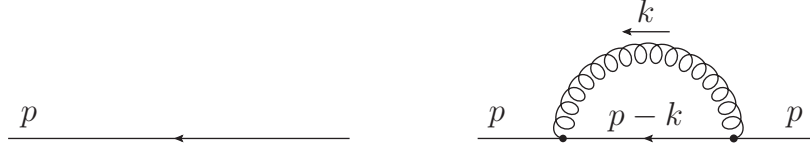


Figure 2.2.: Quark propagator and its one-loop self-energy correction diagram.

is the propagator without higher-order effects. The self-energy $\Sigma(p)$ can be expanded perturbatively with respect to g . To $\mathcal{O}(g^2)$ there is only one contribution represented by the diagram on the right side of figure 2.2. From the Feynman rules (see appendix B) we can deduce

$$\Sigma_{ij}(p) = \int \frac{d^4 k}{(2\pi)^4 i} g \gamma_\mu T_{il}^a \frac{\delta_{ln}}{\not{p} + \not{k}} g \gamma_\nu T_{nj}^b \frac{\delta_{ab}}{k^2} d^{\mu\nu}(k) \quad (2.19)$$

$$= \delta_{ij} \Sigma(p) \quad (2.20)$$

$$= \delta_{ij} g^2 C_F \int \frac{d^4 k}{(2\pi)^4 i} \frac{\gamma_\mu (\not{p} - \not{k}) \gamma_\nu d^{\mu\nu}(p)}{-k^2 (p-k)^2}, \quad (2.21)$$

where we neglected the quark mass, as we will always do from here on. We defined $C_F = (N_C^2 - 1)/(2N_C)$, where $N_C = 3$ is the number of colors. The expression 2.21 is linearly divergent because of the UV region with high momentum $|k| \rightarrow \infty$. The first step to get rid of that divergence is to regularize it. For that we use dimensional regularization. Inserting B.1 the D -dimensional integral

$$\Sigma(p) = g^2 C_F \int \frac{d^D k}{(2\pi)^D i} \frac{1}{k^2 (k-p)^2} \left(\gamma_\mu (\not{k} - \not{p}) \gamma^\mu - (1 - \xi) \frac{\not{k} (\not{k} - \not{p}) \not{k}}{k^2} \right) \quad (2.22)$$

has to be calculated. This is far from trivial. It has to be Feynman parametrized and the momentum k has to be Wick rotated in the complex plane by an angle of 90° . Then the integration can be carried out with the help of D -dimensional polar coordinates. We will just give the result here:

$$\Sigma(p) = \xi \frac{2C_F g^2}{(4\pi)^{D/2}} \not{p} (-p^2)^{D/2-2} (D-1) B\left(\frac{D}{2}, \frac{D}{2}\right) \Gamma\left(2 - \frac{D}{2}\right), \quad (2.23)$$

where the beta function $B(x, y)$ and the gamma function $\Gamma(x)$ were introduced (see appendix A). The step-by-step evaluation can be found in [5]. To make the divergence in the limit $D \rightarrow 4$ visible, we use equation 2.15, substitute $\varepsilon = 2 - \frac{D}{2}$ and make a Laurent expansion around $\varepsilon = 0$ to obtain

$$\Sigma(p) = \xi \frac{g_0^2}{(4\pi)^2} C_F \not{p} \left(\frac{1}{\varepsilon} - \gamma_E + 1 - \ln\left(\frac{-p^2}{4\pi\mu^2}\right) \right) + \mathcal{O}(\varepsilon), \quad (2.24)$$

where $\gamma_E = 0.57721\dots$ is the *Euler-Mascheroni constant*. Now, the regularization procedure is completed. The divergence is regularized by a single pole in ε . Using equation 2.16 and inserting the above expression lead to the one-loop corrected propagator

$$S_{ij}(p) = -\frac{\delta_{ij}}{\not{p}} \frac{1}{1 + \sigma(p^2)}, \quad (2.25)$$

with

$$\sigma(p^2) = -\xi \frac{g_0^2}{(4\pi)^2} C_F \left(\frac{1}{\varepsilon} - \gamma_E + 1 - \ln \left(\frac{-p^2}{4\pi\mu^2} \right) \right) + \mathcal{O}(g_0^4), \quad (2.26)$$

where terms of order ε are neglected.

From here we can start to remove the divergence. This process is called *renormalization*. In our case the quark propagator is what has to be renormalized. This is done by introducing a multiplicative factor Z_2 called *quark-field renormalization constant* and writing

$$S_{ij}^R(p) = \frac{1}{Z_2} S_{ij}(p), \quad (2.27)$$

where S_{ij}^R is the renormalized quark propagator. Inserting 2.25 and expanding Z_2 similar to $\sigma(p^2)$ with respect to g_0 gives

$$Z_2 = 1 - z_2 + \mathcal{O}(g_0^4), \quad (2.28)$$

where z_2 is of order g_0^2 , and we arrive at

$$S_{ij}^R(p) = -\frac{\delta_{ij}}{\not{p}} \frac{1}{1 + \sigma(p^2) - z_2}. \quad (2.29)$$

In this expression it becomes clear how the renormalization constant does its job. Order by order in perturbation theory, it subtracts a divergent part from UV loop contributions, while a finite remainder will be left as virtual correction. Here we are at order g_0^2 and z_2 subtracts the divergence from $\sigma(p^2)$.

To do that, one has to agree on a *renormalization scheme*, since subtracting a divergence is not unique. Different schemes will have different finite remainders. In this manner, different schemes are connected by an additional finite renormalization. In our calculation, as is mostly done in QCD, the *modified minimal subtraction scheme* or $\overline{\text{MS}}$ scheme is chosen. It is defined by not only subtracting the pole $1/\varepsilon$, but the expression

$$\frac{1}{\varepsilon} - \gamma_E + \ln 4\pi. \quad (2.30)$$

It has the advantage of shorten some dimensionally regularized expressions, where the poles are always accompanied by the latter terms. In this scheme, we find

$$z_2 = \xi \frac{g_0^2}{(4\pi)^2} C_F \left(\frac{1}{\varepsilon} - \gamma_E + \ln 4\pi \right). \quad (2.31)$$

The renormalized quark propagator carries finite corrections,

$$S_{ij}^R(p) = -\frac{\delta_{ij}}{\not{p}} \left[\xi \frac{g_0^2}{(4\pi)^2} C_F \left(-1 + \ln \frac{-p^2}{\mu^2} \right) \right]^{-1}. \quad (2.32)$$

Note that the propagator depends on the mass scale μ , which is equally the renormalization scale μ_R in the $\overline{\text{MS}}$ scheme. In the next section, we will see how the complete theory can be made UV finite. The renormalization will lead to the redefinition of the parameters of the theory and they will become scale-dependent as well. For the coupling constant this will lead to the running coupling.

2.2.1. Renormalization

The basic idea of renormalization is to remove the UV divergences by introducing multiplicative factors absorbing the divergence and simultaneously redefine the parameters of the theory. The physical justification for this is that it is no longer demanded that the parameters contained in the Lagrangian are the real physical quantities measured in experiment. One distinguishes between bare and renormalized quantities. It was proven by t'Hooft that a non-Abelian gauge theory like QCD is renormalizable to all orders of perturbation theory by introducing just a finite number of renormalization constants [8]. This procedure will lead to additional *counter terms* in the Lagrangian canceling loop divergences in the same way we saw in the previous section.

Technically, one redefines the fields and the parameters through [5]

$$A_\mu^a = Z_3^{1/2} A_{r\mu}^a, \quad \chi_{1,2}^a = \tilde{Z}_3^{1/2} \chi_{1,2r}^a, \quad \psi = Z_2^{1/2} \psi_r, \quad (2.33)$$

$$g = Z_g g_r, \quad \xi = Z_3 \xi_r, \quad m = Z_m m_r, \quad (2.34)$$

where Z_2 is the already familiar quark-field renormalization constant, Z_3 and \tilde{Z}_3 the gluon-field and ghost-field renormalization constants respectively, Z_m the mass renormalization constant and Z_g the coupling-constant renormalization constant. The index r signals the renormalized version of the equivalent quantity. The ghost-fields were redefined by

$$\chi^a, \chi^{a*} \rightarrow \chi^a = \frac{1}{\sqrt{2}} (\chi_1^a + i\chi_2^a), \quad (2.35)$$

just for practical reasons. When we insert the above expressions into the Lagrangian 2.9, we get

$$\mathcal{L} = \mathcal{L}_{0r} + \mathcal{L}_{1r} + \mathcal{L}_C, \quad (2.36)$$

where \mathcal{L}_{0r} and \mathcal{L}_{1r} are exactly the same as \mathcal{L}_0 and \mathcal{L}_1 from equations 2.10 and 2.11, yet the fields and the parameters exchanged by their renormalized version. The counter-term Lagrangian \mathcal{L}_C contains all remaining terms and is given by

$$\begin{aligned} \mathcal{L}_C = & -(Z_3 - 1) \frac{1}{4} (\partial_\mu A_{r\nu}^a - \partial_\nu A_{r\mu}^a) (\partial^\mu A_r^{a\nu} - \partial^\nu A_r^{a\mu}) \\ & + (\tilde{Z}_3 - 1) i (\partial^\mu \chi_{1r}^a) (\partial_\mu \chi_{2r}^a) + (Z_2 - 1) \bar{\psi}_r^i i \gamma^\mu \partial_\mu \psi_r^i \\ & - (Z_2 Z_m - 1) m_r \bar{\psi}_r^i \psi_r^i \\ & - (Z_g Z_3^{3/2} - 1) \frac{1}{2} g_r f^{abc} (\partial_\mu A_{r\nu}^a - \partial_\nu A_{r\mu}^a) A_r^{b\mu} A_r^{c\nu} \\ & - (Z_g^2 Z_3^2 - 1) \frac{1}{4} g_r^2 f^{abe} f^{cde} A_{r\mu}^a A_{r\nu}^b A_r^{c\mu} A_r^{d\nu} \\ & - (Z_g \tilde{Z}_3 Z_3^{1/2} - 1) i g_r f^{abc} (\partial^\mu \chi_{1r}^a) \chi_{2r}^b A_{r\mu}^c \\ & + (Z_g Z_2 Z_3^{1/2}) g_r \bar{\psi}_r^i T_{ij}^a \gamma^\mu \psi_r^j A_{r\mu}^a. \end{aligned} \quad (2.37)$$

From this expression one obtains the counter-term Feynman rules stated in appendix B. When all renormalization constants are calculated in a way that they cancel the UV divergences at a given order of perturbation theory, considering these new rules

will assure an accurately renormalized result. QCD is made UV finite to all orders of perturbation theory.

Because of the gauge invariance, there are four different ways of determining the constant Z_g , while all four possibilities should give the same result. After the definition of four new constants

$$\begin{aligned} Z_1 &\equiv Z_g Z_3^{3/2}, & Z_4 &\equiv Z_g^2 Z_3^2, \\ \tilde{Z}_1 &\equiv Z_g \tilde{Z}_3 Z_3^{1/2}, & Z_{1F} &\equiv Z_g Z_2 Z_3^{1/2}, \end{aligned} \quad (2.38)$$

this condition gives the *Slavnov-Taylor identity*

$$\frac{Z_1}{Z_3} = \frac{\tilde{Z}_1}{\tilde{Z}_3} = \frac{Z_{1F}}{Z_2} = \frac{Z_4}{Z_1}. \quad (2.39)$$

Its deeper meaning is that the renormalized coupling g_r is universal.

We finally have to discuss the existence of the mass scale introduced in equation 2.15 for having a massless coupling constant in D dimensions. We saw that we can arbitrarily choose the renormalization scheme, which defines how much of the finite terms will remain in an expression after subtracting the divergences. This freedom can be expressed with the help of an additional parameter called *renormalization scale* μ_R . It is a special feature of the \overline{MS} scheme that the mass scale μ and the the renormalization scale μ_R happen to be exactly the same. Anyway, a renormalized quantity will depend on μ after renormalization (see, for instance, the renormalized quark propagator in 2.32). But μ is no physical quantity that is contained in the Lagrangian. It is a technical invention for being consistent. In the end, any observable has to be independent of μ . Otherwise the result we get for an observable would change when we change the renormalization scheme, which is equivalent to a change of the renormalization scale. At this point, perturbation theory causes trouble. Remember that we calculate an observable σ just approximately by truncating the perturbative expansion at some order n . However, this comes at the prize of a scale dependence that will remain in the final result. In order to see this, imagine we carried out the renormalization and for the coupling we have, for example,

$$g_r(\mu) = \frac{1}{Z_g(\mu)} g. \quad (2.40)$$

We might have done the same thing in another scheme, where similar the equation

$$g'_r(\mu') = \frac{1}{Z'_g(\mu')} g \quad (2.41)$$

is valid, but in that scheme we have a different scale μ' and g'_r and Z'_g share finite terms in a different way than g_r and Z_g do. In this sense, both expressions are related by an additional finite renormalization

$$g'_r(\mu') = z_g(\mu', \mu) g_r(\mu) \quad \text{with} \quad z_g(\mu', \mu) = \frac{Z_g(\mu)}{Z'_g(\mu')}, \quad (2.42)$$

where the corresponding renormalization constant z_g is finite. This is guaranteed, because Z_g and Z'_g are multiplicative factors and their poles cancel when they are divided

by each other. It can be shown that the set of finite renormalizations connecting different schemes form a group called the *renormalization group*. Equations like the latter one for the coupling constant define how the quantity will react under a change of the scale. For infinitesimal variations of μ they become differential equations called *renormalization group equations* (RGE). For any observable we demand

$$\sigma'(g'_r, \mu', \dots) = \sigma(g_r, \mu, \dots). \quad (2.43)$$

Here, the dots represent any other dependence like for example on particle momenta or on the renormalized masses. We have to distinguish between σ and σ' , because they will have a different functional form. We claim that their values are the same. But in perturbation theory, we know σ and σ' just to a certain order in g_r . Condition 2.43 gets weakened to

$$\sigma'(g'_r, \mu', \dots) - \sigma(g_r, \mu, \dots) = \mathcal{O}(g_r^{n+2}). \quad (2.44)$$

A finite order result in pQCD will depend on the renormalization scale, yet there is hope that the dependence will decrease if you go to higher orders.

There will be a RGE, like 2.42 for the coupling, for any renormalized field or parameter of QCD. For us, they provide two important things. Firstly, in the massless limit, where quark masses are neglected, the renormalized quark masses remain zero after renormalization [5]. Secondly, the quarks become asymptotically free at high energies. This fact will be discussed in the next subsection.

2.2.2. Running coupling

Imagine we have renormalized the coupling constant g by

$$g_r(\mu) = \frac{1}{Z_g(\mu)} g. \quad (2.45)$$

Apart from that, we want to have dimensionless unrenormalized and renormalized couplings g_0 and g_R , so we claim

$$g = g_0 \mu_0^\varepsilon \quad \text{and} \quad g_r = g_R \mu_R^\varepsilon, \quad (2.46)$$

like it was done in equation 2.15. Inserting this in 2.45 we obtain

$$g_R(\mu_R) = \left(\frac{\mu_0}{\mu_R} \right)^\varepsilon \frac{1}{Z_g(\mu_R)} g_0. \quad (2.47)$$

By making use of the fact that the bare parameter g does not depend on μ_R , we state

$$\frac{dg}{d\mu_R} = 0. \quad (2.48)$$

From this we can deduce the RGE for the renormalized coupling constant:

$$\mu_R \frac{\partial}{\partial \mu_R} g_R(\mu_R) = \mu_R \frac{\partial}{\partial \mu_R} \left(\left(\frac{\mu_0}{\mu_R} \right)^\varepsilon \frac{1}{Z_g(\mu_R)} g_0 \right)$$

$$\begin{aligned}
&= \mu_R \left(-\varepsilon \left(\frac{\mu_0}{\mu_R} \right)^\varepsilon \frac{1}{\mu_R} \frac{1}{Z_g(\mu_R)} g_0 + \left(\frac{\mu_0}{\mu_R} \right)^\varepsilon \left(-\frac{1}{Z_g(\mu_R)^2} \right) \frac{\partial Z_g(\mu_R)}{\partial \mu_R} + 0 \right) \\
&= -\varepsilon g_R(\mu_R) - \frac{\mu_R}{Z_g(\mu_R)} \frac{\partial Z_g(\mu_R)}{\partial \mu_R} g_R(\mu_R) \equiv \beta,
\end{aligned} \tag{2.49}$$

where the β function was introduced, giving the dependence of the coupling constant on the scale. This function can be calculated perturbatively by calculating vertex corrections to a certain order and from that extracting Z_g and g_R . Nowadays, the RGE is normally expressed in terms of $\alpha_s(\mu_R) = g_R^2(\mu_R)/(4\pi)$. For later use of notation we will write [2]

$$\beta(\alpha_s) \equiv \mu_R \frac{d \ln g_R}{d \mu_R} = -\beta_0 \frac{\alpha_s}{4\pi} - \beta_1 \frac{\alpha_s^2}{(4\pi)^2} + \dots, \tag{2.50}$$

where the β -coefficients in one- and two-loop approximation are given by

$$\beta_0 = \frac{1}{3} (11C_A - 2n_f), \tag{2.51}$$

$$\beta_1 = \frac{34}{3} C_A^2 - 2n_f \left(C_F + \frac{5}{3} \right), \tag{2.52}$$

with $C_A = N_C$ and n_f is the number of quark flavors being considered. β_0 and β_1 are the scheme independent part of the β -function. From the three-loop coefficient β_2 on, β is scheme dependent. In the \overline{MS} scheme the β function is not gauge dependent. The β_i are known up to four-loop order [9]. For the determination of β_3 around 50 000 Feynman diagrams had to be calculated. In one-loop approximation an analytical solution of

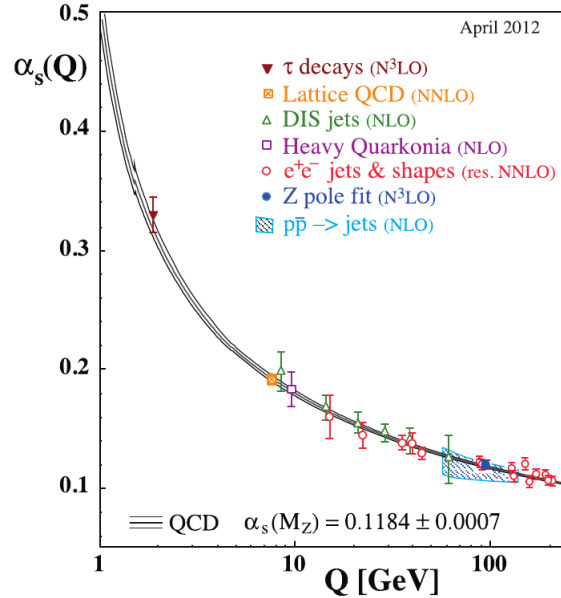


Figure 2.3.: Theoretical estimation of the running coupling constant and collection of experimental data showing good agreement (taken from [10]).

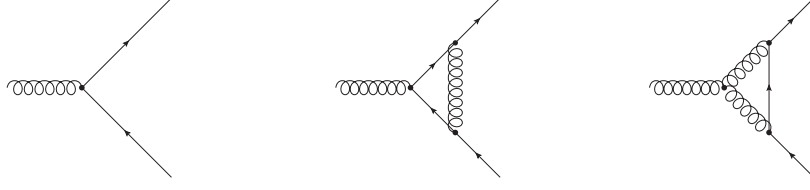


Figure 2.4.: Quark-gluon vertex at tree-level and one-loop vertex corrections via QED-like screening and anti-screening because of gluon self-interaction.

equation 2.50 can be found by

$$\alpha_s(\mu_R^2) = \frac{1}{\beta_0 \ln \left(\frac{\mu_R^2}{\Lambda^2} \right)}, \quad (2.53)$$

where Λ is an integration constant defining the value of α_s at a certain scale. One can see that α_s decreases when μ_R increases, as long as β_0 is positive. Actually, as long as the number of active flavors n_f is smaller than $11C_A/2$, the β -coefficients are positive, what guarantees the falling of α_s . This property is called *asymptotic freedom*. At high energies the strong interaction becomes weak. Experimental data from different type of collider experiments and lattice-QCD calculations confirm this prediction, as it can be seen in figure 2.3. This feature of QCD is the reason why calculations by perturbation theory are meaningful, where a small coupling constant is required. Contrariwise, at small energy scales, the coupling constant becomes large, which is associated to *confinement*, i.e., the non-existence of colored particles at low energies.

Comparing to QED, we find a completely opposite behavior. There the coupling becomes small at low energies, or equivalently higher distances, because of the *screening* effect. The polarized vacuum generated by closed charged fermion lines in Feynman diagrams shields the charge of interacting particles like a virtual dielectric. In principle, the screening effect is also present in QCD. In figure 2.4 we see the quark-gluon vertex at the left-hand side. The vertex gets virtual corrections similar to QED by the diagram depicted in the middle. Indeed, this type of diagram produces screening-effects as in QED. But QCD is based on a non-Abelian symmetry with additional self-interaction vertices of the gluon (see section 2.1). With the help of these vertices one gets vertex corrections not being present in QED, like the one-loop example on the right-hand side of 2.4. It is these contributions that produce *anti-screening* effects countering the screening effect. Assuming the six known quark flavors the anti-screening is dominant and produces asymptotic freedom.

2.3. Mass singularities

In the previous section, it was shown that in pQCD you are confronted with divergent expressions while integrating over the UV part of undefined loop momenta to obtain virtual corrections to a given process. We could get rid of these UV divergences by a renormalization procedure at the cost of the existence of a new parameter μ_R , on

which any finite order calculation will depend. In this section we will see that even the renormalized theory will contain divergent expressions that might spoil the perturbative expansion of a physical quantity. These expressions are called *mass singularities*, because they have their origin in the vanishing mass of virtual particles. Important to note is that the mass singularities appear in two different ways. Firstly, they are present in the integration over undefined loop momentum during the calculation of Feynman amplitudes of loop diagrams. Secondly, they are produced in the integration of Feynman amplitudes over the corresponding final state phase space.

In QCD we can distinguish between two types of mass singularities. First of all, the gluon is massless like the photon in QED. This will accordingly lead to *infrared (IR) divergences*, when the gluon momentum becomes soft. In the limit of vanishing quark masses, also *collinear divergences* will appear.⁴ Mass singularities arise because of our inability to define physical states unambiguously in the quantum field theoretical context of QCD and QED. In experiment you do not collide quarks and gluons with photons, for instance, but electrons with protons. If you assign definite momenta and masses to the electron and the proton, then you have an explicit physical state. On partonic level, things are different. When a particle has no mass, what should be the observable difference between a quark-photon scattering and the same scattering accompanied by the emission of a soft gluon, for example, whose energy lies below any detector sensitivity. In other words, how would you now that there was just a single quark with momentum p initiating the scattering, and not a quark with momentum p' collinearly accompanied by a gluon with momentum k , whose total momentum is $p = p' + k$. To express the electron-proton scattering in the language of QCD, you pick single states out of a bulk of energetically indistinguishable *degenerate states* in the final state as well as in the initial state. Then, we must not be surprised of unphysical singularities in Feynman amplitudes, since they stand for unphysical partonic processes.

So what is the solution for getting rid of the mass singularities? A hint came from the calculation of total decay rates or fully inclusive cross section. It was found that they do not contain any mass singularity, whereas the calculation of the production of definite particles showed singular behavior. For instance, the totally inclusive cross section for e^+e^- -collisions was shown to be finite. Inclusiveness can be interpreted as a sum over all degenerate final states. Thus, the idea was born that the summation over degenerate states might in the end cancel the divergences. In QED this becomes manifest in the *Bloch-Nordsieck theorem* [11]. It says that QED is infrared finite when you sum over degenerate final states. In practice this means that in a perturbative calculation you have to consider additional Feynman diagrams containing the emission of soft photons. In QCD the cancellation is somewhat more elaborate, because you have hadronic matter in the initial state, which are compound and confined states. Therefore, the initial state is also degenerate. Now we can hope to be able to remove all mass singularities in QCD by summing over those states as well. This is exactly the statement of the *Kinoshita-Lee-Nauenberg (KLN) theorem* [12, 13]. It says that the mass singularities coming from

⁴In the literature often collinear divergences are included in the term IR divergences. This is confusing, so we will distinguish between them and refer to the term mass singularities as an umbrella term, since they mutually rise because of vanishing masses.

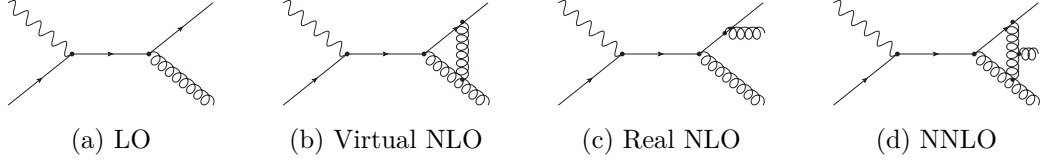


Figure 2.5.: Feynman diagrams for example process and exemplary higher-order diagrams illustrating the application of the KLN theorem.

loop integrals are canceled by mass singularities coming from phase space integrations, if you sum over all degenerate initial and final states.

We will illustrate the application of the KLN theorem in pQCD with the example process depicted in figure 2.5, in particular at NLO. A quark absorbs a photon and emits a gluon, so at LO we have a two-body initial and final state and in figure 2.5a we see one of the two possible diagrams. At NLO we have to consider loop diagrams like the one in figure 2.5b, which will give us corrections called *virtual*, because only virtual particles were added. After renormalization the UV divergences are removed, but soft and collinear divergences remain, until we consider additional diagrams with one further soft or collinear (or both) particle in the initial or final state. In figure 2.5c we see one example diagram with an additional gluon in the final state, producing soft and collinear divergences while integrating the corresponding Feynman amplitude over the three-particle final state phase space. There is no possibility to distinguish the three-particle final state from the one in figure 2.5a and figure 2.5b when the gluon is soft, because any detector will have a lower bound of energy sensibility and if the gluon is collinear to the quark, the final state is not distinguishable in the case of jet measurements. Considering all possibilities to add one particle to the original LO diagram, the KLN theorem assures that by summing these *real* contributions and the virtual ones, all divergences cancel out. The remainder of the cancellation will be called real corrections. Real corrections are classified into initial-state or final-state corrections, depending on whether the particle emitting the extra particle is an initial- or final-state particle. In a perturbative calculation this procedure has to be done order by order, while the number of diagrams increases dramatically already in NNLO. From NNLO on you also lose the separation into real and virtual corrections, which becomes obvious when you see diagrams like the one in figure 2.5d, for instance, where the extra gluon is attached to the loop. The summation over degenerate initial states is carried out by a convolution of the hard-scattering part with suitable distribution functions which are universal in the sense that they only depend on the properties of, in our case, the proton, and not on the actual hard scattering of its constituents (see section 2.5). Nevertheless, in experiment you will not be able to create conditions satisfying the requirement of regarding all degenerate states as the KLN theorem demands. This will be one reason for using resummation techniques introduced in section 2.6.

Technically, the application of the KLN theorem in pQCD involves a lot of effort. As an example, we can consider the $2 \rightarrow 2$ process in figure 2.6a. This diagram gets real correction by, for instance, the process shown in figure 2.6b, in which the incoming quark emits an additional soft gluon. For expressing the phase space integration of the



Figure 2.6.: One Feynman diagram for the process $\gamma^* + q \rightarrow q + g$ and one real correction diagram in NLO to it.

gluon, the variable

$$z = \frac{p_2 \cdot p_3}{q \cdot p} \quad (2.54)$$

is introduced [14]. z is a dimensionless parameter that in principle can take values in the region $0 \leq z \leq 1$. It is a measure for the fraction of the incoming quark momentum p that is entering the hard scattering process. For $z \rightarrow 1$ the gluon momentum k becomes soft. Integrating the Feynman amplitude of diagrams like in figure 2.6b over the phase space, one encounters via dimensional regularization integrals of the form [15]

$$I = \int_0^1 dz \frac{f(z)}{(1-z)^{1-\varepsilon}}, \quad (2.55)$$

where the function $f(z)$ contains all regular parts and distributions functions.⁵ The integral I diverges in the limit $\varepsilon \rightarrow 0$. The reason for that divergence is that the quark propagator right after emitting the gluon becomes on-shell in this limit. The propagator has the form [14]

$$G \sim \frac{1}{(p-k)^2} = \frac{1}{-2p \cdot k} = \frac{1}{-2|p||k|(1-\cos\theta)}. \quad (2.56)$$

When the gluon is soft, $|k|$ goes to zero and G diverges. In the above expression θ is the angle between the incoming quark and the emitted gluon. We can immediately recognize the secondary collinear divergences for $\theta \rightarrow 0$.⁶ With the help of factorization properties (see section 2.4 and 2.3.1) and dimensional regularization the soft and collinear divergence will appear through terms proportional to $1/\varepsilon$ and, when the gluon is soft and collinear at the same time, proportional to $1/\varepsilon^2$. To see this in the case of the soft gluon, let us rewrite equation 2.55 by [15]

$$\begin{aligned} I &= \int_0^1 dz \frac{f(1) + f(z) - f(1)}{(1-z)^{1-\varepsilon}} \\ &= f(1) \int_0^1 dz \frac{1}{(1-z)^{1-\varepsilon}} + \int_0^1 dz \frac{f(z) - f(1)}{(1-z)^{1-\varepsilon}} \\ &= f(1) \frac{1}{\varepsilon} + \int_0^1 dz \frac{1}{(1-z)^{1-\varepsilon}} (f(z) - f(1)) \end{aligned}$$

⁵Because of kinematical reason the lower bound of the z -integration can actually be greater than 0.

⁶Notice that the propagator would be rendered finite, if the quark or the gluon would be massive.

$$\begin{aligned}
&= f(1) \frac{1}{\varepsilon} + \int_0^1 dz \left(\frac{1}{1-z} + \varepsilon \frac{\ln(1-z)}{1-z} + \mathcal{O}(\varepsilon^2) \right) (f(z) - f(1)) \\
&= f(1) \frac{1}{\varepsilon} + \int_0^1 dz \left(\left[\frac{1}{1-z} \right]_+ + \varepsilon \left[\frac{\ln(1-z)}{1-z} \right]_+ + \mathcal{O}(\varepsilon^2) \right) f(z). \tag{2.57}
\end{aligned}$$

Now the KLN theorem can come into action. The first term in 2.57 contains the pole in ε . Note that the argument of f is $z = 1$, i.e., all incoming momentum goes into the hard scattering and nothing is left for the soft gluon. That corresponds to the case of virtual diagrams, where from the outset are no additional external particles stealing momentum. And indeed, the KLN theorem tells us that in virtual corrections the exact same pole but with different sign will appear, canceling the first term in 2.57. So we do not have to care about it anymore, but the remaining terms are important. They were expressed with the help of the *plus distribution*, which is defined by [16]

$$\int_0^1 dz [f(z)]_+ g(z) = \int_0^1 dz f(z) [g(z) - g(1)]. \tag{2.58}$$

The remainder is finite, but still can get large. What is even more painful is that equivalent terms will be present in any order of perturbation theory. In that way they spoil the expansion 2.12. The truncation at any order would neglect significant contributions at higher orders. We will discuss in section 2.6 how this is dealt with.

Even after executing the above cancellation, some collinear divergences will remain. They have to be absorbed into the parton distribution functions that become scale dependent through this procedure. The heuristic reason to do this is that by means of the KLN theorem some of the poles will cancel by summing over degenerate initial states.

2.3.1. Phase Space Slicing

We saw that it is necessary to cancel mass singularities from loop diagrams and from real emission diagrams by each other. The problem is that the singularities stemming from the real emission do not appear until the phase space integration over the additional degrees of freedom is carried out. The *phase space slicing* algorithm provides a solution to perform the cancellation analytically. As the name suggests, it is based on the idea of separating the three-particle phase space into two different regions. The first region is the one in which no divergences are created. The second one is the infrared and collinear sensitive regime, where the final state partons generate singularities. For the separation one introduces a *cutoff parameter* y_c and writes [14]

$$\int_0^1 d\text{PS}^{(3)} |\mathcal{M}_{2 \rightarrow 3}|^2 = \int_0^{y_c} d\text{PS}^{(3)} |\mathcal{M}_{2 \rightarrow 3}|^2 + \int_{y_c}^1 d\text{PS}^{(3)} |\mathcal{M}_{2 \rightarrow 3}|^2, \tag{2.59}$$

where the first integral on the right-hand side of the equation is the infrared and collinear sensitive part and the second integral is finite in 4 dimensions. In principle you might need two different cutoffs to distinguish soft and collinear regions of phase space, but you can define both in a way that they are represented by just one cutoff y_c . The latter integral can be directly evaluated analytically or, preferentially, by a Monte-Carlo

simulation. This has the advantage that you can generate events and analyze them in histograms, which can be easily adapted to different observables or experimental cuts. So practically you can say that y_c separates the integration in what you calculate by hand and what is done by Monte-Carlo simulations [17].

Until now, we did not really gain anything. We constrained the phase space to the problematic regions, but we did not remove anything. To do that, we have to isolate the poles and write them in a way to be comparable to the poles from the loop diagrams. Therefore you have to factorize the three-particle phase space in D dimensions

$$d\text{PS}^{(3)} = \frac{d^{D-1}p_1}{2E_1(2\pi)^{D-1}} \frac{d^{D-1}p_2}{2E_2(2\pi)^{D-1}} \frac{d^{D-1}p_3}{2E_3(2\pi)^{D-1}} (2\pi)^D \delta^D(p + q - p_1 - p_2 - p_3) \quad (2.60)$$

in the region $[0, y_c]$ into the two-particle phase space that expressed by the Mandelstam variables 3.39 is given by

$$d\text{PS}^{(2)} = \frac{1}{\Gamma(1-\varepsilon)} \left(\frac{4\pi}{stu} \right) (s + Q^2)^{-1+2\varepsilon} \frac{dt}{8\pi}, \quad (2.61)$$

and a remaining part $d\text{PS}^{(r)}$ that will be integrated out analytically together with the approximate matrix elements [14]. The remainder will differ in case of initial- or final-state corrections. In the initial state it will also depend on whether we consider emission from the massless parton or the virtual photon. For example, the remaining phase space for parton initial state singularities is

$$\begin{aligned} d\text{PS}^{(r)} &= \frac{\Gamma(1-\varepsilon)}{4^\varepsilon \pi \Gamma(1-2\varepsilon)} d\phi \sin^{-2\varepsilon}(\phi) \left(\frac{4\pi}{s} \right)^\varepsilon \frac{s}{16\pi^2} \\ &\times dz_1 z_1^\varepsilon \left(1 - z_1 \frac{s - zQ^2}{s(1-z) - zQ^2} \right)^{-\varepsilon} \\ &\times \frac{dz}{z} \left(\frac{1-z}{z} - \frac{Q^2}{s} \right) \left(1 + \frac{Q^2(1-z)}{z(zs - (1-z)Q^2)} \right)^{1-\varepsilon}, \end{aligned} \quad (2.62)$$

where $\phi \in [0, \pi]$ is the angle between the momentum p and the momentum p_1 of the soft or collinear particle, $z \in [\eta, 1]$ was introduced in equation 2.54 and the variable

$$z_1 \equiv \frac{p_1 \cdot p}{q \cdot p} \in \left[0, \min \left(\frac{-u}{s + Q^2}, y_c \right) \equiv y_I \right] \quad (2.63)$$

is used to restrict the integration to the singular regions.⁷

Approximating the matrix element makes it possible to solve the integral analytically over $d\text{PS}^{(r)}$. In the case of infrared sensitivity, the *soft gluon approximation* is used, i.e., the gluon momentum is set to 0 in the numerator of the matrix element. In the case of collinear sensitivity, the *leading pole approximation* is used, where the poles arise when expressions like $(p + p_1)^2 = p_1 \cdot p$ in the denominator of the matrix elements become much smaller than the total incoming energy [17]. After this is done, the generated poles

⁷Note that z_1 vanishes in the soft ($p_1 \rightarrow 0$) and the collinear ($p_1 \cdot p \rightarrow 0$) limit.

can be canceled by the ones in the virtual matrix elements. The sum of virtual and real corrections can then be safely integrated over $dPS^{(2)}$ by Monte-Carlo simulations.

Both integrations on the right-hand side of equation 2.59 depend on the cutoff parameter. This dependence should cancel in the sum, because y_c is no physical parameter. However, the cancellation of the y_c -dependence is only exact when y_c goes to zero [18]. Of course that does not make sense in practice. Technically, we want to calculate an integral of the form

$$I = \lim_{\varepsilon \rightarrow 0} \left(\int_0^1 \frac{dx}{x} x^\varepsilon F(x) - \frac{1}{\varepsilon} F(0) \right), \quad (2.64)$$

where F might be any function, containing in our case finite parts of the matrix element, and in 4 dimensions the singularity appears when the parameter x goes to 0 [19]. The singularity is canceled by the latter term, which corresponds in our case to a pole from virtual loops. Using phase space slicing, we approximate the integral by

$$\begin{aligned} I &\approx \lim_{\varepsilon \rightarrow 0} \left(F(0) \int_0^{y_c} \frac{dx}{x} x^\varepsilon + \int_{y_c}^1 \frac{dx}{x} x^\varepsilon F(x) - \frac{1}{\varepsilon} F(0) \right) \\ &= F(0) \ln(y_c) + \int_{y_c}^1 \frac{dx}{x} F(x). \end{aligned} \quad (2.65)$$

The approximation lies in the fact that we set $F(x) \rightarrow F(0)$ in the region $0 < x < y_c$. With the help of this schematic formula we can decide how the cutoff should be chosen in practice. The approximation above is only valid for small cutoffs and also the dependence on the integral in the second term will be small, if y_c is chosen as small as possible. The limit is given because of numerical reasons. The smaller y_c is, the more contributions of the divergence is put into the Monte-Carlo integration, and the numerical error increases. In practice, you choose different values for y_c and find a more or less stable regime, in which the dependence on y_c is minimal. Actually, the existence of such a regime is a good test to see, if your calculation is done properly.

Nevertheless, with phase space slicing you introduce an additional parameter. That is the prize to pay for being able to cancel mass singularities analytically before entering your formulas into a computer code. Nowadays, it is more common to use the *dipole subtraction method* [18]. For calculating the exclusive NLO part of a cross section

$$\sigma^{NLO} = \sigma - \sigma^{LO} = \int_{m+1} d\sigma^R + \int_m d\sigma^V, \quad (2.66)$$

with m particles in the final state at LO and the integral denoting the phase space integration over the m - and $m+1$ -particle phase space, this method introduces a counter term $d\sigma^A$. That term has the task to make both integrations on the right-hand side of the upper equation finite. Remember that in general only their sum is finite. The counter term shall have the same pointwise singular behavior as $d\sigma^R$ and the integration over the extra degree of freedom in the phase space of real corrections shall be possible analytically. Then we can write using dimensional regularization

$$\sigma^{NLO} = \int_{m+1} \left[(d\sigma^R)_{\varepsilon=0} - (d\sigma^A)_{\varepsilon=0} \right] + \int_m \left[d\sigma^V + \int_1 d\sigma^A \right]_{\varepsilon=0}. \quad (2.67)$$

The first integrand is now finite by definition of $d\sigma^A$, so the limes $\varepsilon \rightarrow 0$ can be performed and then the integration can be carried out by Monte-Carlo routines. In the second integrand you first analytically integrate the counter term over the additional phase space and after that cancel the singularities with the ones from the virtual part in the limes $\varepsilon \rightarrow 0$. The integration over the m -particle phase space then again can be done by Monte-Carlo routines. Of course here we assumed that the UV divergences in $d\sigma^V$ were already removed by renormalization. We will not go into details of dipole subtraction in this thesis, because the calculations here make use of phase space slicing. We just state it as an alternative that avoids introducing an auxiliary parameter. The challenge of dipole subtraction lies in the proper definition of the counter term $d\sigma^A$. If it has not the same singularities as $d\sigma^R$ your Monte-Carlo integration will simply give meaningless results and the debugging attempt will be cumbersome.

2.4. Factorization

“In fact, we shall see that factorization theorems may be thought of as field theoretic realizations of the parton model.”

– Collins, Soper, Sterman [20]

We saw that any perturbative calculation relies on some constraints, and in the last section we had to discover that there are regions in the phase space, where the constraints are violated. Soft and collinear parts cause divergences spoiling any attempt to obtain reasonable finite order results, when it is not taken care of their cancellation following the KLN theorem. Luckily, QCD contains a feature called *factorization*. Not before factorization was found, pQCD calculations were possible just in cases, where there are no hadronic components in the initial state, for instance, in e^+e^- scattering. Aiming to find reasonable results for higher order cross sections with initial hadrons, the basic idea was to split the calculation into a part perturbatively calculable, and a part not perturbatively calculable [20]. The first part is denoted by short-distance part, while the latter on is called long-distance part. This separation should not be underestimated. If the starting point is not being able to calculate anything, it is a big advantage to be able to factorize out the troublemakers. And what is equally important is that the long-distance effects are universal in a sense that they are the same, for example, in eP or PP collisions, because they represent just properties of the proton and do not depend on the actual scattering process. So even if we cannot calculate them theoretically, we can deduce them from one experiment involving protons and transfer them to other experiments involving protons. If correct results are obtained in the second case, we have a good justification for claiming the universality of the long-distance effects.

Here, we will content ourselves with just stating the principle factorization theorems, while for the proofs the interested reader is referred to the literature [20, 21]. This will be sufficient, yet a heuristic and truly intuitive justification for the factorization properties will be given by the parton model in section 3.1. We will closely follow the argumentation of reference [20], focussing on the case of deep inelastic scattering. To start the factorization, you have to define regarding what attribute you want to separate. We realize that the scattering involves to different energy scales, on which

any event happens. We divide the cross section into a hard-scattering cross section, involving huge momentum transfers and highly virtual particles, and the rest is the soft remainder, containing everything that happens on comparably low energy scales. The hard scattering is happening on partonic level, where the physical energy scale is given by the exchanged photon virtuality Q^2 and the transferred transverse momentum p_T in DIS. Because the photon or any other internal propagator is highly off-shell, the hard scattering is happening at short distances. The hard piece is the one that can be obtained by pQCD with the help of asymptotic freedom. The soft part is not perturbatively calculable. It is given by the distributions of partons in the hadron, fragmentation processes in the final state and of course emission of soft and collinear particles, like extra gluons, happening at longer distances, because the virtual particles connecting these soft parts to the hard scattering become close to being on-shell and can propagate farther.

In the case of inclusive jet production in DIS, where we have a reaction like

$$\text{lepton} + \text{hadron} \rightarrow \text{lepton}' + \text{Jet} + X,$$

X representing the inclusiveness and standing for anything else, one finds a factorization theorem that can be written like [22]

$$Q^2 \sigma(Q, m) = \omega_{SD} \left(\frac{Q}{\mu_F}, \alpha_s \right) \otimes f_{LD}(\mu_F, m) + \mathcal{O} \left(\frac{1}{Q^p} \right). \quad (2.68)$$

Here, μ_F is the factorization scale, separating the short-distance effects ω_{SD} from the long-distance effects f_{LD} . Q represents the hard scale, while the parameter m collects the non-perturbative scales and p is an integer number. The operator \otimes usually is a convolution, at least as long you stay in the ordinary momentum space. However, the factorization is not always possible in momentum space. The reason for that is that σ is built out of the Feynman amplitudes and a phase space integration. The phase space is constrained by momentum conservation. It may, for example, contain δ -functions [16]

$$dz_1 \cdots dz_n \delta(z - z_1 \cdot z_2 \cdot \cdots \cdot z_n) \quad (2.69)$$

expressed in terms of momentum fractions z, z_1, z_2, \dots, z_n , obviously not factorized. Therefore, it is helpful to work in the space of *Mellin moments* N , defined by the transformation

$$\tilde{f}(N) = \int_0^1 dz z^{N-1} f(z). \quad (2.70)$$

As it is usually done in literature, we will omit the tilde indicating functions in Mellin space, because they can be identified by their argument N . The Mellin transformation factorizes the δ -function

$$\int_0^1 \frac{dz}{z} z^N \delta(z - z_1 \cdot z_2 \cdot \cdots \cdot z_n) = z_1^{N-1} z_2^{N-1} \cdots z_n^{N-1}, \quad (2.71)$$

where the limit $z \rightarrow 1$ is now given by $N \rightarrow \infty$. Another important result in the context of resummation is the Mellin transformation of plus distributions appearing in the soft part of the cross section [23]

$$\int_0^1 dz z^{N-1} \left[\frac{\ln^m(1-z)}{1-z} \right]_+ = \frac{-1}{m+1} \ln^{m+1} \frac{1}{N} + \mathcal{O}(\ln^{m-1} N). \quad (2.72)$$

The factorization theorem 2.68 underlies two conditions. Firstly, all Lorentz invariant parameters characterizing the process must be large and comparable. This is the case for DIS, when we force the jets to have a transverse momentum at the order of magnitude of the parton momenta. In particular, the virtuality of the photon Q^2 is large, so the contributions with $\mathcal{O}(1/Q^p)$ will be negligible. The only exceptions to that condition are the quark masses, which are set to 0. This does not prohibit the factorization. The second requirement is that the cross section has to be inclusive enough. With enough it is meant that the final-state long-distance interactions can be completely factorized out from the short-distance effects. In DIS the inclusiveness is guaranteed by a sum over all hadronic final states. We do not care about what definite hadrons can be found in the jet, we just assume that it is created by a hard parton that afterwards will fragment in whatsoever, independently of the hard process. Heuristically, both conditions together motivate the factorization of final-state interactions by saying that a jet with high transverse momentum, originated in a single hard event, will not interact again in a second hard event, or at least this is extremely unlikely.

The short-distance part ω_{SD} is the part which is calculable by perturbation theory. The long-distance part f_{LD} contains the partonic soft and collinear interactions in the proton and the final state and is not calculable in perturbation theory, but universal for many processes. It will therefore contain the *parton distribution functions (PDF)* $f_{c/H}(x, \mu_F)$ that give the probability to find a parton c inside a hadron H with the fraction x of longitudinal momentum of the hadron at a given momentum scale μ_F . Equation 2.68 can then be written as

$$Q^2 \sigma_{AB \rightarrow F}(Q) = f_{a/A}(x_a) \otimes f_{b/B}(x_b) \otimes \omega_{ab \rightarrow F+X} \quad (2.73)$$

for a collision of two hadrons A and B , producing the final state F . Of course, in DIS we only have one hadron and one PDF, but we introduce this more general formula for the discussion of resummation.

If we want to have a physical cross section, you naturally have to transform σ back from Mellin to momentum space. This can be a tricky task to do, which cannot be discussed in this thesis, but the result will be a convolution of the PDFs and the partonic differential cross section obtained by pQCD. In the case of DIS, we find⁸

$$d\sigma = \sum_a \int dx f_{a/P}(x, \mu_F) d\sigma_{ea}(\alpha, \alpha_s, \mu_R, \mu_F). \quad (2.74)$$

In the last two sections of this chapter we will make use of the fact that, while long-distance part f_{LD} and short-distance part ω_{SD} each depend on a scale μ_F , their product (or convolution) σ does not. This will lead us to the scale dependence of the PDFs in the following.

2.5. Parton Distribution Functions

In the last section we argued that by factorization it is possible to separate the perturbatively not calculable contributions to the cross section into universal functions called

⁸We will see later, that the electronic part factorizes additionally and we will be left with calculating matrix elements for $\gamma^* a$ scattering $d\sigma_{\gamma^* a}$.

parton distribution functions (PDFs). The procedure of how to obtain these functions is the following. For a given process, for instance DIS, you determine experimentally the cross section σ . On the theoretical side we can calculate the short-distance effects ω_{SD} . By using equation 2.68 you can then extract the PDFs in the long-distance part f_{LD} . In practice, this is not that simple to do, because of the huge amount of parameters coming into play, the PDFs are obtained by a global fit. You calculate the short-distance part to a certain order, perform the convolution with a type of functions depending on a set of parameters, and find the values for that parameters, so as to get a result for σ that describes best the experimental data. The good thing is that you can use data of different experiments, because we know that the PDFs are universal. Indeed, the experimental verification of this universality justifies the factorization theorems.

One still has to consider that different types of experiments happen at different energy scales. At different energies the proton, considering DIS, will appear different to the colliding electron. The higher the energies, the more important will be additional splittings of the partons into each other. One says that the partonic structure of hadrons smears out at high energies. Technically, this is represented by the dependence of the PDFs on the factorization scale μ_F . So it is not enough to just obtain the PDFs for one special energy scale in a single experiment. To compare theoretical calculations to experiments at different energy scales you need to know how the PDFs depend on μ_F . Luckily, there is a way out, by using the fact that an observable like σ in equation 2.68 cannot depend on auxiliary scales. By differentiating that equation, one gets the *QCD evolution equation* [22]

$$\mu_F \frac{d}{d\mu_F} \ln f_{LD}(\mu_F, m) = -P(z, \alpha_s) = -\mu_F \frac{d}{d\mu_F} \ln \omega_{SD}(Q/\mu_F, \alpha_s), \quad (2.75)$$

where $P(z, \alpha_s)$ stands for the *Altarelli Parisi splitting functions*. The above equation on the PDF-side is called *DGLAP equation* (for Dokshitzer, Gribov, Lipatow, Altarelli and Parisi) [24–26]. The splitting functions can be calculated perturbatively in orders of the coupling constant,

$$P_{i \leftarrow j}(z, \alpha_s) = \frac{\alpha_s}{2\pi} P_{i \leftarrow j}^{(0)}(z, \alpha_s) + \left(\frac{\alpha_s}{2\pi}\right)^2 P_{i \leftarrow j}^{(1)}(z, \alpha_s) + \dots, \quad (2.76)$$

and give the probability of a certain parton j to emit another parton i with a definite momentum fraction z of its initial momentum in the collinear limit at leading order. The initial parton can remain the same parton after the splitting, or become another type of parton. You can, for instance, distinguish between the emission of a gluon by a quark that itself remains being a quark, and a quark emitting a quark and becoming a gluon. The difference is, whether after splitting the gluon or the quark is considered to be in the collinear regime. At lowest order the splitting functions are given by [14]

$$P_{q \leftarrow g}^{(0)}(z) = \frac{1}{2} \left(z^2 + (1-z)^2 \right), \quad (2.77)$$

$$P_{q \leftarrow q}^{(0)}(z) = C_F \left(\frac{1+z^2}{(1-z)_+} + \frac{3}{2} \delta(1-z) \right), \quad (2.78)$$

$$P_{g \leftarrow q}^{(0)}(z) = C_F \frac{1 + (1 - z)^2}{z}, \quad (2.79)$$

$$P_{g \leftarrow g}^{(0)}(z) = 2N_C \left(\frac{1}{(1 - z)_+} + \frac{1}{z} + z(1 - z) - 2 \right) + \frac{\beta_0}{2} \delta(1 - z), \quad (2.80)$$

where the plus distributions defined by 2.58 was used. For later use we will state here the splitting functions in moment space in the soft limit [25]

$$P_{q \leftarrow g}^{(0)}(N) \sim \frac{1}{2N}, \quad P_{q \leftarrow q}^{(0)}(N) = C_F \left(\frac{3}{2} - 2(\ln N + \gamma_E) \right) + \mathcal{O}\left(\frac{1}{N}\right), \quad (2.81)$$

$$P_{g \leftarrow q}^{(0)}(N) \sim \frac{C_F}{N}, \quad P_{g \leftarrow g}^{(0)}(N) = \frac{\beta_0}{2} - 2N_C (\ln N + \gamma_E) + \mathcal{O}\left(\frac{1}{N}\right), \quad (2.82)$$

what can be obtained using the transformation 2.72.

In the scope of this work, we do not aim to determine the PDFs. Instead we will use existing proton PDFs for any quark flavor⁹ and the gluon to convolute them with our hard-scattering function to obtain a result for the cross section. There are PDFs of different research groups like MSTW or the CTEQ collaboration and a platform is available using different types of PDFs in a computer code. The difference in the PDFs of different collaborations lies mostly in the type of experimental data that was fitted. The values of the PDFs are recalled depending on the momentum fraction and the factorization scale. Each collaboration offers their PDFs to LO, NLO and nowadays NNLO accuracy. To be consistent, the running coupling formula 2.50, providing the value for the coupling constant α_s depending on the renormalization scale μ_R , should be used in the same order as the PDFs. The proton PDFs fulfill certain sum rules resulting from the partonic structure of the proton. Details on that can be found in section 3.1. As already mentioned, the PDFs are derived by a globe fit of experimental data, adjusting the fit parameters to minimize a global goodness-of-fit quantity χ^2 . This inevitably comes with a statistical uncertainty. That is why each PDF is given to a 68% or 90% confidence level. The fitting can be carried out fitting the PDFs and the coupling constant simultaneously. In this case a PDF set with α_s fixed at a certain scale μ_R will be used. Such PDF sets usually contain different PDF members, each with a fixed value for $\alpha_s(M_Z)$, from which the user can choose his preferred one, or rather go through a certain range of $\alpha_s(M_Z)$ to determine a best value for this quantity.

2.6. Resummation

In section 2.3 the cancellation of mass singularities according to the KLN theorem was explained. The singularities appear because we use a perturbative expansion regarding the coupling constant to calculate a physical quantity. The coefficients of that expansion contain virtual and real corrections, each including infrared and collinear divergences that cancel by summing both contributions. The remainder of that summation can be expressed by means of plus distributions, as we can see in formula 2.57. The problem

⁹Information about the different types of flavors are mostly obtained by neutrino scattering experiments.

with these remainders is that they can grow large in certain regions of the phase space, and what is even worse is that they are present in any order of perturbation theory. In NLO, for instance, where we consider the radiation of a single gluon, we find expressions proportional to

$$\left[\frac{1}{1-z} \right]_+ \quad \text{and} \quad \left[\frac{\ln(1-z)}{1-z} \right]_+ . \quad (2.83)$$

In higher orders there will be multiple gluon emission. At n -th order behind LO we will encounter so-called *towers* of logarithms of the form [16]

$$\alpha_s^n \left[\frac{\ln^l(1-z)}{1-z} \right]_+ , \quad 0 \leq l \leq 2n-1 . \quad (2.84)$$

Since, in the limit $z \rightarrow 1$ we will enter a region of the phase space where

$$\alpha_s \ln^2(1-z) \approx 1 , \quad (2.85)$$

the truncation of the perturbative expansion at any finite order neglects significant contributions and is therefore meaningless in that regime. Speaking in the language of Feynman diagrams that corresponds to the situation, in which all incoming parton momentum is just enough to produce the hard scattering final state and the additionally radiated gluons become soft. Heuristically we can imagine that the phase space of the soft gluons, which is limited by their energies, results in an incomplete cancellation of virtual mass singularities. Thus, when we cannot trust a fixed-order calculation in the contemplated regime, is there any loop hole? The answer is yes and no. No, because we will have to give up on fixed-order calculations, but yes, because it is partially possible to sum the problematic contributions to all orders of perturbation theory. This procedure is called *resummation*. More precisely, in our case we make use of *soft-gluon* or *threshold resummation*, where the threshold refers to the partonic threshold

$$z = \frac{M^2}{\hat{s}} \rightarrow 1 , \quad (2.86)$$

M^2 being the invariant mass of the target final state and $\sqrt{\hat{s}}$ the partonic center-of-mass energy. The fundamental condition making it possible to resum the problematic terms is that they can be determined to all orders due to factorization. To be more specific, in the given limit the matrix elements and the phase space integration can be separated into the soft gluonic part and the rest. It might be necessary to transform everything into the Mellin space though.

To illustrate the factorization we follow an example of reference [16]. Consider the emission of n gluons from a partonic quark line, as you can see in figure 2.7. In the soft limit, i.e., where all gluons are soft, using the *eikonal approximation*, the corresponding matrix element $\mathcal{M}_n(z_1, \dots, z_n)$ can be written in factorized form as

$$\mathcal{M}_n(z_1, \dots, z_n) = \frac{1}{n!} \prod_{i=1}^n \mathcal{M}_1(z_i) , \quad (2.87)$$

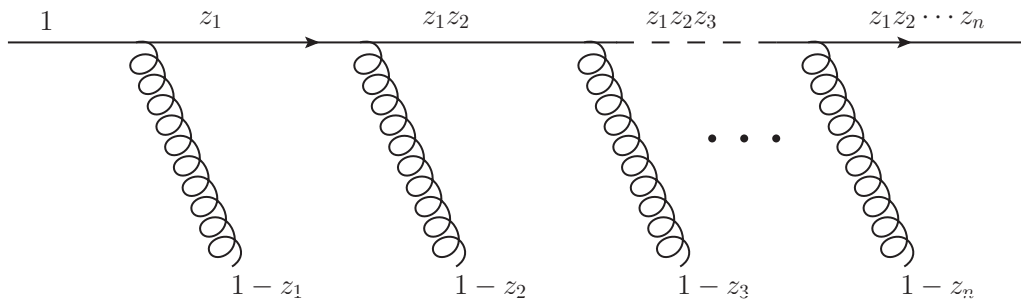


Figure 2.7.: Emission of n gluons with momentum fraction z_i , $i = 1, 2, \dots, n$, referring to the momentum of the emitting quark.

where \mathcal{M}_1 is the matrix element for the emission of just one soft gluon. Important to note is that the non-Abelian nature of QCD does not spoil the factorization, but the proof is much more evolved than in QED. The soft gluonic phase space $d\text{PS}_{soft}^n$ contains $\delta(z - z_1 \cdot z_2 \cdot \dots \cdot z_n)$ because of momentum conservation. The factorization of the phase space has to be done in Mellin space using the transformation from equation 2.71. We then can write accordingly to the matrix element

$$d\text{PS}_{soft}^n = \left(d\text{PS}_{soft}^1\right)^n. \quad (2.88)$$

The cross section for the emission of n extra soft gluons schematically can be expressed by

$$\sigma(n) \sim \int d\text{PS}_{soft}^{1+n}(p, z_1, \dots, z_n) |\mathcal{M}(p, z_1, \dots, z_n)|^2, \quad (2.89)$$

where p denotes the initial quark momentum. Inserting the factorization properties we find in Mellin space

$$\sigma(n) \sim \int d\text{PS}(p) |\mathcal{M}(p)|^2 \times \frac{1}{n!} \left(\int d\text{PS}_{soft}^1 |\mathcal{M}_1|^2 \right)^n. \quad (2.90)$$

The final important step is now obvious. If we sum this expression over n , which is the same as summing all orders of perturbation theory, the soft part of the cross section *exponentiates*. Writing the first integral regarding the quark phase space as $\sigma(0)$ we arrive at [27]

$$\sum_n \sigma_n \sim \sigma(0) \times \exp \left(\int d\text{PS}_{soft}^1 |\mathcal{M}_1|^2 \right). \quad (2.91)$$

The exponential absorbs all potentially large logarithms. We did not take into account the running coupling effects, what in QCD in principle should not be neglected. Here, we will just give the remark and do not investigate this problem further. Thus, you can call the approach *Sudakov resummation* [28], since it would be valid in QED.

This section on resummation is intended to give an introduction on this topic. We hope to have given the reader the motivation to resum perturbative coefficients to all orders and how this is possible, namely by factorization and exponentiation. We refer to section 4.1 to a more detailed discussion. In the end, a *re-expansion* of the exponential functions obtained by resummation will be used to predict the NNLO contributions that are calculated in the scope of this thesis.

3. Deep Inelastic Scattering

In deep inelastic scattering (DIS), generally a hadron is probed by a point-like lepton. As already mentioned in the introduction, DIS historically played a fundamental role in the formulation of the quark-parton model and thereby for QCD, as we will discuss in the following. In DIS experiments the partons were *seen* the first time [20]. In year 1990 Jerome I. Friedman, richard E. Taylor and Henry W. Kendall received the Nobel price for their DIS experiments at SLAC in the 1960th, where they provided the confirmation of the quark-parton model.

In our case the hadron is a proton and the lepton is either an electron or a positron. The sign of the charge does not matter because the cross sections are proportional to the square of the charge). The reaction can be depicted by

$$e^{+/-} + P \rightarrow e^{+/-} + X, \quad (3.1)$$

where X is any final state, containing also our jet observables. We will specify the final state later. This kind of experiments had the aim to analyze hadronic matter. Most information for the determination of PDF sets were extracted from DIS data. DIS experiments represent the idea of probing the unknown inner structure of an object (proton) with a sensor being much smaller (lepton).

The hadronic cross section for inclusive eP-scattering can be written as [29]

$$d\sigma = \frac{(4\pi\alpha)^2}{Q^4} \frac{4\pi M}{4\sqrt{(k \cdot p)^2 - m_e^2 M^2}} L_{\mu\nu} W^{\mu\nu} \frac{d^3 k'}{2E' (2\pi)^3}, \quad (3.2)$$

where m_e is the mass, k the momentum before and k' and E' the momentum and energy after the scattering of the electron, M and p are the mass and the momentum of the incoming proton and

$$Q^2 = -q^2 = (k - k')^2 \quad (3.3)$$

is the virtuality of the exchanged virtual photon in the one-photon-exchange approximation. α is the electromagnetic coupling constant and $L^{\mu\nu}$ and $H^{\mu\nu}$ are the lepton and the hadron tensor (for the detailed calculation of these expressions the interested reader may have a look at appendix C)

$$L^{\mu\nu} = 2 \left[k^\mu k'^\nu + k'^\mu k^\nu + \frac{q^2}{2} g^{\mu\nu} \right], \quad (3.4)$$

$$e^2 W^{\mu\nu} = \frac{1}{M^2} W_2(Q^2, \nu) \left[p^\mu - \frac{(p \cdot q)}{q^2} q^\mu \right] \left[p^\nu - \frac{(p \cdot q)}{q^2} q^\nu \right] + W_1(Q^2, \nu) \left[-g^{\mu\nu} + \frac{q^\mu q^\nu}{q^2} \right], \quad (3.5)$$

where $\nu = (p \cdot q)/M$ is the energy transferred in the rest frame of the proton and W_1 and W_2 are called structure functions. Here we omitted a third term in the hadron tensor containing a third structure function W_3 that represents processes where a Z_0 boson is exchanged instead of a photon. We want to leave this process aside at this stage. In the rest frame of the proton neglecting m_e one finds

$$\frac{d^2\sigma}{dQ^2 d\nu} = \frac{\pi\alpha^2}{4E^2 \sin^4\left(\frac{\theta}{2}\right)} \frac{1}{EE'} \left[W_2(Q^2, \nu) \cos^2\left(\frac{\theta}{2}\right) + 2W_1(Q^2, \nu) \sin^2\left(\frac{\theta}{2}\right) \right], \quad (3.6)$$

where θ is the angle between \vec{k} and \vec{k}' and E and E' the energy of the electron before and after scattering. Important to note is that the complete information about the inner structure of the proton is hidden in the functions W_1 and W_2 arbitrarily depending on Q^2 and ν . Now the theoretical physicist Bjorken comes into play. He predicted the following properties of the structure functions which today go under the name of *Bjorken Scaling* [30].

In the elastic limit

$$\nu \rightarrow \infty \quad \text{and} \quad Q^2 \rightarrow \infty \quad \text{with} \quad x \equiv \frac{Q^2}{2M\nu} \quad \text{fixed}, \quad (3.7)$$

the functions $W_1(Q^2, \nu)$ and $W_2(Q^2, \nu)$ scale to two functions $F_1(x)$ and $F_2(x)$

$$MW_1(Q^2, \nu) \rightarrow F_1(x), \quad (3.8)$$

$$\nu W_2(Q^2, \nu) \rightarrow F_2(x), \quad (3.9)$$

while $F_1(x)$ and $F_2(x)$ are finite and non-zero functions only depending on the fraction Q^2/ν [29].

In fact, the Bjorken scaling was verified approximately in experiment shortly after [31]. To understand the observation of Bjorken scaling the next section will explain the parton model. It was introduced by Feynman [32] in order to give an intuitive picture of what is going on. This is surely one of Feynman's outstanding qualities as a physicist.

3.1. The Parton Model

“Eine perfekte Formulierung des Problems ist schon die halbe Lösung.”

– David Hilbert

Feynman imagined a proton - or any other hadron - as an extended object consisting of point-like partons tied by a mutual interaction. At a given time the structure of the proton is given by the partonic state in that exact moment. How exactly such states look like and how they change in time we do not know, but let us assume it is there and the incoming electron is faced with these partonic conditions. The fundamental idea now is that we might be able to consider the inelastic electron-proton scattering to be an elastic scattering of the electron on one quasi-free parton, in the hope that we can calculate the latter process in some way. This assumption seems to be contradictory. We said there is an interaction between the partons inside the protons, so why would we

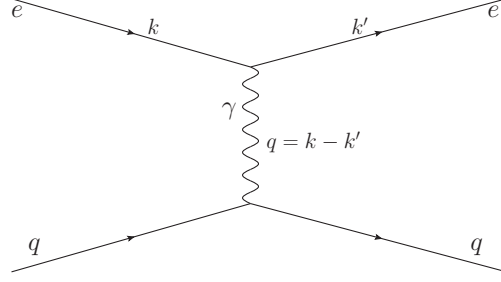


Figure 3.1.: Feynman diagram for elastic electron-parton scattering in the one-photon-exchange approximation.

claim the partons to be free during the scattering process? To answer that we specify our partons and demand their interaction with the electron to be electromagnetic, or in other words, the partons carry an electric charge. Additionally, we assume that the partonic interaction does not influence the electron itself, but exclusively the partons. What will the scattering look like under these assumptions, say in the center-of-mass frame of electron and proton, where both particles move in opposite direction with highly relativistic velocities?

Firstly, because of length contraction the proton is contracted in the beam direction. That shortens the time that it takes the electron to transit the proton. Secondly, there is time dilatation. The internal partonic interaction is delayed and the lifetime of the partonic state is lengthened. For the moving electron the proton metaphorically speaking appears to be frozen and it has only a small time window to interact via a photon exchange. In DIS the transferred momentum is high, so the exchanged particles must be highly virtual. This corresponds to a small lifetime of the photon. It has only time to interact with a single parton. And because the scattering happens on a much smaller timescale than the partonic interaction the parton can be regarded as a free particle and it carries a definite fraction $0 < \xi < 1$ of the proton momentum.

Overall, it is plausible that the scattering happens in the one-photon-exchange approximation depicted in figure 3.1. The inelastic electron-proton scattering is split into the elastic electron-parton scattering happening on a very small timescale and everything that might happen before or after it on much larger timescales that do not anymore interfere with the scattering quantum mechanically. One also speaks of short- and long-range effects in this context. Technically it means that the hadronic cross section factorizes and we are left with multiplying probabilities [20]

$$\sigma_{eP}(x, Q^2) = \sum_a \int_x^1 d\xi f_{a/P}(\xi) \sigma_{ea}(x/\xi, Q^2). \quad (3.10)$$

Here σ_{eP} is the cross section for the inelastic electron-proton scattering, σ_{ea} is the cross section for the elastic electron-parton scattering where there can be different types of partons denoted by a and $f_{a/P}$ are probability distributions giving the probability of finding a parton of type a with momentum fraction ξ inside the proton. Q^2 is the virtuality of the exchanged photon already defined in 3.3. It is always a positive quantity

because of the elasticity. The integral is carried out over all kinematically allowed values $\xi > Q^2/2(p \cdot q) = x$, where we identified the Bjorken variable x as the lower bound of ξ . We see that Q^2 and ν are not free parameters just because of the kinematics in the parton model. With Bjorken scaling in mind we get the impression that we are on the right way. So let us specify the partons.

In the quark-parton model we assume the partons to be quarks and gluons and the partonic interaction is the strong interaction. Of course this step is motivated by hadron spectroscopy, yet it is also a reasonable step concerning the basic assumptions of the parton model. First of all, the elastic electron-parton scattering can be seen as the LO contribution of electron-quark scattering. The gluon does not couple directly to the electron nor the photon, so the electron is indeed not influenced by the partonic interaction. Additionally, we have asymptotic freedom in QCD. This validates the assumption of quasi-free partons. Generally, we see that the parton model is nothing else as the heuristic explanation of factorization properties of QCD already mentioned in section 2.4. And what is most important is that the separated hard scattering part is actually calculable by the methods of pQCD (see section 2.1).

The cross section for elastic electron-quark scattering in LO results by calculating the Feynman amplitude of the diagram in figure 3.1 and expressing the two-body phase space in terms of the variables Q^2 and ν [29]

$$\frac{d^2\sigma_{ea}}{dQ^2 d\nu} = \frac{\pi\alpha^2}{4E^2 \sin^4\left(\frac{\theta}{2}\right)} \frac{1}{EE'} \left(q_a^2 \cos^2\left(\frac{\theta}{2}\right) + q_a^2 \frac{Q^2}{4m_a^2} 2 \sin^2\left(\frac{\theta}{2}\right) \right) \times \delta\left(\nu - \frac{Q^2}{2m_a}\right), \quad (3.11)$$

where q_a is the charge and m_a the mass of parton a . Equation 3.10 tells us that for getting the hadronic cross section we have to sum over a , which is a sum over all quark flavors and the gluon in the quark-parton model and integrate over all momentum fractions weighted by the probability distribution $f_{a/P}(\xi)$. With setting $m_a = xM$ the fraction ξ is just the Bjorken variable x and it runs from 0 to 1. Hence one finds

$$\frac{d^2\sigma}{dQ^2 d\nu} = \frac{\pi\alpha^2}{4E^2 \sin^4\left(\frac{\theta}{2}\right)} \frac{1}{EE'} \sum_a \int_0^1 dx f_{a/P}(x) \times \left(q_a^2 \cos^2\left(\frac{\theta}{2}\right) + q_a^2 \frac{Q^2}{4M^2 x^2} 2 \sin^2\left(\frac{\theta}{2}\right) \right) \delta\left(\nu - \frac{Q^2}{2Mx}\right). \quad (3.12)$$

Comparing to 3.6 yields

$$W_2(\nu, Q^2) = \sum_a \int_0^1 dx f_{a/P}(x) q_a^2 \delta\left(\nu - \frac{Q^2}{2Mx}\right) = \frac{1}{\nu} \sum_a q_a^2 x f_{a/P}(x), \quad (3.13)$$

$$W_1(\nu, Q^2) = \sum_a \int_0^1 dx f_{a/P}(x) q_a^2 \frac{Q^2}{4M^2 x^2} \delta\left(\nu - \frac{Q^2}{2Mx}\right) = \frac{1}{M} \sum_a \frac{q_a^2}{2} f_{a/P}(x). \quad (3.14)$$

The Bjorken scaling becomes manifest. By defining new structure functions

$$F_2(x) \equiv \sum_a q_a^2 x f_{a/P}(x) \quad \text{and} \quad F_1(x) \equiv \sum_a \frac{q_a^2}{2} f_{a/P}(x), \quad (3.15)$$

we obtain the Callan-Gross relation [33]

$$2xF_1(x) = F_2(x). \quad (3.16)$$

The Callan-Gross relation is a consequence of the assumption that the quarks are spin-1/2 particles. It is experimentally well satisfied in DIS regions of the phase space. This is a further hint that identifying the partons with quarks was a good idea. So let us take this idea more seriously. Up to now, we have the unknown functions $f_{a/P}(x)$ in our calculation, which cannot be calculated, but can only be taken from experiment. The good thing is that these functions are universal in a way that they do not depend on the actual hard scattering process, but only on the structure of the proton.

Using the quantum numbers of the quarks we expect from QCD and recalling the interpretation of $f_{a/P}(x)$, being the the probability to find a parton of type a with momentum fraction x , we should be able to write the structure function as

$$F_2(x) = x \left[\frac{4}{9} \left(u(x) + \bar{u}(x) + c(x) + \bar{c}(x) + t(x) + \bar{t}(x) \right) + \frac{1}{9} \left(d(x) + \bar{d}(x) + s(x) + \bar{s}(x) + b(x) + \bar{b}(x) \right) \right], \quad (3.17)$$

where we assigned probability distributions for each flavor of quarks and antiquarks respectively. From the quantum numbers of the proton different sum rules emerge. The proton has no charm, strangeness, topness or bottomness. Translated into the quark-parton model we therefore demand

$$\int_0^1 dx [c(x) - \bar{c}(x)] = [s(x) - \bar{s}(x)] = [t(x) - \bar{t}(x)] = [b(x) - \bar{b}(x)] = 0. \quad (3.18)$$

From the electrical charge of the proton one gets

$$\int_0^1 dx [u(x) - \bar{u}(x)] = 2 \quad \text{and} \quad \int_0^1 dx [d(x) - \bar{d}(x)] = 1. \quad (3.19)$$

Both sum rules were tested experimentally. They symbolize the picture of the proton being built out of two up-quarks and one down-quark as constituent quarks, while all other flavor are just present as sea quarks arising through the mutual interaction. Important is that they are not zero, even though the probability to find the heavy flavors is suppressed. In our calculation the top-quark contributions are neglected and we calculated with 5 active flavors. Perhaps the most surprising sum rules arises from summing the total momentum carried by the quarks

$$\int_0^1 dx x \left[u(x) + \bar{u}(x) + d(x) + \bar{d}(x) + c(x) + \bar{c}(x) + s(x) + \bar{s}(x) + t(x) + \bar{t}(x) + b(x) + \bar{b}(x) \right] = 1 - \varepsilon, \quad (3.20)$$

where ε accounts for all momentum carried by uncharged objects, i.e., by gluons. It was found that nearly 50% of the proton momentum is carried by gluons.

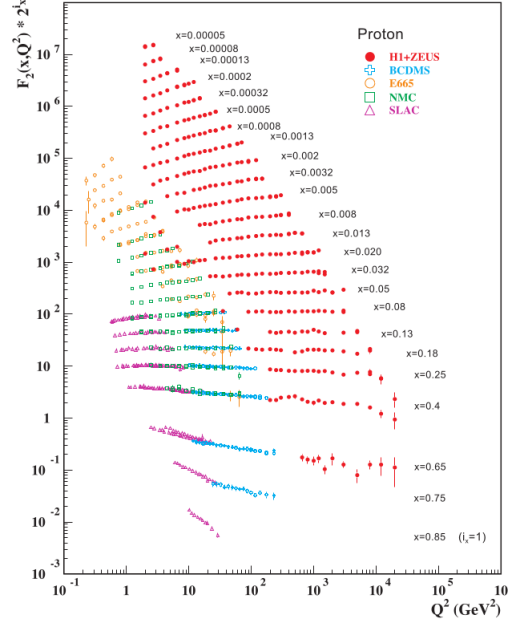


Figure 3.2.: Proton structure function measured by ep-scattering (H1, Zeus, SLAC) and by muon scattering on a fixed target (BCDMS, E665, NMC). The plot is taken from [10], where also the data references are given.

While this story was a long one, it is not the full story. Luckily it is not, because otherwise this work would be useless. The Bjorken scaling is an approximation and refers to the first order approximation in perturbation theory. If you look more closely (see figure 3.2) you see scaling violation. The structure functions do depend only on x up to a certain degree of accuracy (nearly 10% [34]), but beyond that accuracy they become functions of x and Q^2 each. To understand scaling violation perturbative calculations had to be extended to NLO in α_s . In section 2.1 it was explained that this means to deal with additional emission of gluons and virtual corrections from loop diagrams. Additionally, the electron-proton scattering becomes sensitive to gluon initiated processes by considering the splitting of the gluon into a quark-antiquark pair. This will be the topic of the next sections in the context of jet production, where beside the parton distribution functions discussed here also fragmentation functions in the final state have to be discussed.

3.2. LO cross section

In this section we demonstrate the calculation of the hadronic LO cross section $d\sigma_{eP}$ for the production of two jets through an electron-proton scattering event, characterized by the reaction

$$e(k) + P(p) \rightarrow e(k') + \text{Jet}_1(p_{T_1}, \eta_1) + \text{Jet}_2(p_{T_2}, \eta_2) + X. \quad (3.21)$$

Here and in the following section we will follow reference [14], because the program JetViP is based on this work. The outgoing jets are described by their transverse momentum p_T and rapidities η . As explained in the previous chapter, the hadronic cross section is obtained by the convolution of the partonic cross section $d\sigma_{ea}$ with the parton distribution functions of the proton $f_{a/P}(x)$. Hence, we can write

$$d\sigma_H = \sum_a \int dx f_{a/P}(x) d\sigma_{ea}(xs_H), \quad (3.22)$$

where $s_H = (p + k)^2$ is the hadronic center-of-mass energy and x is the momentum fraction of the proton momentum carried by the parton. The partonic cross section is given as usual by

$$d\sigma_{ea} = \frac{1}{2xs_H} |\mathcal{M}|^2 d\text{PS}^{(n+1)}, \quad (3.23)$$

thus the product of the matrix elements \mathcal{M} squared and the phase space $d\text{PS}^{(n+1)}$ of the partonic subprocess with n final state particles ($n = 2$ in leading order) and the electron, divided by the flux factor $2xs_H$. Both the matrix elements and the phase space factorize into a leptonic and a hadronic part. By using QED Feynman rules in the one-photon exchange approximation we find

$$|\mathcal{M}|^2 = \frac{1}{2xs_H} \frac{4\pi\alpha}{Q^4} L_{\mu\nu} H^{\mu\nu}, \quad (3.24)$$

where α is the QED coupling constant and the hadron tensor $H^{\mu\nu}$ and lepton tensor

$$L_{\mu\nu} = 4 \left(k_\mu k'_\nu - k'_\mu k_\nu - g_{\mu\nu} (k \cdot k') \right) \quad (3.25)$$

were introduced. Accordingly, the phase space factorizes into the leptonic part dL and the partonic part $d\text{PS}^{(n)}$. We find

$$d\text{PS}^{(n+1)} = dL d\text{PS}^{(n)} \quad \text{with} \quad dL = \frac{Q^2}{16\pi^2} \frac{d\phi dy dQ^2}{Q^2}. \quad (3.26)$$

The leptonic phase space is expressed by the polar angle of the outgoing electron ϕ , the virtuality of the photon Q and the variable $y \equiv (p \cdot q)/(p \cdot k)$. Integrating out the polar angle gives

$$\frac{1}{4Q^2} \int \frac{d\phi}{2\pi} L_{\mu\nu} H^{\mu\nu} = \frac{1 + (1 - y)^2}{2y^2} H + \frac{4(1 - y) + 1 + (1 - y)^2}{2y^2} \bar{H}, \quad (3.27)$$

where we defined

$$H = -g^{\mu\nu} H_{\mu\nu} \quad \text{and} \quad \bar{H} = \frac{4Q^2}{(s_H y)^2} p^\mu p^\nu H_{\mu\nu}. \quad (3.28)$$

Introducing the functions

$$f_{\gamma/e}^T(y) = \frac{\alpha}{2\pi} \frac{1 + (1 - y)^2}{y} \frac{1}{Q^2}, \quad (3.29)$$

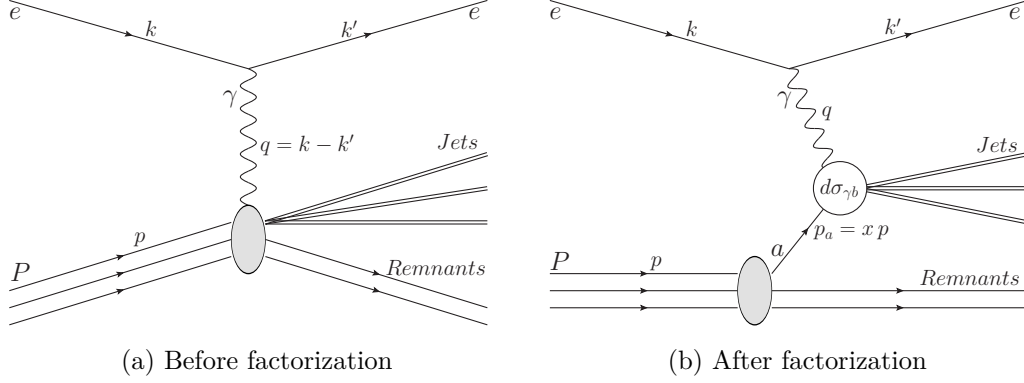


Figure 3.3.: Schematic diagrams representing the DIS process and the production of jets.

$$f_{\gamma/e}^L(y) = \frac{\alpha}{2\pi} \frac{4(1-y) + 1 + (1-y)^2}{y} \frac{1}{Q^2}, \quad (3.30)$$

where T and L denote transverse and longitudinal polarization of the photon, we find for the hadronic cross section

$$d\sigma_H = d\sigma_H^T + d\sigma_H^L, \quad (3.31)$$

with

$$d\sigma_H^T(s_H) = \sum_a \int dx \int dy f_{a/P}(x) f_{\gamma/e}^T(y) d\sigma_{\gamma a}^T(xys_H), \quad (3.32)$$

$$d\sigma_H^L(s_H) = \sum_a \int dx \int dy f_{a/P}(x) f_{\gamma/e}^L(y) d\sigma_{\gamma a}^L(xys_H) \frac{4Q^2}{(s_H y)^2}. \quad (3.33)$$

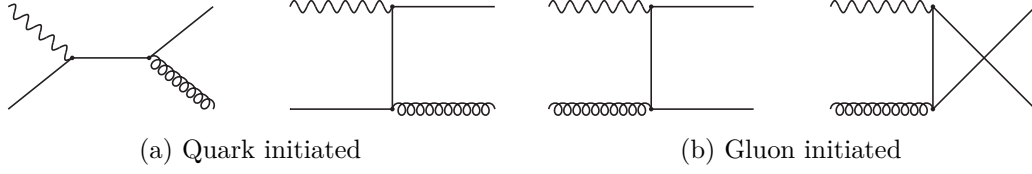
In the last step we defined the cross section for photon-parton scattering

$$d\sigma_{\gamma a}^{T/L}(xys_H) = \frac{1}{2xys_H} H_{\gamma a}^{T/L} d\text{PS}^{(n)}. \quad (3.34)$$

We see that by using the factorization into the leptonic and the hadronic part, we are left with calculating matrix elements for the scattering of a parton with a virtual photon, producing a partonic final state with n particles. This phenomena is illustrated in figure 3.3.

$d\sigma_{\gamma a}$ can now be calculated by pQCD. In figure 3.4 you can see the four generic Feynman diagrams contributing in LO. The fermion line represents a quark or an antiquark of any flavor. In the initial state we sum over the color states and the spins, while in the final state we take the average. We can group the processes into quark initiated (or anti-quark initiated) reactions defined by $\gamma^* q \rightarrow qg$ and gluon initiated reactions $\gamma^* g \rightarrow q\bar{q}$. For the matrix elements one finds

$$H_B^T(\gamma^* q \rightarrow qg) = (16\pi^2 \alpha \alpha_s) Q_b^2 2C_F \left(-\frac{t}{s} - \frac{s}{t} + 2Q^2 \frac{u}{st} \right), \quad (3.35)$$

Figure 3.4.: LO Feynman diagrams contributing to $d\sigma_{\gamma a}$.

$$H_B^T(\gamma^* g \rightarrow q\bar{q}) = (16\pi^2 \alpha \alpha_s) Q_b^2 \left(\frac{t}{u} + \frac{u}{t} + 2Q^2 \frac{s}{ut} \right), \quad (3.36)$$

$$H_B^L(\gamma^* q \rightarrow qg) = (16\pi^2 \alpha \alpha_s) Q_b^2 2C_F \left(-\frac{u}{2} \right), \quad (3.37)$$

$$H_B^L(\gamma^* g \rightarrow q\bar{q}) = (16\pi^2 \alpha \alpha_s) Q_b^2 \left(s \right), \quad (3.38)$$

expressed with the help of the Mandelstam variables

$$\begin{aligned} s &= (q + p_a)^2 = (p_1 + p_2)^2, \\ t &= (q - p_1)^2 = (p_a - p_2)^2, \\ u &= (q - p_2)^2 = (p_a - p_1)^2. \end{aligned} \quad (3.39)$$

Here q is the momentum of the virtual photon, p_a is the momentum of the incoming parton a and p_1 and p_2 are the momenta of the final state partons. Q_b is the electric charge of the quark or anti-quark taking part in the hard scattering. The two-body final state phase space simply reads

$$d\text{PS}^{(2)} = \frac{1}{s + Q^2} \frac{dt}{8\pi}. \quad (3.40)$$

The integration over the phase space can be carried out together with the integration over x and y in formula 3.32 and 3.33 by making use of the kinematics. If we define the center-of mass energy of the photon-proton subsystem

$$W^2 \equiv (q + p), \quad (3.41)$$

we find from momentum conservation

$$W = p_T (e^{-\eta_1} + e^{-\eta_2}), \quad (3.42)$$

$$y = \frac{W^2 + Q^2}{s_H}, \quad (3.43)$$

$$x = 1 + \frac{2W}{W^2 + Q^2} p_T (\sinh \eta_1 + \sinh \eta_2). \quad (3.44)$$

Hence, the integrations can be expressed by the experimental observables as

$$d\text{PS}^{(2)} dx dy = \frac{W}{W^2 + Q^2} \frac{p_T}{2s_H} \frac{dp_T}{(2\pi)^2} d\eta_1 d\eta_2. \quad (3.45)$$

3.3. NLO cross section

In next-to-leading order we are faced with virtual and real corrections. In both cases we have to remove divergences properly, so the integrations have to be done in D dimensions. Additionally, life becomes harder, because the amount of Feynman diagrams that have to be considered increases factorially with the order of perturbation theory. We start with discussing the virtual corrections.

Virtual corrections arise from loop diagrams that have to be multiplied with corresponding Born diagrams. In NLO we have one-loop diagrams for quark-initiated and gluon-initiated processes. The generic diagrams that play a role here are listed in figure 3.5. The integration over undefined loop momenta as well as the phase space integration have to be done dimensionally regularized. Apart from that, the Born contributions have to be calculated in D dimensions, even if we know that they are finite in 4 dimensions. The reason for that is that they contain terms proportional to ε , giving finite contributions when they are multiplied with terms from loop-diagrams containing a single pole in ε . The Born matrix element from equation 3.35, for instance, becomes

$$H_B^T(\gamma^* q \rightarrow qg) = (16\pi^2 \alpha \alpha_s) Q_b^2 2C_F \left[(1 - \varepsilon) \left(-\frac{t}{s} - \frac{s}{t} \right) + 2Q^2 \frac{u}{st} - 2\varepsilon \right]. \quad (3.46)$$

The other Born matrix elements in D dimensions can be found in [14] for transverse polarization. The two-body final state phase space can be written as

$$d\text{PS}^{(2)} = \frac{1}{\Gamma(1 - \varepsilon)} \left(\frac{4\pi}{stu} \right)^\varepsilon (s + Q^2)^{-1+2\varepsilon} \frac{dt}{8\pi}. \quad (3.47)$$

The full virtual corrections are of the form

$$H_V^{T/L}(\gamma^* q \rightarrow qg) = 16\pi^2 \frac{\alpha \alpha_s}{2\pi} 2(1 - \varepsilon) \left(\frac{4\pi \mu_R^2}{s} \right)^\varepsilon \frac{\Gamma(1 - \varepsilon)}{\Gamma(1 - 2\varepsilon)} \left[C_F^2 E_1^{T/L} - \frac{1}{2} N_C C_F E_2^{T/L} + \frac{1}{\varepsilon} \left(\frac{1}{3} n_f - \frac{11}{6} N_C \right) C_F T_{\gamma q}^{T/L} \right], \quad (3.48)$$

$$H_V^{T/L}(\gamma^* g \rightarrow q\bar{q}) = 16\pi^2 \frac{\alpha \alpha_s}{2\pi} \left(\frac{4\pi \mu_R^2}{s} \right)^\varepsilon \frac{\Gamma(1 - \varepsilon)}{\Gamma(1 - 2\varepsilon)} \left[C_F E_3^{T/L} - \frac{1}{2} N_C E_4^{T/L} + \frac{1}{\varepsilon} \left(\frac{1}{3} n_f - \frac{11}{6} N_C \right) T_{\gamma g}^{T/L} \right], \quad (3.49)$$

where the functions $E_1^{T/L}$, $E_2^{T/L}$, $E_3^{T/L}$, $E_4^{T/L}$ are lengthy functions depending on the Mandelstam variables. For the case of transverse polarization of the virtual photon, they can be found in [14] to $\mathcal{O}(\varepsilon)$. After renormalization they still contain single and double poles in ε , but we know from the KLN theorem that they will cancel against the poles from the real corrections. The functions $T_{\gamma q}^{T/L}$ and $T_{\gamma g}^{T/L}$ represent the kinetic part of the Born matrix elements and depend on the Mandelstam variables as well. For the quark initiated process with transverse polarization, for instance, we can read off from equation 3.46

$$T_{\gamma q}^T = (1 - \varepsilon) \left(-\frac{t}{s} - \frac{s}{t} \right) + 2Q^2 \frac{u}{st} - 2\varepsilon. \quad (3.50)$$

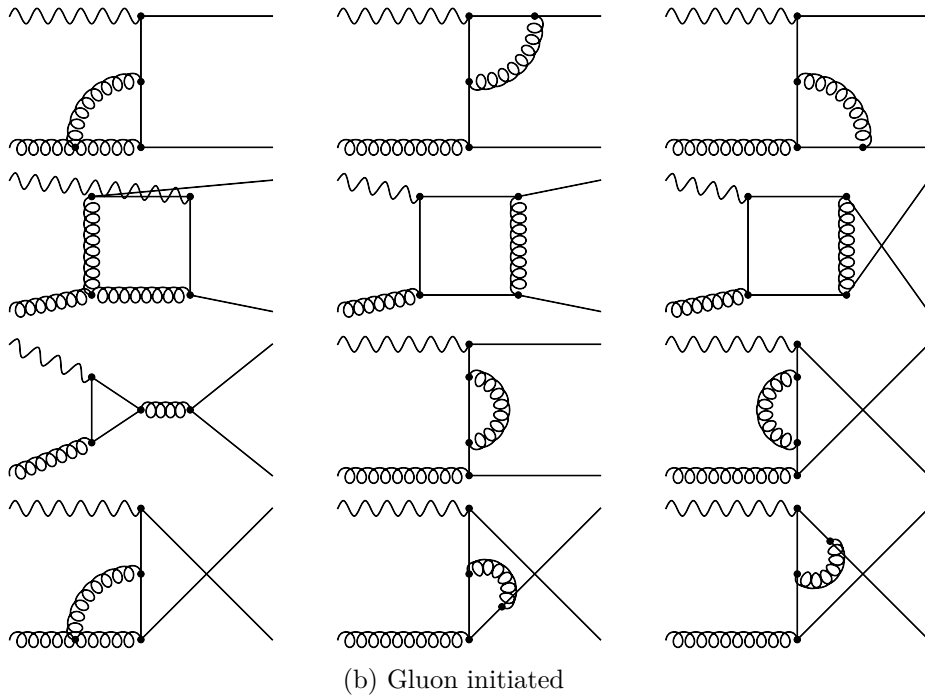
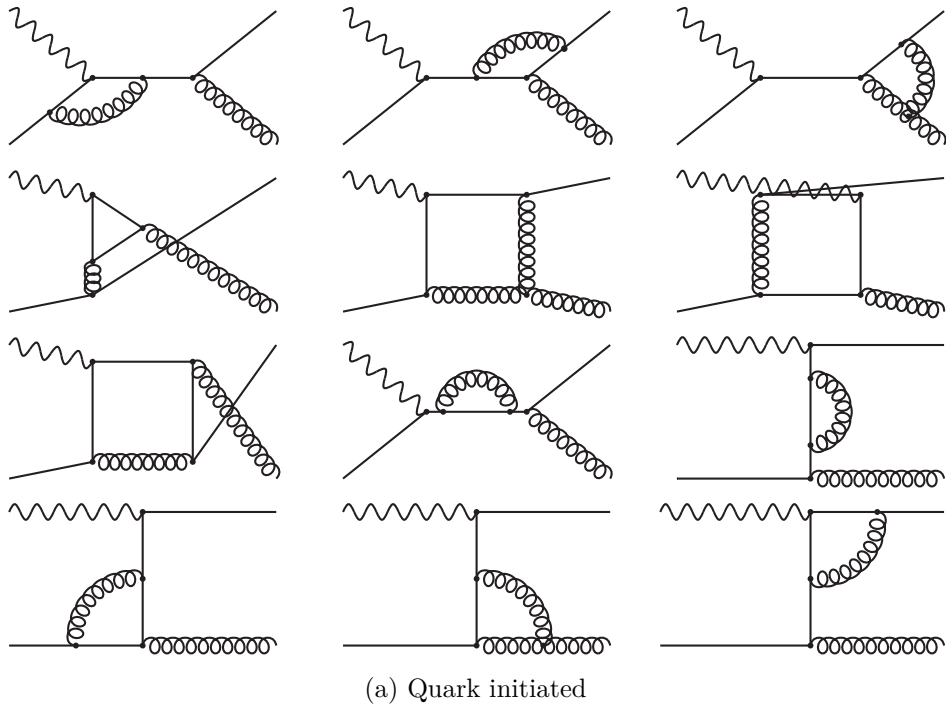


Figure 3.5.: One-loop Feynman diagrams contributing to NLO virtual corrections.

After the poles have been removed, the limes $\varepsilon \rightarrow 0$ can be taken and all finite terms contribute to the virtual corrections.

For the real corrections we consider diagrams with one additional parton in the final state. The generic Feynman diagrams that have to be considered are listed in figure 3.6. We can summarize the processes into four types of reactions, whose matrix elements we call

$$H_{R1} = H_R(\gamma^* q \rightarrow qgg), \quad (3.51)$$

$$H_{R2} = H_R(\gamma^* q \rightarrow qq'\bar{q}'), \quad (3.52)$$

$$H_{R3} = H_R(\gamma^* q \rightarrow qq\bar{q}), \quad (3.53)$$

$$H_{R4} = H_R(\gamma^* g \rightarrow q\bar{q}g). \quad (3.54)$$

We do not distinguish between transverse and longitudinal polarization, because up to the Born contribution that always factorizes out in real corrections, the formulas are the same in both cases. We see that only H_{R4} belongs to the gluon initiated process. The primed quark and anti-quark in H_{R2} can have a different flavor than the incoming quark or anti-quark.

As we learned in section 2.3, divergences will arise by integrating the corresponding matrix elements over the three-body final-state phase space. By means of phase space slicing the contributions are separated into finite and divergent parts. The finite parts can be safely integrated over

$$d\text{PS}^{(3)} = \frac{d^{D-1}p_1}{2E_1(2\pi)^{D-1}} \frac{d^{D-1}p_2}{2E_2(2\pi)^{D-1}} \frac{d^{D-1}p_3}{2E_3(2\pi)^{D-1}} (2\pi)^D \delta^D(q + p_a - p_1 - p_2 - p_3) \quad (3.55)$$

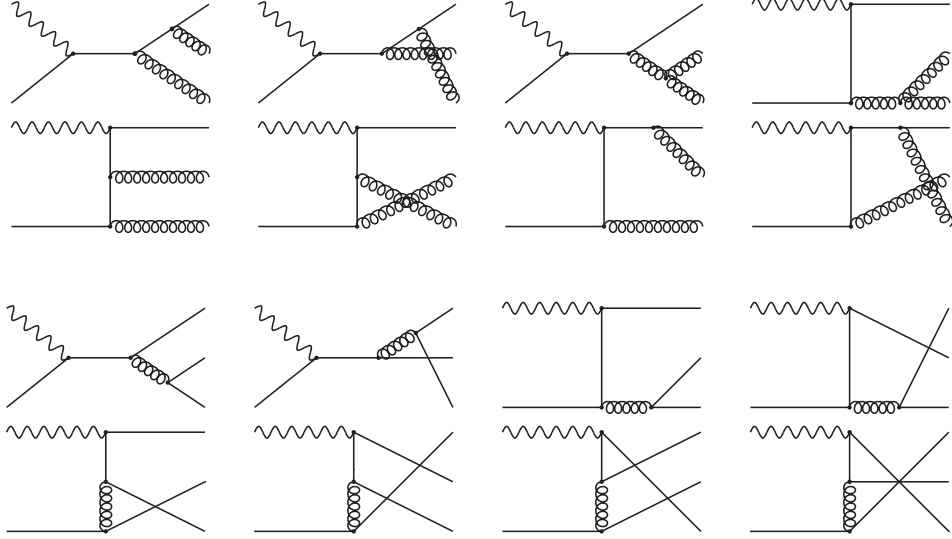
in $D = 4$ dimensions. Here we denoted the energy and momentum of the i -th particle in the final state with E_i and p_i . For the singular parts this is of course not true. We have to bring the expressions in a form comparable to the virtual corrections to be able to cancel the mass singularities. To do that, it is convenient to distinguish between initial- and final-state corrections. In section 2.3.1 we already saw how to separate $d\text{PS}^{(3)}$ into the two-body phase space $d\text{PS}^{(2)}$ and a remainder $d\text{PS}^{(r)}$ (see equation 2.62) for initial-state singularities caused by radiation from the incoming massless parton. Taking the limit $z_1 \rightarrow 0$ of the matrix elements and integrate analytically over $d\text{PS}^{(r)}$, one obtains

$$\int d\text{PS}^{(r)} H_{Ri}^I = \int_{\eta}^1 \frac{dz}{z} 8\pi \left(\frac{4\pi\mu_F^2}{s} \right)^{\varepsilon} \frac{\Gamma(1-\varepsilon)}{\Gamma(1-2\varepsilon)} (1-\varepsilon) I_i + \mathcal{O}(\varepsilon), \quad (3.56)$$

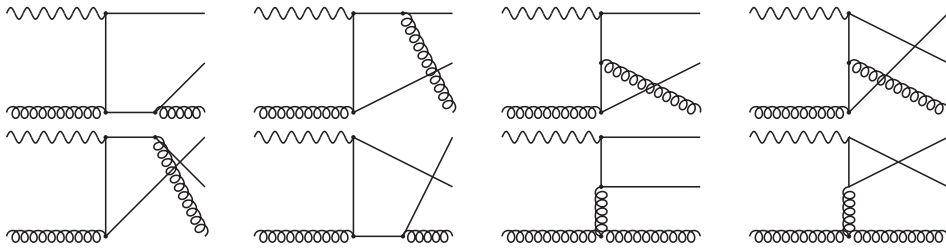
where the integration over z defined by equation 2.54 remains. z measures the fraction of the momentum p_a entering the hard scattering subprocess after the parton a radiated another soft parton.¹ The lower bound of the integration is given by $\eta = xz$. The actual information is contained by the functions I_i . They are given in reference [14] and are functions of the Mandelstam variables, the phase space slicing parameter y_c and the integration variable z . They contain terms proportional to

$$\delta(1-z), \quad \mathcal{D}_0 = \left[\frac{1}{1-z} \right]_+ \quad \text{and} \quad \mathcal{D}_1 = \left[\frac{\ln(1-z)}{1-z} \right]_+, \quad (3.57)$$

¹In our notation the soft momentum in the final state is p_1 , while p_2 and p_3 are the final state parton momenta of the hard scattering subprocess.



(a) Quark initiated



(b) Gluon initiated

Figure 3.6.: Feynman diagrams contributing to NLO real corrections. Depending on the choice of handling the gluon polarization sums, one might need additional diagrams including ghosts in the final state, to remove longitudinal modes of the external gluons in the two diagrams at the right-hand side of the upper line.

as well as single and double poles in ε . Poles appearing in terms with $\delta(1-z)$ will cancel the mass singularities from virtual corrections. Nevertheless, some collinear divergences remain. They appear together with the splitting functions introduced in 2.77, 2.78, 2.79 and 2.80, and are removed by a re-definition of the parton distribution functions of the proton in NLO that by this procedure become factorization scale dependent. I_1 , for instance, has the term

$$I_1 = \alpha \alpha_s^2 Q_b^2 C_F T_{\gamma q} \left(C_F \left[-\frac{1}{\varepsilon} \frac{1}{C_F} P_{q \leftarrow q} + \dots \right] + \dots \right), \quad (3.58)$$

The re-definition of the PDFs is done by transition functions $\Gamma_{a \leftarrow b}(z, \mu_F)$ that are defined by the demand that the collinear singularities will be removed.² The justification for that is that the collinear divergences, that remain after cancellation between real and virtual corrections, are universal in a sense, that they always appear when there is an incoming proton initiating the reaction. The redefinition can be written as [14]

$$\bar{f}_{a/P}(\eta, \mu_F) = \int_{\eta}^1 \frac{dz}{z} \left(\delta_{ab} \delta(1-z) + \frac{\alpha_s}{2\pi} \Gamma_{a \leftarrow b}(z, \mu_F) \right) f_{b/P} \left(\frac{\eta}{z} \right), \quad (3.59)$$

where $\bar{f}_{a/P}(\eta, \mu_F)$ is the renormalized NLO PDF and $f_{b/P}$ is the LO PDF. Since the argument of that PDF may not be bigger than one, we can retain that z must be bigger than η . This is the reason why the lower bound of the z -integration in equation 3.56 is not zero, but η . Expressions for $\Gamma_{a \leftarrow b}$ can be found in [14] for NLO.

The final state corrections are obtained by a similar procedure. Just the separation of the phase space works a bit different. Final state singularities appear, when the variable

$$r = \frac{2 p_2 \cdot p_3}{2 q \cdot p_a - Q^2} \quad (3.60)$$

goes to 0, i.e., when the propagator of the massless parton in the finale state before splitting becomes on-shell. In the limit $r \rightarrow 0$ we find $d\text{PS}^{(3)} = d\text{PS}^{(2)} d\text{PS}^{(r)}$ with

$$d\text{PS}^{(r)} = \frac{\Gamma(1-\varepsilon)}{4^\varepsilon \pi \Gamma(1-2\varepsilon)} d\phi \sin^{-2\varepsilon} \phi \left(\frac{4\pi}{s} \right)^\varepsilon \frac{s}{16\pi^2} dr r^{-\varepsilon} \left[1 - \frac{r}{1-z} \right]^{-\varepsilon} db \frac{1}{[b(1-b)]^\varepsilon}, \quad (3.61)$$

where is used $b \equiv (1 - \cos \theta)/2$, θ being the angle between p_3 and p_a . Integrating the corresponding approximated matrix elements in the same limit over the regions $b \in [0, 1]$, $\phi \in [0, \pi]$ and $r \in [0, \min(-u/(s+Q^2), y_c) \equiv y_I]$ gives the final state corrections in the form

$$\int d\text{PS}^{(r)} H_{Ri}^F = 8\pi \left(\frac{4\pi\mu_F^2}{s} \right)^\varepsilon \frac{\Gamma(1-\varepsilon)}{\Gamma(1-2\varepsilon)} (1-\varepsilon) F_i + \mathcal{O}(\varepsilon). \quad (3.62)$$

²Here, it has to be defined how much finite parts are put into the PDFs while absorbing collinear divergences. This is done by the *factorization scheme*. Most commonly used is the $\overline{\text{MS}}$ scheme, defined analogously to the $\overline{\text{MS}}$ renormalization scheme. Alternatively, there is the DIS scheme which demands that the DIS structure function F_2 gets no higher order corrections, motivated by the fact that it is directly measurable in experiment.

The functions F_i can be found in reference [14]. As the initial state corrections I_i they depend on the Mandelstam variables and the phase space slicing parameter. Mass singularities are canceled accordingly by the KLN theorem. If there is a real gluon in the final state, it is necessary to do partial fractioning to separate simultaneously arising singularities.

3.4. The program JetViP

The calculations described in the previous two sections are implemented in a Fortran code. The program JetViP (short for *Jets with Virtual Photons*) [35] is able to compute inclusive single- and dijet cross sections in eP - and $e\gamma$ -scattering [36, 37]. There is a public download of this code available, but it is slightly different comparing to the code that was provided by the supervisor of this thesis, which was used in this work. Already some differences in the input format could be noticed. Anyway, the source code was changed, so there is no guarantee that there is comparability between both versions.

The aim of this work was to extend the existing full NLO calculation with NNLO contributions. But before we added the NNLO contributions we wanted to be sure that the results of the NLO calculation are consistent with results from other groups. So we reproduced the H1 analysis of DIS data in section 3.5. In the following the basic computation steps of the program are explained, where we will restrict ourselves to the case of eP -scattering.

JetViP makes use of a Monte Carlo integration to evaluate two functions. The function **twobody** contains all partonic processes with two particles in the final state, i.e., the LO tree-level processes and the virtual, initial state and final state corrections when NLO accuracy is desired. The function **threebody** contains all partonic processes with three particles in the final state and is evaluated for the NLO calculation. These functions are integrated by the **Vegas** routine [38], while the full event record is available in a subroutine called **user**. There it is possible to analyze the events and fill histograms with a user defined binning. Additionally, this subroutine is a good place to implement cuts on the final-state phase space, what might be necessary because of detector properties, for instance.

JetViP comes with a steering file that lets the user decide, if he wants to calculate in LO or NLO. Further parameters that are defined in the steering file are the renormalization μ_R as linear functions of Q^2 and p_T^2 , the beam energies E_e and E_P , the number of flavors n_f , bounds on the phase-space integration, the number of points evaluated by the Vegas routine and the number of its iterations, and the phase space slicing parameter y_c .³ For convoluting the partonic functions **twobody** and **threebody** with parton distribution functions to the hadronic cross section, the PDFs are included by a standard interface. Originally this interface was **PDFLIB** [39], but we changed it for the proton PDFs to the **LHAPDF** interface [40], which is more modern and provides all important proton PDFs. Because of technical reasons not the newest but the LHAPDF version 5.9.1 was used. JetViP offers two different **user** subroutines, each for two different kinds of jet algorithms. In our case we choose **user-kt** suitable for

³The factorization scale μ_F was changed directly in the code.

kT-clustering jet algorithms instead of **user–cone** for cone-type jet algorithms. The need for such an algorithm is explained in the following section.

3.4.1. The jet algorithm

To compare experimental results and theoretical predictions you have to define what you measure in one case and what you calculate in the other. In experiment we observe so-called jets. It was first of all in e^+e^- -annihilation [41], where in the initial state you do not even have a single strongly interacting particle, but a huge amount of hadronic particles moving nearly in the same direction were measured. The idea was to collect these particles to a single observable, namely a jet. The counterpart to a jet that comes out of our theoretical calculation is a parton in the final state. Because of showering and hadronization to colorless particles a parton can generate a jet and the total momentum of all particles attached to the jet is the initial parton momentum.

With this in mind, the task arises to accurately define what we call a jet, and both sides, experiment and theory, must stick to the same definition. Therefore, we need an appropriate jet definition and an algorithm that builds a jet out of the final state particles. In reference [1] the *k_T-clustering algorithm* was used [41]. Besides the necessary property of being infrared and collinear safe to all order of pQCD it has two advantages, especially associated to deep inelastic scattering. It allows the factorization of universal initial-state collinear singularities, which are not present in e^+e^- -annihilation where there is no hadronic matter in the initial state, and it minimizes contamination from the proton remnant.

Technically, the algorithm is an iterative method that assigns a relative distance-measure d_{ij} to all particles by

$$d_{ij} = \min \left(p_{T_i}^{2a}, p_{T_j}^{2a} \right) \frac{\Delta_{ij}^2}{R^2}, \quad (3.63)$$

$$d_i = p_{T_i}^{2a}, \quad (3.64)$$

where

$$\Delta_{ij}^2 = (\phi_i - \phi_j)^2 + (\eta_i - \eta_j)^2. \quad (3.65)$$

Here ϕ_i is the azimuthal angle and η_i the pseudorapidity of particle i , so Δ_{ij} measures the distance of two particles. R is a dimensionless parameter in correspondence to a second kind of jet algorithms called *jet cone-algorithms* [42]. In case of k_t -clustering it is $a = 1$, so the softest particles are recombined first. An alternative is the anti- k_t -clustering with $a = -1$ to start the recombination with the hardest particles.

Afterwards the algorithm performs the following steps:

1. Find the smallest d_{ij} and d_i and label it d_{min} .
2. If d_{min} is d_{ij} recombine particle i and j to a new pseudo-particle and add it to the list.
If d_{min} is d_i define particle i as a jet and remove it from the list.
3. Recalculate all d_{ij} and go back to step 1 as long as only jets remain.

The recombination of the pseudo-particles for massless particles is given by

$$p_{T,ij} = p_{T_i} + p_{T_j} , \quad (3.66)$$

$$\phi_{i,j} = \frac{(\phi_i p_{T_i} + \phi_j p_{T_j})}{p_{T,ij}} , \quad (3.67)$$

$$\eta_{i,j} = \frac{(\eta_i p_{T_i} + \eta_j p_{T_j})}{p_{T,ij}} . \quad (3.68)$$

Important to note is that the k_T -clustering is only Lorentz invariant under longitudinal boosts along the collision axis, so you have to be careful to use the momenta in the same frame or at least in frames that are connected by a longitudinal boost. In reference [1] the jets were constructed in the Breit frame while the program JetVip produces the final state partons in the center-of-mass system of the virtual photon and the incoming parton. As it will be explained in chapter 3.5.1, you indeed can get from one to another by a boost along the beam axis, so in principle there was no problem to stick to the center-of-mass system and construct the jets there. Yet, the program had to be changed anyway in order to use the k_T -clustering instead of a cone-algorithm and the Fortran code we used, presented in [41] in its edition of year 2000, offered a boost routine from the center-of-mass system to the Breit frame before letting the jet algorithm do its job, which was then implemented without much effort. Additionally, it was a good test to see if we used the algorithm correctly and to check if we get the same results in both frames.

In our NLO calculation we have two-body and three-body contributions. Showering and hadronization is left out because there is no program available offering these processes on full NLO basis. Pythia [43] for example calculates mainly in LO, despite the fact that it contains some NLO corrections. Luckily reference [1] gave correction factors containing the implications of hadronization to cross section predictions. That is why in our case the jet algorithm is left with just two or three particles. If there are two partons they will leave the reaction in the opposite direction in the Breit frame and a merging of those could only take place if they carry low transverse momentum, which is excluded by the p_T -cut (see chapter 3.5.1). Only in the three-body final state it might happen that the algorithm merges two of the three partons. So basically the algorithm decides if there was an dijet or trijet event.

3.5. Reproduction of H1-Analysis

To test the NLO calculation, we reproduced the NLO analysis of inclusive jet cross sections in DIS from the H1 collaboration [1]. Experimental data was obtained by $e^{+/-}P$ -collisions in the HERA collider (from german *Hadron Elektron Ring Anlage*) at DESY in Hamburg during the HERA-II phase, after the collider was upgraded to reach higher luminosities in year 2002. The beam pipe energies were $E_e = 27.6$ GeV for electrons or positrons and $E_P = 920$ GeV for protons, which gives a center-of-mass energy of

$$S = \sqrt{4E_e E_P} = 319 \text{ GeV} , \quad (3.69)$$

p_T -bins [GeV]	Q^2 -bins [GeV ²]
$7 \leq p_T < 11$	$150 \leq Q^2 < 200$
$11 \leq p_T < 18$	$200 \leq Q^2 < 270$
$18 \leq p_T < 30$	$270 \leq Q^2 < 400$
$30 \leq p_T < 50$	$400 \leq Q^2 < 700$
	$700 \leq Q^2 < 5\,000$
	$5\,000 \leq Q^2 < 15\,000$

Table 3.1.: p_T - and Q^2 -bins for which $d^2\sigma/(dp_T dQ^2)$ was measured.

neglecting the particle masses. The integrated luminosity during running time was

$$\mathcal{L} = 357.60 \pm 8.9 \text{ pb}^{-1}. \quad (3.70)$$

Because of the geometric properties of the H1 detector, the neutral-current DIS phase space was constrained by several conditions. The leptonic phase space was given by

$$150 \text{ GeV}^2 < Q^2 < 15\,000 \text{ GeV}^2 \quad \text{and} \quad 0.2 < y < 0.7. \quad (3.71)$$

The Jets were reconstructed in the Breit frame of reference (see subsection 3.5.1) using the k_T -clustering jet algorithm with $R_0 = 1$. The jet phase space was constrained by

$$7 \text{ GeV} < p_T < 50 \text{ GeV} \quad (3.72)$$

in the Breit frame or the center-of-mass system of virtual photon and incoming parton⁴ and by

$$-1.0 < \eta_{lab} < 2.5, \quad (3.73)$$

where η_{lab} is the pseudorapidity in the laboratory frame. The experimental cuts had to be included in our program to get reasonable results. While the cuts on Q^2 and y could be set in the input file, the cuts on p_T and η_{lab} had to be implemented into the code. Therefore, we modified the event record in the **user** routine so that a jet of a certain event was not considered to fill the histogram, if it was outside the allowed region of phase space. The inclusive one jet cross section σ was given bin-wise and double differentially in Q^2 and p_T . The bins regarding these variables are listed in table 3.1. Since we want to calculate single differential cross sections $d\sigma/dp_T$ and $d\sigma/Q^2$, the data had to be summed up. For instance, for getting $d\sigma/dp_T$ in the lowest p_T -bin, all the values for $d\sigma/(dp_T dQ^2)$ lying in that p_T -region were multiplied by the corresponding Q^2 -width and summed up. The uncertainty was then obtained by usual error propagation.

For the theoretical NLO calculation the renormalization and the factorization scale were chosen to be

$$\mu_R = \sqrt{p_T^2 + Q^2} \quad \text{and} \quad \mu_F = \sqrt{Q^2}. \quad (3.74)$$

The partonic NLO predictions had to be multiplied by bin-wise correction factors because of electroweak and hadronization effects. Hence, we corrected our NLO results

⁴The transverse momentum is equal in both frame, because they are related by a longitudinal boost along the collision axis (see subsection 3.5.1)

using the same factors. They are given in subsection 3.5.2. The theoretical uncertainty of the NLO calculation in reference [1] was mostly due to scale variation of μ_R and μ_F by a factor 1/2 and 2. In section 3.5.3 we present our NLO analysis and compare it to the experimental data and the NLO results of the H1 collaboration. Hence, we used the same PDF set, which was the MSTW2008 set in NLO with fixed α_s [44]. The coupling strength was chosen to be

$$\alpha_s(M_Z) = 0.118. \quad (3.75)$$

For the phase space slicing cut parameter we choose a central value of

$$y_c = 10^{-4}. \quad (3.76)$$

This choice was motivated by relatively high stability of the calculation. Nevertheless, we tested the dependence on the cut parameter y_c separately.

3.5.1. The Breit frame

As already mentioned in chapter 3.4.1 the Breit frame of references is used to analyze the jets. This has to do with the parton model picture depicted in figure 3.7. The Breit frame is defined by the condition [1]

$$2x\vec{p} + \vec{q} = 0. \quad (3.77)$$

The frame is oriented in a way that both, virtual photon and quark, move along the z -axis colliding head on. Because equation 3.77 depends on q the transformation into the Breit frame has to be done for each event separately. The photon becomes completely spacelike

$$q = (0, 0, 0, -Q), \quad (3.78)$$

while the quark carries the longitudinal momentum $p_z = Q/2$ before and $p'_z = -Q/2$ after absorbing the photon, so in the parton model it bounces off and moves now in negative z -direction with the same velocity. The crux of the matter comes with the transverse momentum. Up to now the quark has no transverse momentum. It is totally balanced by the electron. Only if we have an additional quark-gluon vertex both resulting partons generate transverse momentum. Actually, this is a good thing. We can distinguish between processes we are interested in, to say depending on α_s , and irrelevant exclusively electroweak processes by demanding a minimum amount of transverse momentum in the final state. In our case the cut was $p_T > 7$ GeV. Another reason to imply this cut is a technical one. Perturbation theory becomes invalid in the kinematic region of soft total transverse momentum, because of a universal collinear divergence that already appears in the calculation of the partonic process in zeroth order of α_s . Nevertheless, the cut shall be small and already in the region close to the cut the cross section gets enhanced.

The Breit frame is closely related to the center-of-mass system of virtual photon and quark. The difference is that in the center-of-mass system the quark is at rest after absorbing the photon and does not bounce off. It becomes clear that you can get from one frame to another by simply carrying out a longitudinal boost along the z -axis.

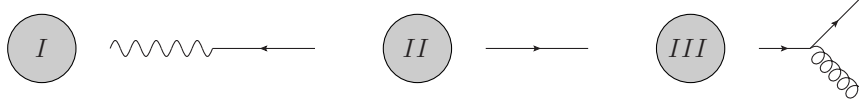


Figure 3.7.: Illustration of the partonic collision process in the Breit frame: **I** Virtual photon and quark collide. **II** Quark absorbed photon and leaves in opposite direction with same velocity. **III** Transverse momentum is generated by additional quark-gluon vertex.

3.5.2. Corrections to perturbative calculation

To compare our calculations to the experimental data we have to include correction factors c_i^{EW} and c_i^{had} for electroweak and hadronization effects in the following way [1]:

$$d\sigma_i = c_i^{\text{EW}} c_i^{\text{had}} d\sigma_i^{\text{pQCD}}, \quad (3.79)$$

where $d\sigma_i^{\text{pQCD}}$ is the the differential cross section prediction from our NLO pQCD analysis and $d\sigma_i$ the final theoretical result. The correction factors are given for each bin i .

They were obtained by using Monte Carlo event generators and comparing their results with and without fragmentation of the final state in the hadronic case

$$c_i^{\text{had}} = \frac{d\sigma_i^{\text{hadron}}}{d\sigma_i^{\text{parton}}}, \quad (3.80)$$

and with and without including Z -boson exchange and γZ -interference terms in the electroweak case

$$c_i^{\text{EW}} = \frac{\sigma_i^{(\gamma, \gamma Z, Z^0)}}{\sigma_i^{\gamma}}. \quad (3.81)$$

The hadronic coefficients c_i^{had} take into account energy loss by the hadronization process, so they are always smaller than 1. The electroweak corrections c_i^{EW} on the other hand can increase the cross section when the energy scale Q^2 goes to the mass of the Z -boson squared M_Z^2 and above.

The coefficients are given in the appendix of reference [1] for the bins of the double differential cross section $d^2\sigma/(dp_T dQ^2)$. We calculated single differential cross sections $d\sigma/dp_T$ and $d\sigma/dQ^2$. To get the coefficients as needed we simply took the average value of the ones given for each p_T -bin and Q^2 -bin. As the corrections are small, we think that this is sufficient. In table 3.2 the obtained coefficients are depicted by which any of our results were corrected. The errors were obtained by usual uncertainty propagation of the uncertainty estimates given in the reference.

3.5.3. Results

Now we will present the results of our NLO calculation and compare it to experimental data and the NLO analysis from the H1 collaboration. In figure 3.8a the results for the p_T -distribution are shown. The bigger error bars on the NLO calculation of H1 is due

p_T -bin [GeV]	c_i	δc [%]	Q^2 -bin [GeV ²]	c_i	δc [%]
$7 < p_T < 11$	0.95	0.63	$150 < Q^2 < 200$	0.95	0.76
$11 < p_T < 18$	0.99	0.49	$200 < Q^2 < 270$	0.96	0.80
$18 < p_T < 30$	0.99	0.39	$270 < Q^2 < 400$	0.96	0.53
$30 < p_T < 50$	0.98	0.29	$400 < Q^2 < 700$	0.96	0.42
			$700 < Q^2 < 5000$	0.98	0.28
			$5000 < Q^2 < 15000$	1.07	0.41

Table 3.2.: Coefficients $c_i = c_i^{\text{EW}} \cdot c_i^{\text{had}}$ for bin-wise hadronization and electroweak correction of cross section results.

to scale variation, while the scales are fixed in our calculation. The uncertainty in our results is given due to the uncertainty of the Monte-Carlo integration and the errors of the electroweak and hadronization correction factors. We see very good agreement to the data. There is a small tendency that results are getting too big compared to the data for high transverse momentum. This tendency is also present in the H1 analysis. Nevertheless, our results seem to be closer to the data in that region than the H1 results.

We also see good agreement to the data in the Q^2 -distribution plotted in figure 3.8b. Our results fall into the error band of the H1 analysis in every bin. All in all, considering both the p_T - and the Q^2 -distribution, we are left with big confidence that our results are reasonable, since it describes the data pretty well over the complete region of phase space. The deviations are just a few percent and of the same size as the ones from the H1 analysis.

We still have to check the dependence on the phase space slicing cut parameter y_c . This was done by using three different values for y_c . Besides the preset value $y_c = 10^{-4}$ we carried out the calculation with $y_c = 10^{-3}$ and $y_c = 10^{-5}$. The results are plotted in figure 3.9. Apparently, the results for $y_c = 10^{-4}$ and $y_c = 10^{-3}$ are more or less the same. Just in the highest p_T - and Q^2 -bins there is a small discrepancy. For $y_c = 10^{-5}$ there certainly is a significant gap. See for example, the highest two p_T -bins in figure 3.9a. In the Q^2 -distribution we can additionally see that the uncertainty of the Monte-Carlo integration becomes too big in the latter case. This suggests that y_c may not be so small, because too much of the mass singularities is put into the Monte-Carlo integration over the three-particle phase space, which then becomes numerically unstable. The Monte-Carlo error was the shortest for $y_c = 10^{-4}$. This and the fact that in that case our results coincides most with the H1 analysis, we were convinced that it is the best choice for the phase space slicing cut parameter.

Having fixed y_c we can finally analyze the dependence on the renormalization and factorization scale μ_R and μ_F . The idea is to vary the scales over a physically reasonable range to get an estimation of the lack of higher order effects. Of course, the range you choose is in principle as arbitrary as the scales themselves, so you have to follow a convention. Usually, what one does is to divide and multiply one or both scales by a factor of 2. To get comparable results we adopted the procedure of the H1 analysis and varied both scales by that factor. Figure 3.10 shows the resulting error bands for $d\sigma/dp_T$ and $d\sigma/dQ^2$ compared to the H1 results and the experimental data. In the lowest two

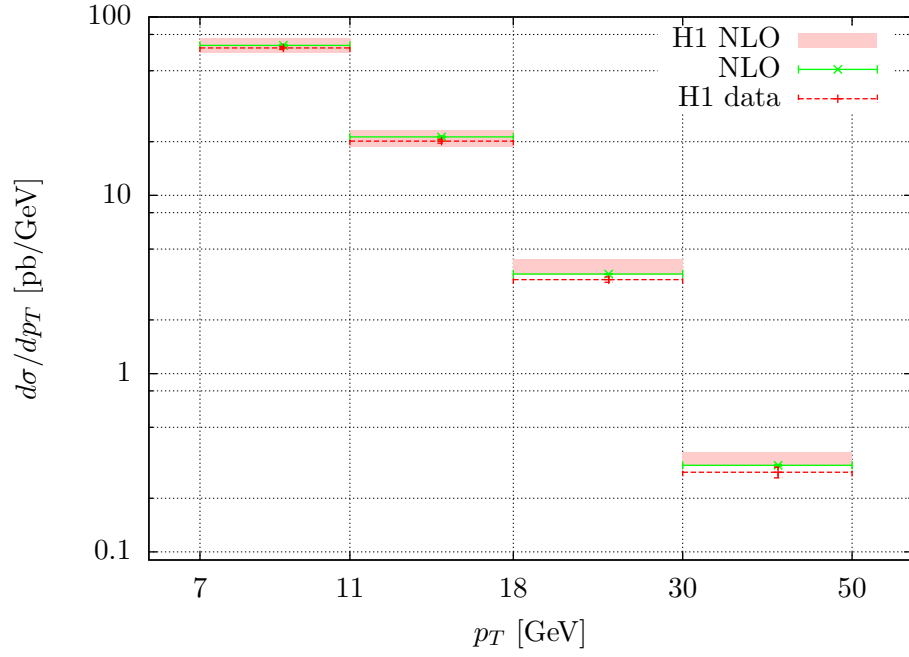
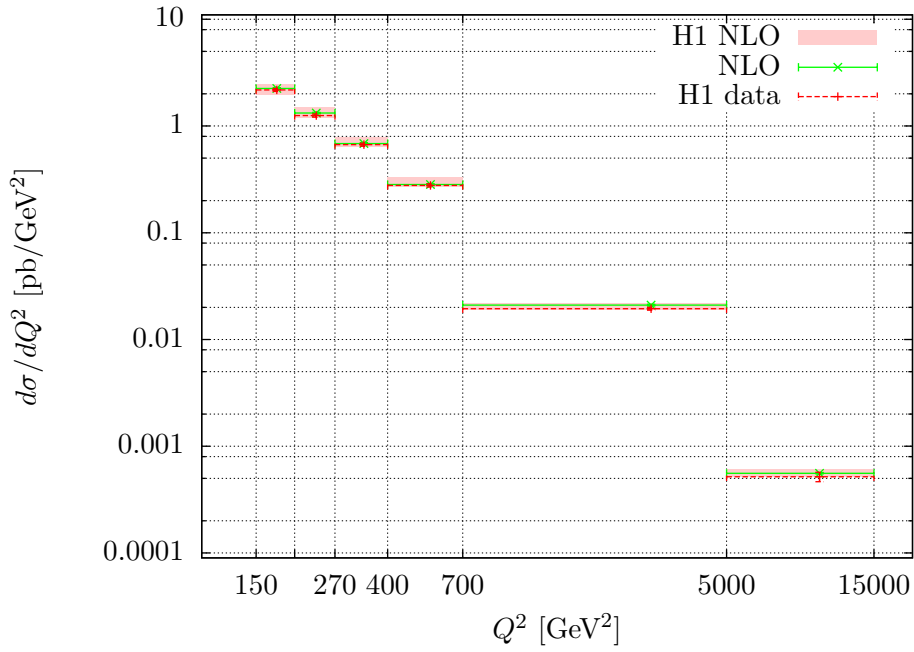
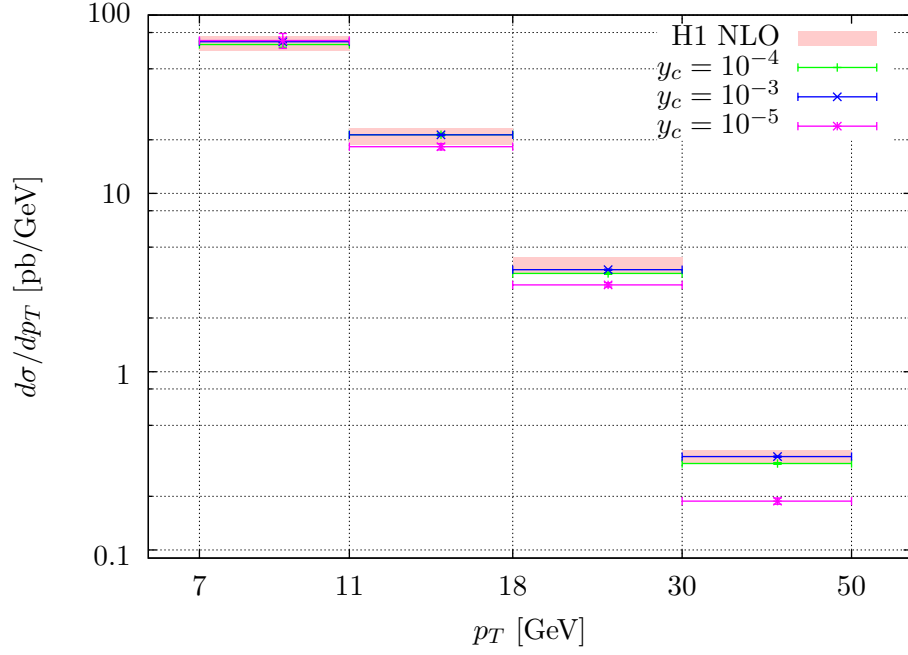
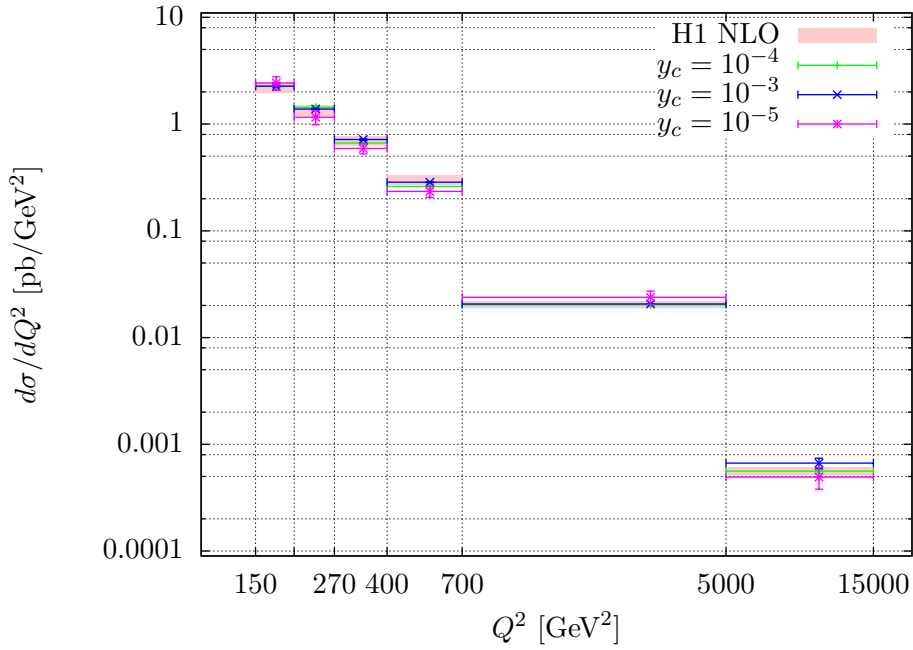
(a) $d\sigma/dp_T$ -distribution(b) $d\sigma/dQ^2$ -distribution

Figure 3.8.: NLO results compared to experimental data and NLO analysis from H1 collaboration.

(a) $d\sigma/dp_T$ -distribution(b) $d\sigma/dQ^2$ -distributionFigure 3.9.: NLO results for different values of the phase space slicing cut parameter y_c .

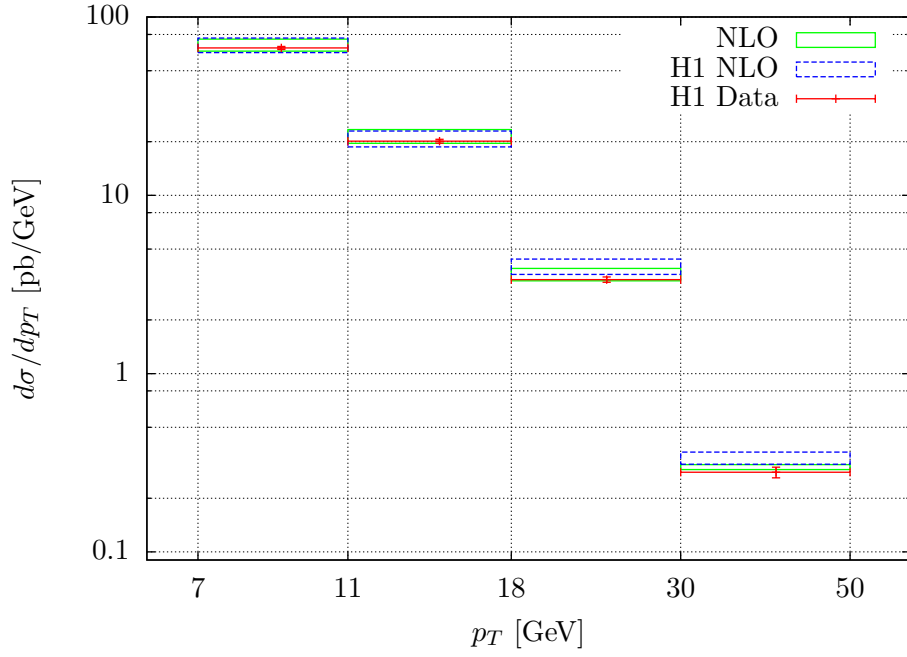
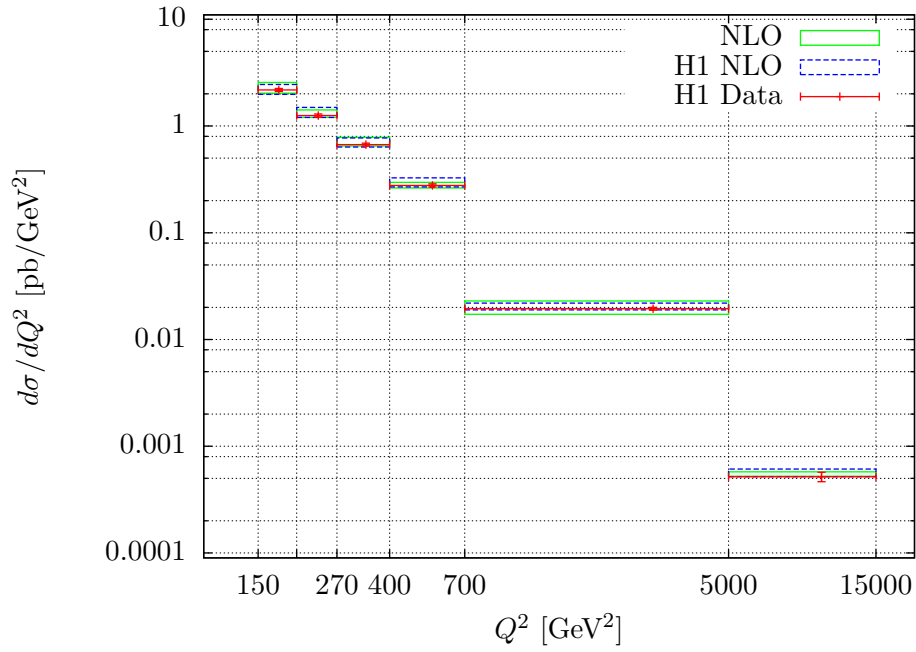
(a) $d\sigma/dp_T$ -distribution(b) $d\sigma/dQ^2$ -distribution

Figure 3.10.: NLO results with error bands obtained by variation of μ_R and μ_F by a factor of 1/2 and 2.

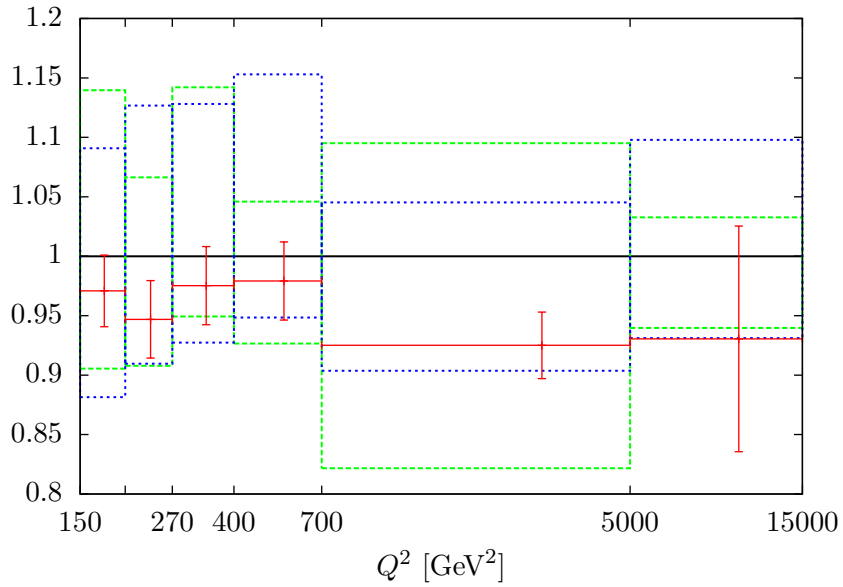
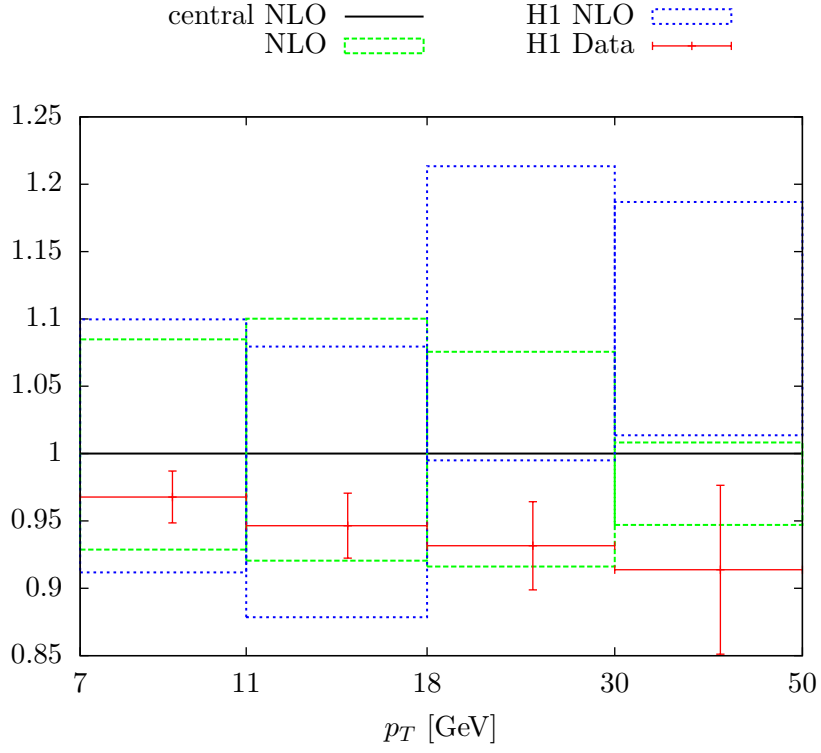


Figure 3.11.: NLO results for the differential cross section normalized to our central NLO result. The error bands are due to scale variation.

p_T -bins we see excellent agreement to the H1 analysis. The error bands nearly overlap completely. For higher transverse momentum the tendency of our results to decrease the differential cross section gets confirmed. Remarkably, the data points therefore lie within the error bands of our calculation in all p_T -bins, in contrast to the H1 analysis. In the last bin we can see that the width of the scale uncertainty is much smaller than in the H1 analysis. The Q^2 -distribution shows good agreement to the H1 analysis in all bins. Also the data points coincide with the error bands.

To see the width of the uncertainties more clearly we normalized both distributions to the central NLO result. Here, central means that the scales were not changed. The results are illustrated in figure 3.11. In the p_T -distribution we can see that the error due to scale variation is in our calculation roughly around 20%, as well as for the H1 analysis. In the region $18 \text{ GeV} < p_T < 50 \text{ GeV}^2$ the error decreases to approximately 5% to 10% in our result, while the H1 error does not become smaller there. The Q^2 -distribution shows a scale uncertainty of around 15% to 20% as well. An exception is the the region $700 \text{ GeV}^2 < Q^2 < 5000 \text{ GeV}^2$, where the scale uncertainty becomes very large (nearly 30%).

All in all, our plots show excellent agreement to the H1 analysis and describe the experimental data pretty well. We see a tendency that the NLO predictions overestimate the differential cross sections by a few percent. Since this is the case in our and in the H1 result, we are convinced that our NLO results are correct and we can continue to implement NNLO contributions in the next step.

4. From NLO to NNLO

This chapter presents the extension of the calculation of the DIS cross section to NNLO contributions, based on threshold resummation predictions. Our extensions are based on the master formulas of Kidonakis [2]. The procedure was previously done in our work group for the case of jet photoproduction [45]. The basic steps towards the master formulas are the following. The cross section for a hadron-hadron or lepton-hadron collision in general can schematically be written as [2]

$$\sigma = \sum_a \int \left[\prod_i dx_i \phi_{f_a/h_i}(x_i, \mu_F^2) \right] \hat{\sigma}(s, t_i, \mu_F, \mu_R), \quad (4.1)$$

where i runs over the initial-state hadrons h_i , a over the different parton flavors and $\phi_{a/H_i}(x_i, \mu_F)$ are the PDFs, giving the probability of finding a parton of type a with momentum fraction x_i in hadron H_i . For DIS we could in principle set $i = 1$ since there is just one incoming proton, but we stick to the general form until we arrive at the master formulas. The hadronic and the partonic cross section σ and $\hat{\sigma}$ stand for any total or differential cross section at this stage. $\hat{\sigma}$ contains soft and virtual corrections including plus distributions, i.e.,

$$\mathcal{D}_l(z) \equiv \left[\frac{\ln^l(1-z)}{1-z} \right]_+, \quad l \leq 2n-1, \quad (4.2)$$

with $n = 1$ at NLO, $n = 2$ at NNLO, etc. The variable z defines the partonic threshold (see equation 2.86). The highest power of logs at a given order is called *leading log* (LL), the second highest *next-to-leading log* (NLL), etc. It should be noted that it is not unlikely to reach the partonic threshold, even if we are far from the hadronic threshold

$$\tau = \frac{M^2}{S}, \quad (4.3)$$

with S being the hadronic center-of-mass energy. This happens at scales, where the PDFs are huge in small x -regions. That is why the above distributions become especially important when there is a gluon in the initial state.

In Moment space the logs can be resummed to all orders of perturbation theory and one obtains a resummed partonic cross section $\hat{\sigma}^{res}(N)$. In section 4.1 we give the result for $\hat{\sigma}^{res}(N)$ and point out the main steps of its derivation. In section 4.2 we state the NLO and NNLO master formulas presented in reference [2], which were gained by the re-expansion of $\hat{\sigma}^{res}(N)$ and matching to NLO results. In section 4.3 we compare the NLO master formula to the NLO calculation described in section 3.3. This will provide us with coefficients appearing in the NNLO master formula. Since the NLO master formula does not predict the full NLO result, but just contributions from soft-gluon

radiation, the reduction of the full NLO result to those being predicted by the master formula will give us an approximated NLO result. In section 4.4 we present the NNLO contributions for DIS predicted by the NNLO master formula. We discuss how the contributions influence the cross section results and give some remarks concerning the implementation of the new terms into the code of JetViP.

4.1. Threshold resummation

In this section, following the work of references [23, 46–50], we will find a resummed expression for the partonic cross section in Mellin space. More precisely, we will focus on dijet production [23]. The general procedure for calculating the resummed partonic cross section consists of the following steps. We start with the usual hadronic cross section, defined by a convolution of a hard-scattering function and certain distribution functions. From that we deduce a corresponding partonic cross section, which will factorize due to a Mellin transform. Next, the partonic cross section is *refactorized*, i.e., reorganized by using the factorization of soft gluons from high-energy partons and the exponentiation of soft-gluon effects [47]. Consequently, the primary factorized and the refactorized expressions are compared and the hard-scattering function is obtained in a form that can be resummed. The resummation of large logarithms of N is done by using RGEs that follow from the renormalization of jet and soft functions.

The process we want to deal with in this section is inclusive dijet production in the collision of two hadrons,

$$h_A(p_A) + h_B(p_B) \longrightarrow J_1(p_1) + J_2(p_2) + X(k), \quad (4.4)$$

at a fixed rapidity interval

$$\Delta y = \frac{1}{2} \ln \left(\frac{p_1^+ p_2^-}{p_1^- p_2^+} \right), \quad (4.5)$$

with total rapidity

$$y_{JJ} = \frac{1}{2} \ln \left(\frac{p_1^+ + p_2^+}{p_1^- + p_2^-} \right), \quad (4.6)$$

both expressed in light-cone variables. The partonic threshold is quantified by the variable

$$z = \frac{M^2}{x_A x_B S} = \frac{M^2}{\hat{s}}, \quad (4.7)$$

where M^2 is a large invariant that is fixed. The form of the cross section depends on the choice of M . It can, for instance, be the invariant final state mass or the invariant of a produced electroweak boson. Threshold is reached for $z_{\max} = 1$, when contributions of the form as in equation 4.2 become large. The lower bound of z is reached when the momentum fractions take their maximum value $x_A = x_B = 1$, so $z_{\min} = \tau$. The hadronic cross section then can be written as a convolution of parton distribution functions ϕ and a partonic hard-scattering function $\hat{\sigma}$,

$$\frac{d\sigma_{h_A h_B \rightarrow J_1 J_2}(S, \delta_1, \delta_2)}{dM^2 dy_{JJ} d\Delta y} = \frac{1}{S^2} \sum_{f_A, f_B=q, \bar{q}, g} \int_{\tau}^1 dz \int dx_A dx_B \phi_{f_A/h_A}(x_A, \mu^2)$$

$$\begin{aligned}
& \times \phi_{f_B/h_B}(x_B, \mu^2) \delta\left(z - \frac{M^2}{\hat{s}}\right) \delta\left(y_{JJ} - \frac{1}{2} \ln \frac{x_A}{x_B}\right) \\
& \times \sum_{f_1, f_2} \hat{\sigma}_{f_A f_B \rightarrow f_1 f_2} \left(1 - z, \frac{M}{\mu}, \Delta y, \alpha_s(\mu^2), \delta_1, \delta_2\right). \quad (4.8)
\end{aligned}$$

Here, μ is the factorization scale and δ_1 and δ_2 represent the parametrization of the jet definition. $\hat{\sigma}$ is defined for every partonic subprocess. A corresponding partonic cross section can be written by introducing *light-cone parton distribution functions* ϕ_{f_I/f_J} , giving the probability to find parton I in parton J , in the soft limit as

$$\begin{aligned}
\frac{d\sigma_{f_A f_B \rightarrow J_1 J_2}(S, \delta_1, \delta_2)}{dM^2 dy_{JJ} d\Delta y} &= \frac{1}{S^2} \int_{\tau}^1 dz \int dx_A dx_B \phi_{f_A/f_A}(x_A, \mu^2) \\
&\times \phi_{f_B/f_B}(x_B, \mu^2) \delta\left(z - \frac{M^2}{\hat{s}}\right) \delta\left(y_{JJ} - \frac{1}{2} \ln \frac{x_A}{x_B}\right) \\
&\times \sum_{f_1, f_2=q, \bar{q}, g} \hat{\sigma}_{f_A f_B \rightarrow f_1 f_2} \left(1 - z, \frac{M}{\mu}, \Delta y, \alpha_s(\mu^2), \delta_1, \delta_2\right). \quad (4.9)
\end{aligned}$$

Only the flavor diagonal distribution functions play a role, because the parton mixing is negligible for $N \rightarrow \infty$, what can be seen in equations 2.81 and 2.82.¹ The partonic cross section gets factorized by transform it in Mellin space with respect to the hadronic threshold τ ,

$$\begin{aligned}
\int_0^1 d\tau \tau^{N-1} \int dy_{JJ} S^2 \frac{d\sigma_{f_A f_B \rightarrow J_1 J_2}(S, \delta_1, \delta_2)}{dM^2 dy_{JJ} d\Delta y} \\
= \sum_{\mathbf{f}} \tilde{\phi}_{f_A/f_A}(N+1, \mu^2, \epsilon) \tilde{\phi}_{f_B/f_B}(N+1, \mu^2, \epsilon) \\
\times \tilde{\sigma}_{\mathbf{f}}(N, M/\mu, \alpha_s(\mu^2), \delta_1, \delta_2), \quad (4.10)
\end{aligned}$$

where by the δ -function depending on z , the transformations $\tilde{\sigma}(N) = \int_0^1 dz z^{N-1} \hat{\sigma}(z)$, and $\tilde{\phi}(N+1) = \int_0^1 dx x^N \phi(x)$ result. To shorten the notation we write \mathbf{f} for $f_A + f_B \rightarrow f_1 + f_2$. Since we are in the soft limit, we can set $N+1 \approx N$ in the following. In a perturbative expansion of $\hat{\sigma}$, they will factorize out initial-state collinear divergences, so they will depend on ϵ as well.

Now, although we already found a factorized form of the partonic cross section, it is necessary to *refactorize* it to perform the exponentiation. By refactorization we separate in particular soft-gluon contributions into a *soft gluon function* S from collinear radiation of the incoming and outgoing partons. This is important, because when S is free of collinear effects, we avoid double counting, because by definition they are included in jetlike distributions. The refactorized partonic cross section is of the form

$$\begin{aligned}
\frac{d\sigma_{f_A f_B \rightarrow J_1 J_2}(S, \delta_1, \delta_2)}{dM^2 d\Delta y} &= \frac{1}{S^2} \sum_{\mathbf{f}} \sum_{IL} H_{IL}^{(\mathbf{f})} \left(\frac{M}{\mu}, \Delta y, \alpha_s(\mu^2)\right) \\
&\times K_{LI}^{(\mathbf{f})} \left(\frac{M}{\mu}, \frac{(1-\tau)M}{\mu}, \Delta y, \alpha_s(\mu^2), \delta_1, \delta_2\right) + \mathcal{O}(1-\tau), \quad (4.11)
\end{aligned}$$

¹The light-cone PDFs fulfill the same evolution equations than the usual hadronic PDFs.

where $H_{IL}^{(f)}$ contains the hard-scattering components and describes the short-distance effects, and $K_{LI}^{(f)}$ contains everything happening at long distances. Both depend on the underlying partonic subprocess and are matrices in the color basis of the scattering event, so they carry color indices denoted by capital letters. The hard function is built out of the amplitude and its complex conjugate,

$$H_{IL}^{(f)}\left(\frac{M}{\mu}, \Delta y, \alpha_s(\mu^2)\right) = h_L^{*(f)}\left(\frac{M}{\mu}, \Delta y, \alpha_s(\mu^2)\right) h_I^{(f)}\left(\frac{M}{\mu}, \Delta y, \alpha_s(\mu^2)\right).$$

$K_{LI}^{(f)}$ consists of a convolution of five functions, depending on kinematical weights w_A , w_B , w_1 , w_2 and w_S measuring the amount of momentum each function contributes to the final state. Their exact definition depends on the choice of M^2 , so we will not specify them in detail. We find

$$\begin{aligned} K_{LI}^{(f)}\left(\frac{M}{\mu}, \frac{(1-\tau)M}{\mu}, \Delta y, \alpha_s(\mu^2), \delta_1, \delta_2\right) \\ = \int_0^1 dw_A dw_B dw_1 dw_2 dw_S \delta(1-\tau-w_A-w_B-w_1-w_2-w_S) \\ \times \psi_{f_A/f_A}\left(w_A, \frac{M}{\mu}, \alpha_s(\mu^2), \epsilon\right) \psi_{f_B/f_B}\left(w_B, \frac{M}{\mu}, \alpha_s(\mu^2), \epsilon\right) \\ \times S_{LI}^{(f)}\left(\frac{w_S M}{\mu}, \Delta y, \alpha_s(\mu^2)\right) \\ \times J^{(f_1)}\left(w_1, \frac{M}{\mu}, \alpha_s(\mu^2), \delta_1\right) J^{(f_2)}\left(w_2, \frac{M}{\mu}, \alpha_s(\mu^2), \delta_2\right) \\ + \mathcal{O}(1-\tau). \end{aligned} \quad (4.12)$$

The *jet functions* $J^{(f_1)}$ and $J^{(f_2)}$ contain gluonic effects by radiation collinear to the outgoing jets. The *center-of-mass distributions* ψ_{f_A/f_A} and ψ_{f_B/f_B} accordingly represent gluons radiated collinear to the incoming jets. In contrast to the light-cone PDFs they are defined at fixed energies and not at momentum fractions. In the axial gauge all collinear logarithms are incorporated in these four functions. $S_{LI}^{(f)}$ consequently accounts for soft, but not collinear, gluon radiation. $K_{LI}^{(f)}$ again factorizes in Mellin space,

$$\begin{aligned} \int_0^1 d\tau \tau^{N-1} S^2 \frac{d\sigma_{f_A f_B \rightarrow J_1 J_2}(S, \delta_1, \delta_2)}{dM^2 d\Delta y} &= \sum_f \sum_{IL} H_{IL}^{(f)}\left(\frac{M}{\mu}, \Delta y, \alpha_s(\mu^2)\right) \\ &\times \tilde{\psi}_{f_A/f_A}\left(N, \frac{M}{\mu}, \alpha_s(\mu^2), \epsilon\right) \tilde{\psi}_{f_B/f_B}\left(N, \frac{M}{\mu}, \alpha_s(\mu^2), \epsilon\right) \\ &\times \tilde{S}_{LI}^{(f)}\left(\frac{M}{\mu N}, \Delta y, \alpha_s(\mu^2)\right) \\ &\times \tilde{J}^{(f_1)}\left(N, \frac{M}{\mu}, \alpha_s(\mu^2), \delta_1\right) \tilde{J}^{(f_2)}\left(N, \frac{M}{\mu}, \alpha_s(\mu^2), \delta_2\right) \\ &+ \mathcal{O}(1/N). \end{aligned} \quad (4.13)$$

This is the refactorized partonic cross section. By setting equal equation 4.10 and 4.13

we can solve for the hard-scattering function

$$\begin{aligned} \tilde{\sigma}_f(N) &= \left[\frac{\tilde{\psi}_{f_A/f_A}(N, M/\mu, \epsilon) \tilde{\psi}_{f_B/f_B}(N, M/\mu, \epsilon)}{\tilde{\phi}_{f_A/f_A}(N, \mu^2, \epsilon) \tilde{\phi}_{f_B/f_B}(N, \mu^2, \epsilon)} \right] \\ &\times \sum_{IL} H_{IL}^{(f)} \left(\frac{M}{\mu}, \Delta y, \alpha_s(\mu^2) \right) \tilde{S}_{LI}^{(f)} \left(\frac{M}{\mu N}, \Delta y, \alpha_s(\mu^2) \right) \\ &\times \tilde{J}^{(f_1)} \left(N, \frac{M}{\mu}, \alpha_s(\mu^2), \delta_1 \right) \tilde{J}^{(f_2)} \left(N, \frac{M}{\mu}, \alpha_s(\mu^2), \delta_2 \right), \end{aligned} \quad (4.14)$$

that in this form can be exponentiated by making use of renormalization properties. In the product $H_{IL}S_{LI}$ appearing UV divergences have to cancel, because that is guaranteed by the renormalization of the underlying theory. But UV divergences in each factor appear, because of approximations for soft gluons that are extended to all momenta [23]. They can be removed by multiplicative renormalization constants. With Z_i being the field renormalization constants for parton field i and Z_S being the renormalization constant for the soft gluon function one can write

$$H_{IL}^{(f)(0)} = \prod_{i=A,B,1,2} Z_i^{-1} \left(Z_S^{(f)-1} \right)_{IC} H_{CD} [(Z_S^{(f)\dagger})^{-1}]_{DL} \quad (4.15)$$

$$S_{LI}^{(f)(0)} = (Z_S^{(f)\dagger})_{LB} S_{BA} Z_{S,AI}^{(f)}. \quad (4.16)$$

From that one deduces for S the RGE

$$\left(\mu \frac{\partial}{\partial \mu} + \beta(g) \frac{\partial}{\partial g} \right) S_{LI}^{(f)} = -(\Gamma_S^{(f)\dagger})_{LB} S_{BI}^{(f)} - S_{LA}^{(f)} (\Gamma_S^{(f)})_{AI}, \quad (4.17)$$

where the *soft anomalous dimension matrix* is given by the UV divergences of the soft gluon function,

$$\Gamma_S^{(f)}(g) = -\frac{g}{2} \frac{\partial}{\partial g} \text{Res}_{\epsilon \rightarrow 0} Z_S^{(f)}(g, \epsilon). \quad (4.18)$$

The solution to equation 4.17 is given by

$$\begin{aligned} &\text{Tr} \left\{ H^{(f)} \left(\frac{M}{\mu}, \Delta y, \alpha_s(\mu^2) \right) \tilde{S}^{(f)} \left(\frac{M}{N\mu}, \Delta y, \alpha_s(\mu^2) \right) \right\} \\ &= \text{Tr} \left\{ H^{(f)} \left(\frac{M}{\mu}, \Delta y, \alpha_s(\mu^2) \right) \right. \\ &\quad \times \bar{P} \exp \left[\int_{\mu}^{M/N} \frac{d\mu'}{\mu'} \Gamma_S^{(f)\dagger}(\alpha_s(\mu'^2)) \right] \\ &\quad \times \tilde{S}^{(f)} \left(1, \Delta y, \alpha_s(M^2/N^2) \right) \\ &\quad \left. \times P \exp \left[\int_{\mu}^{M/N} \frac{d\mu'}{\mu'} \Gamma_S^{(f)}(\alpha_s(\mu'^2)) \right] \right\}. \end{aligned} \quad (4.19)$$

Here, the trace is taken regarding the color indices and P and \bar{P} stand for path ordering in the same sense as μ' and against it. This expression resums all large logarithms of N . For the initial-state jets, resummed at the scale $\mu = M$, one finds

$$\left[\frac{\tilde{\psi}_{f/f}(N, 1, \epsilon)}{\tilde{\phi}_{f/f}(N, M^2, \epsilon)} \right] = R_{(f)}(\alpha_s(M^2)) \exp[E_{(f)}(N, M)] , \quad (4.20)$$

by making use of factorization properties, where the N -dependence is put into $E_{(f)}$ in the exponential. Its form depends on the factorization scheme. In $\overline{\text{MS}}$ one finds

$$\begin{aligned} E_{(f)}(N, M) = & - \int_0^1 dz \frac{z^{N-1} - 1}{1 - z} \left\{ \int_{(1-z)^2}^1 \frac{d\lambda}{\lambda} A_{(f)}[\alpha_s(\lambda M^2)] \right. \\ & \left. + B_{(f)}[\alpha_s(M^2)] + \frac{1}{2} \nu^{(f)}[\alpha_s((1-z)^2 M^2)] \right\} . \end{aligned} \quad (4.21)$$

The functions $A_{(f)}$, $B_{(f)}$, and $\nu^{(f)}$ are finite concerning their arguments and can be expanded in α_s . To evolve this result to different factorization scales, one uses the RGEs of the individual distribution functions, namely

$$\begin{aligned} \mu \frac{d\tilde{\psi}_{f/f}(N, M/\mu, \epsilon)}{d\mu} &= 2\gamma_f(\alpha_s(\mu^2)) \tilde{\psi}_{f/f}(N, M/\mu, \epsilon) , \\ \mu \frac{d\tilde{\phi}_{f/f}(N, \mu^2, \epsilon)}{d\mu} &= 2\gamma_{f/f}(N, \alpha_s(\mu^2)) \tilde{\phi}_{f/f}(N, \mu^2, \epsilon) . \end{aligned} \quad (4.22)$$

In the former equation we defined the anomalous dimension of the parton field f γ_f , given by the virtual part of the splitting functions, and the anomalous dimension of the operator corresponding to $\phi_{f/f}$ $\gamma_{f/f}$ in the latter equation. It depends on the scheme and the gauge you choose. Combining the result of that RGEs with equation 4.21 gives

$$\begin{aligned} \left[\frac{\tilde{\psi}_{f/f}(N, M/\mu, \epsilon)}{\tilde{\phi}_{f/f}(N, \mu^2, \epsilon)} \right]_{\overline{\text{MS}}} &= R_{(f)}(\alpha_s(\mu^2)) \exp[E_{(f)}(N, M)] \\ &\times \exp \left\{ -2 \int_\mu^M \frac{d\mu'}{\mu'} [\gamma_f(\alpha_s(\mu'^2)) - \gamma_{f/f}(N, \alpha_s(\mu'^2))] \right\} . \end{aligned} \quad (4.23)$$

Finally, for the final-state jets, one can find a similar exponential result. Its exact form depends strongly on the choice of M , because different definitions lead to different final-state phase spaces at partonic threshold. Nevertheless, we can write

$$\tilde{J}^{(f_i)}\left(N, \frac{M}{\mu}, \alpha_s(\mu^2), \delta_i\right) = \exp[E'_{(f_i)}(N, M)] , \quad (4.24)$$

while we skip giving a precise form of $E'_{(f_i)}$ for the moment. Combining equation 4.19, 4.23 and 4.24 we find the resummed partonic hard-scattering function in Mellin space, which includes large the contributions of large logarithms of N to all orders. To get the physical cross section, a transformation back to ordinary momentum space has to be done. Carrying this out is far from trivial, because of Landau poles in the complex

plane, demanding a *prescription* how to choose an integration path. We will not go into detail on that problem and refer to the literature (for instance reference [16]). To sum up our result, we state the resummed cross section in its full glory:

$$\begin{aligned}
\tilde{\sigma}_f(N) = & R_{(f)} \exp \left\{ \sum_{i=A,B} \left[E_{(f_i)}(N, M) \right. \right. \\
& \left. \left. - 2 \int_{\mu}^M \frac{d\mu'}{\mu'} [\gamma_{f_i}(\alpha_s(\mu'^2)) - \gamma_{f_i f_i}(N, \alpha_s(\mu'^2))] \right] \right\} \\
& \times \exp \left\{ \sum_{j=1,2} E'_{(f_j)}(N, M) \right\} \\
& \times \text{Tr} \left\{ H^{(f)} \left(\frac{M}{\mu}, \Delta y, \alpha_s(\mu^2) \right) \right. \\
& \times \bar{P} \exp \left[\int_{\mu}^{M/N} \frac{d\mu'}{\mu'} \Gamma_S^{(f)\dagger}(\alpha_s(\mu'^2)) \right] \tilde{S}^{(f)} \left(1, \Delta y, \alpha_s(M^2/N^2) \right) \\
& \left. \times P \exp \left[\int_{\mu}^{M/N} \frac{d\mu'}{\mu'} \Gamma_S^{(f)}(\alpha_s(\mu'^2)) \right] \right\}. \tag{4.25}
\end{aligned}$$

4.2. The master formula

Kidonakis presented master formulas predicting NLO and NNLO contributions containing logarithms of the form 4.2 for inclusive processes like hadron-hadron collisions and hadron-lepton collisions

$$f_1(p_1) + f_2(p_2) \rightarrow F + X \quad \text{and} \quad f_1(p_1) + l(p_2) \rightarrow F + X, \tag{4.26}$$

where F is the observed hadronic final state and X is anything else [2]. The master formulas were obtained by the re-expansion of the resummed partonic cross section

$$\begin{aligned}
\hat{\sigma}^{res}(N) = & \exp \left[\sum_i E^{(f_i)}(N_i) \right] \exp \left[\sum_j E'^{(f_j)}(N_j) \right] \\
& \times \exp \left[\sum_i 2 \int_{\mu_F}^{\sqrt{s}} \frac{d\mu'}{\mu'} \left(\frac{\alpha_s(\mu'^2)}{\pi} \gamma_i^{(1)} + \gamma'_{i/i}(\alpha_s(\mu'^2)) \right) \right] \\
& \times \exp \left[2 d_{\alpha_s} \int_{\mu_R}^{\sqrt{s}} \frac{d\mu'}{\mu'} \beta(\alpha_s(\mu'^2)) \right] \\
& \times \text{Tr} \left\{ H(\alpha_s(\mu_R^2)) \bar{P} \exp \left[\int_{\sqrt{s}}^{\sqrt{s}/\tilde{N}_j} \frac{d\mu'}{\mu'} \Gamma'_S(\alpha_s(\mu'^2)) \right] \tilde{S}(\alpha_s(s/\tilde{N}_j^2)) \right. \\
& \left. \times P \exp \left[\int_{\sqrt{s}}^{\sqrt{s}/\tilde{N}_j} \frac{d\mu'}{\mu'} \Gamma'_S(\alpha_s(\mu'^2)) \right] \right\}, \tag{4.27}
\end{aligned}$$

and matching it to full NLO calculations. The summation over i runs over initial-state partons, with

$$E^{(f_i)}(N_i) = - \int_0^1 dz \frac{z^{N_i-1} - 1}{1-z} \times \left\{ \int_{(1-z)^2 s}^{\mu_F^2} \frac{d\mu'^2}{\mu'^2} A^{(f_i)}(\alpha_s(\mu'^2)) + \nu_{f_i} [\alpha_s((1-z)^2 s)] \right\}. \quad (4.28)$$

The N -dependence of the final-state partons is resummed by the summation over j and

$$E'^{(f_j)}(N_j) = \int_0^1 dz \frac{z^{N_j-1} - 1}{1-z} \times \left\{ \int_{(1-z)^2}^{1-z} \frac{d\lambda}{\lambda} A^{(f_j)}(\alpha_s(\lambda s)) - B'_j [\alpha_s((1-z)s)] - \nu_j [\alpha_s((1-z)^2 s)] \right\}. \quad (4.29)$$

Here, we used

$$A^{(f_i)} = C_{f_i} [\alpha_s/\pi + (\alpha_s/\pi)^2 K/2] + \dots, \quad (4.30)$$

$$\nu_{f_i} = (\alpha_s/\pi) C_{f_i} + (\alpha_s/\pi)^2 \nu_{f_i}^{(2)} + \dots, \quad (4.31)$$

$$B'_j = (\alpha_s/\pi) B_j'^{(1)} + (\alpha_s/\pi)^2 B_j'^{(2)} + \dots, \quad (4.32)$$

where $C_{f_i} = C_F$ for a quark or antiquark and $C_{f_i} = C_A = N_c$ for a gluon, and $K = C_A(67/18 - \pi^2/6) - 5n_f/9$. Also, we find $B_q'^{(1)} = 3C_F/4$ and $B_g'^{(1)} = \beta_0/4$, with β_0 defined by equation 2.51. In the second line of equation 4.27 it was defined the one-loop parton anomalous dimensions $\gamma_q^{(1)} = 3C_F/4$ and $\gamma_g^{(1)} = \beta_0/4$. $\gamma'_{i/i}$ is the anomalous dimension of $\tilde{\phi}_{i/i}$ (see equation 4.22) minus its one-loop and its N -dependent two-loop components. For later use we state the N -independent two-loop part of $\gamma_{i/i}$ for quarks and gluons,

$$\gamma'_{q/q}^{(2)} = C_F^2 \left(\frac{3}{32} - \frac{3}{4} \zeta_2 + \frac{3}{2} \zeta_3 \right) + C_F C_A \left(-\frac{3}{4} \zeta_3 + \frac{11}{12} \zeta_2 + \frac{17}{96} \right) + n_f C_F \left(-\frac{\zeta_2}{6} - \frac{1}{48} \right), \quad (4.33)$$

$$\gamma'_{g/g}^{(2)} = C_A^2 \left(\frac{2}{3} + \frac{3}{4} \zeta_3 \right) - n_f \left(\frac{C_F}{8} + \frac{C_A}{6} \right). \quad (4.34)$$

$\zeta_2 = \pi^2/6$ and $\zeta_3 = 1.2020569 \dots$ are values of the Riemann zeta function. In the third line of 4.27 we made use of the beta function already defined by equation 2.50. In our case, the constant $d_{\alpha_s} = 1$, because our Born cross section is of order α_s^1 . The prime on Γ'_S indicates that all gauge-dependent terms are ignored. This is possible, because it was proven that gauge-dependence cancels out.

The re-expansion of formula 4.27 to NLO and NNLO accuracy gives the desired master formulas. Since we have a colorless virtual photon in the initial state, we need just the master formulas for simple color-flow. It also means that Γ_S is a 1×1 matrix. The NLO master formula reads

$$\hat{\sigma}^{(1)} = \sigma^B \frac{\alpha_s(\mu_R^2)}{\pi} \{ c_3 \mathcal{D}_1(z) + c_2 \mathcal{D}_0(z) + c_1 \delta(1-z) \}, \quad (4.35)$$

where σ^B is the Born term and the coefficients are defined by

$$c_3 = \sum_i 2C_{f_i} - \sum_j C_{f_j}, \quad (4.36)$$

$$c_2 = c_2^\mu + T_2, \quad (4.37)$$

$$c_2^\mu = - \sum_i C_{f_i} \ln \left(\frac{\mu_F^2}{s} \right), \quad (4.38)$$

$$T_2 = 2\text{Re}\Gamma_S^{\prime(1)} - \sum_i \left[C_{f_i} + 2C_{f_i} \delta_K \ln \left(\frac{-t_i}{M^2} \right) \right] - \sum_j \left[B_j^{\prime(1)} + C_{f_j} + C_{f_j} \delta_K \ln \left(\frac{M^2}{s} \right) \right], \quad (4.39)$$

$$c_1 = c_1^\mu + T_1, \quad (4.40)$$

$$c_1^\mu = \sum_i \left[C_{f_i} \delta_K \ln \left(\frac{-t_i}{M^2} \right) - \gamma_i^{(1)} \right] \ln \left(\frac{\mu_F^2}{s} \right) + d_{\alpha_s} \frac{\beta_0}{4} \ln \left(\frac{\mu_R^2}{s} \right). \quad (4.41)$$

All coefficients have to be determined for every type of partonic reaction that contributes to the inclusive cross section. c_2 and c_3 are split into a scale-dependent part and the rest that does not contain a dependence neither on the factorization scale μ_F nor on the renormalization scale μ_R . In our case the mass scale M was chosen to be the natural scale at hand for deep inelastic scattering, namely the virtuality of the exchanged photon Q , and the constant δ_K is set to zero, what is valid in pair-invariant-mass (PIM) kinematics. β_0 was defined in equation 2.51. Using the expansion

$$\Gamma_S' = \left(\frac{\alpha_s}{\pi} \right) \Gamma_S^{\prime(1)} + \left(\frac{\alpha_s}{\pi} \right)^2 \Gamma_S^{\prime(2)} + \dots, \quad (4.42)$$

we identify the real part of the one-loop anomalous dimension matrix neglecting gauge-dependent terms $\text{Re}\Gamma_S^{\prime(1)}$ in the definition of T_2 . t_i is a kinematical variable only important in different kinematics than PIM. It appears in terms containing δ_K , so they vanish anyway, and we do not need to specify t_i . T_1 contains the scale-independent corrections proportional to $\delta(1-z)$. They are given by the virtual NLO corrections, which cannot be predicted by the threshold resummation formalism. They have to be taken from a full NLO calculation, if available.

The NNLO master formula reads

$$\hat{\sigma}^{(2)} = \sigma^B \frac{\alpha_s^2(\mu_R^2)}{\pi^2} \hat{\sigma}'^{(2)}, \quad (4.43)$$

with

$$\begin{aligned} \hat{\sigma}'^{(2)} &= \frac{1}{2} c_3^2 \mathcal{D}_3(z) + \left[\frac{3}{2} c_3 c_2 - \frac{\beta_0}{4} c_3 + \sum_j C_{f_j} \frac{\beta_0}{8} \right] \mathcal{D}_2(z) \\ &+ \left\{ c_3 c_1 + c_2^2 - \zeta_2 c_3^2 - \frac{\beta_0}{2} T_2 + \frac{\beta_0}{4} c_3 \ln \left(\frac{\mu_R^2}{s} \right) + \sum_i C_{f_i} K \right\} \end{aligned}$$

$$\begin{aligned}
& + \sum_j C_{f_j} \left[-\frac{K}{2} + \frac{\beta_0}{4} \delta_K \ln \left(\frac{M^2}{s} \right) \right] - \sum_j \frac{\beta_0}{4} B_j'^{(1)} \Big\} \mathcal{D}_1(z) \\
& + \left\{ c_2 c_1 - \zeta_2 c_2 c_3 + \zeta_3 c_3^2 - \frac{\beta_0}{2} T_1 + \frac{\beta_0}{4} c_2 \ln \left(\frac{\mu_R^2}{s} \right) + 2 \operatorname{Re} \Gamma_S'^{(2)} - \sum_i \nu_{f_i}^{(2)} \right. \\
& + \sum_i C_{f_i} \left[\frac{\beta_0}{8} \ln^2 \left(\frac{\mu_F^2}{s} \right) - \frac{K}{2} \ln \left(\frac{\mu_F^2}{s} \right) - K \delta_K \ln \left(\frac{-t_i}{M^2} \right) \right] \\
& - \sum_j (B_j'^{(2)} + \nu_j^{(2)}) + \sum_j C_{f_j} \delta_K \left[\frac{\beta_0}{8} \ln^2 \left(\frac{M^2}{s} \right) - \frac{K}{2} \ln \left(\frac{M^2}{s} \right) \right] \\
& \left. - \sum_j \frac{\beta_0}{4} B_j'^{(1)} \delta_K \ln \left(\frac{M^2}{s} \right) \right\} \mathcal{D}_0(z) \\
& + \left\{ \frac{1}{2} c_1^2 - \frac{\zeta_2}{2} c_2^2 + \frac{1}{4} \zeta_2^2 c_3^2 + \zeta_3 c_3 c_2 - \frac{3}{4} \zeta_4 c_3^2 + \frac{\beta_0}{4} c_1 \ln \left(\frac{\mu_R^2}{s} \right) \right. \\
& + 2 \operatorname{Re} \Gamma_S'^{(2)} \delta_K \ln \left(\frac{M^2}{s} \right) - \frac{\beta_0}{2} \delta_K T_1 \ln \left(\frac{M^2}{s} \right) + \frac{\beta_0}{4} \delta_K T_2 \ln^2 \left(\frac{M^2}{s} \right) \\
& + \frac{d_{\alpha_s}}{16} \left[-\frac{\beta_0^2}{2} \ln^2 \left(\frac{\mu_R^2}{s} \right) + \beta_1 \ln \left(\frac{\mu_R^2}{s} \right) \right] \\
& + \sum_i \frac{\beta_0}{8} \left[\gamma_i^{(1)} - C_{f_i} \delta_K \ln \left(\frac{-t_i}{M^2} \right) \right] \ln^2 \left(\frac{\mu_F^2}{s} \right) \\
& + \sum_i C_{f_i} \frac{K}{2} \delta_K \ln \left(\frac{-t_i}{M^2} \right) \ln \left(\frac{\mu_F^2}{s} \right) - \sum_i \gamma_{i/i}^{(2)} \ln \left(\frac{\mu_F^2}{s} \right) \\
& + \sum_i C_{f_i} \delta_K \left[\frac{\beta_0}{6} \ln^3 \left(\frac{-t_i}{M^2} \right) + \left(\frac{\beta_0}{4} + \frac{K}{2} \right) \ln^2 \left(\frac{-t_i}{M^2} \right) \right] \\
& + \sum_i C_{f_i} \frac{\beta_0}{2} \delta_K \ln \left(\frac{M^2}{s} \right) \left[\ln^2 \left(\frac{-t_i}{M^2} \right) - \ln \left(\frac{-t_i}{M^2} \right) \ln \left(\frac{M^2}{s} \right) \right. \\
& \left. - \frac{1}{2} \ln \left(\frac{M^2}{s} \right) + \ln \left(\frac{-t_i}{M^2} \right) \right] + \sum_i \nu_{f_i}^{(2)} \delta_K \ln \left(\frac{-t_i}{M^2} \right) \\
& - \sum_j (B_j'^{(2)} + \nu_j^{(2)}) \delta_K \ln \left(\frac{M^2}{s} \right) + \sum_j \left[\frac{\beta_0}{8} C_{f_j} \ln \left(\frac{M^2}{s} \right) \right. \\
& \left. \left. - \frac{K}{4} C_{f_j} - \frac{\beta_0}{8} B_j'^{(1)} \right] \delta_K \ln^2 \left(\frac{M^2}{s} \right) + R \right\} \delta(1-z). \tag{4.44}
\end{aligned}$$

Here we find $\zeta_4 = \pi^4/90$ and the real part of the two-loop Γ_S after dropping gauge-dependent terms $\operatorname{Re} \Gamma_S'^{(2)}$ in the $\mathcal{D}_0(z)$ -part. It appears followed by $-\sum_i \nu_{f_i}^{(2)}$, which both are two-loop quantities. We could not find an expression for that part in literature, so we neglected it in our calculation. The same problem arose for the expression $\sum_j (B_j'^{(2)} + \nu_j^{(2)})$ that could not be found in literature and therefore was neglected. K

was introduced in equation 4.30 and given beneath. β_1 is given by equation 2.52. R denotes all contributions that can only be known from a full NNLO calculation. Note that many terms, especially in the $\delta(1-z)$ -part, vanish, because $\delta_K = 0$. $\gamma'_{q/q}^{(2)}$ and $\gamma'_{g/g}^{(2)}$ were defined in equations 4.33 and 4.34.

4.3. Matching coefficients to NLO

We have defined the ingredients to evaluate the general expressions of the coefficients c_i appearing in the NLO and NNLO master formula in equation 4.35 and 4.44. This has to be done for both contributing partonic two-body processes $\gamma^*q \rightarrow qg$ and $\gamma^*g \rightarrow q\bar{q}$. Afterwards we compare the predicted NLO contributions with the virtual and initial-state corrections of the full NLO calculation. In principle, we should be able to find all the predicted contributions in the formulas that we either took from reference [14] or directly from the code of the program JetViP. In the following we will calculate the coefficients for both processes and illustrate the identification of the resulting terms in the NLO corrections with one example for each process.

$\gamma^*q \rightarrow qg$

By the unified approach of Kidonakis we find

$$c_3 = C_F - N_C. \quad (4.45)$$

For c_2 we need additionally $\text{Re}(\Gamma_S'^{(1)}) = 2C_F \ln\left(\frac{-u}{M^2}\right) + 2C_F + N_C \ln\left(\frac{t}{u}\right) + N_C$ [2],² and find

$$c_2 = 2C_F \ln\left(\frac{-u}{M^2}\right) + N_C \ln\left(\frac{t}{u}\right) - C_F \ln\left(\frac{\mu_F^2}{M^2}\right) - \frac{3}{4}C_F - \frac{\beta_0}{4}. \quad (4.46)$$

Finally, the scale-dependent part of c_1 is given by

$$c_1^\mu = -\frac{3}{4}C_F \ln\left(\frac{\mu_F^2}{M^2}\right) + \frac{\beta_0}{4} \ln\left(\frac{\mu_R^2}{M^2}\right). \quad (4.47)$$

Note that we substitute all s by M^2 . Originally, this was motivated by the fact that otherwise no agreement was found regarding the formulas implemented in the code. The actual reason for this might be the differences between the resummed partonic cross section from equations 4.25 and 4.27, where we already see that some integration boundaries are s in the former and M^2 in the latter equation. Anyway, the substitution is necessary according to the full NLO formulas and since we choose $M^2 = Q^2$ we also find agreement to DIS coefficients explicitly stated in [2], where likewise Q^2 appears instead of s more or less out of the blue.

We choose the term $c_1^\mu = \frac{\beta_0}{4} \ln(\mu_R^2/M^2) + \dots$ as an example of the identification in the full NLO corrections. The term contains the renormalization scale μ_R , which gives us

²The expression is given for the reversed partonic process in direct photon production, but it is the same in our case.

the hint that it must be part of the virtual corrections. β_0 includes the number of active quark flavors n_f . The only term containing n_f in the virtual corrections corresponding to the given process is

$$H_V^{T/L} = 16\pi^2 \frac{\alpha_s}{2\pi} 2(1-\varepsilon) \left(\frac{4\pi\mu_R^2}{s} \right)^\varepsilon \frac{\Gamma(1-\varepsilon)}{\Gamma(1-2\varepsilon)} \frac{1}{\varepsilon} \left(\frac{1}{3}n_f - \frac{11}{6}N_C \right) C_F T_{\gamma q}^{T/L} + \dots, \quad (4.48)$$

which is the last term of equation 3.48. Using the expansion

$$\left(\frac{4\pi\mu_R^2}{s} \right)^\varepsilon = \exp \left[\ln \left(\frac{4\pi\mu_R^2}{s} \right)^\varepsilon \right] \approx 1 + \varepsilon \cdot \ln \left(\frac{4\pi\mu_R^2}{s} \right) = \varepsilon \cdot \ln \left(\frac{\mu_R^2}{s} \right) + \dots, \quad (4.49)$$

and inserting β_0 and the Born contributions of equations 3.35 or 3.37 that we, following the notation of reference [2], generically denote σ_B , we can identify the finite term

$$H_V^{T/L} = \frac{\alpha_s}{\pi} \sigma_B \ln \left(\frac{\mu_R^2}{s} \right) \frac{\beta_0}{4} + \dots = \int_\eta^1 \frac{dz}{z} \frac{\alpha_s}{\pi} \sigma_B [c_1 \delta(1-z) + \dots]. \quad (4.50)$$

Remembering that for virtual corrections the z -integration is already carried out analytically, we can read off $c_1^\mu = \frac{\beta_0}{4} \ln(\mu_R^2/s) + \dots$ on the left-hand side, which is the sought term when we substitute s by M^2 . That this substitution is necessary shall not worry us, because reference [14] is about jet photoproduction with small Q^2 , while here we work in the DIS high- Q^2 regime. Indeed, in the code the corresponding term was found with M^2 instead of s , in agreement with the threshold resummation prediction.

$\gamma^* g \rightarrow q \bar{q}$

For the gluon-initiated process we find

$$c_3 = 2(N_C - C_F). \quad (4.51)$$

For c_2 we need $\text{Re}(\Gamma_S'^{(1)}) = 2C_F + N_C \ln \left(\frac{tu}{M^4} \right) + N_C$ [2], and thus

$$c_2 = N_C \ln \left(\frac{tu}{M^4} \right) - N_C \ln \left(\frac{\mu_F^2}{M^2} \right) - \frac{3}{2}C_F. \quad (4.52)$$

Finally, we find

$$c_1^\mu = -\frac{\beta_0}{4} \ln \left(\frac{\mu_F^2}{M^2} \right) + \frac{\beta_0}{4} \ln \left(\frac{\mu_R^2}{M^2} \right). \quad (4.53)$$

As a second example we try to recover the term $c_2 = -N_C \ln(\mu_F^2/M^2) + \dots$. This time, the wanted term contains the factorization scale μ_F , so it must be part of the initial-state corrections. They are given for the gluon-initiated process by (see equation 3.56)

$$\int d\text{PS}^{(r)} H_{R^4}^I = \int_\eta^1 \frac{dz}{z} 8\pi \left(\frac{4\pi\mu_F^2}{s} \right)^\varepsilon \frac{\Gamma(1-\varepsilon)}{\Gamma(1-2\varepsilon)} (1-\varepsilon) I_4 + \mathcal{O}(\varepsilon), \quad (4.54)$$

with I_4 being a lengthy function that can be looked up in reference [14].³ c_2 collects terms proportional to $\mathcal{D}_0(z)$. We find the term

$$I_4 = \alpha_s^2 Q_b^2 \left(-\frac{N_C}{4} \right) T_{\gamma g}^{T/L} \left[\frac{2}{\varepsilon} \frac{1}{N_C} P_{g \leftarrow g}(z) + \dots \right] + \dots, \quad (4.55)$$

with

$$P_{g \leftarrow g}(z) = 2N_C \left(\left[\frac{1}{1-z} \right]_+ + \dots \right). \quad (4.56)$$

Inserting the latter expressions in 4.54, using again the expansion 4.49, and inserting the Born contributions 3.36 or 3.38 we find in the limit $\varepsilon \rightarrow 0$ the finite term

$$\int_{\eta}^1 \frac{dz}{z} \frac{\alpha_s}{\pi} \sigma_B \left(-\frac{N_C}{2} \right) \ln \left(\frac{\mu_F^2}{s} \right) \mathcal{D}_0 + \dots = \int_{\eta}^1 \frac{dz}{z} \frac{\alpha_s}{\pi} \sigma_B [c_2 \mathcal{D}_0 + \dots]. \quad (4.57)$$

We recognize $c_2 = -(N_C/2) \ln(\mu_F^2/s) + \dots$, which differs from our expectation, besides the s instead of M^2 in the argument of the logarithm, by a factor of $1/2$. This would be problematic, but luckily the corresponding formula in the code does not have the factor $1/2$ in the prefactor and is in agreement with the threshold resummation prediction. That the formulas in the code differ by a factor of $1/2$ to the ones in reference [14] was also seen in other terms. That is why we focused our attention to the formulas implemented in the code.

The complete results of the matching of the coefficients to the full NLO calculation are summarized in table D.1. All in all, most of the predicted terms could be identified in the code. In c_2 and c_3 there were some terms that could not be found in the code. They all come from final-state parton contributions in the approach of Kidonakis. The reason for that is that our NLO calculation uses phase space slicing, rather producing alternative logarithms that depend on the phase space slicing cut parameter. The threshold resummation procedure of course cannot reproduce these contributions, so we shall not be surprised to find a mismatch that becomes manifest in the prediction of terms not being present in the code. In c_2 there are three predicted terms differing by a factor of 2 to the corresponding terms in the code. They all stem from the expression $2\text{Re}(\Gamma_S^{(1)})$, whose form we took from [2]. Interestingly, the same issue was found in previous work on jet photoproduction [45].

Having identified the NLO contributions in the code that are predicted by the threshold resummation approach, we can define an approximate NLO calculation that we call kNLO in the following. It consists of the LO contributions, the scale-independent virtual NLO contributions that are grouped in T_1 , the predicted NLO contributions, using the coefficients from the right column of table D.1, and the terms in the full NLO calculation that depend on the phase space slicing cut parameter. The results of the kNLO approximation are compared to the full NLO calculation and the H1 data in figure 4.1, by which we can estimate how big the fraction of contributions predicted by the Kidonakis approach is in contrast to the full NLO contributions in different kinematical regions. In the p_T -distribution we see that for small transverse momentum the kNLO

³The notation was changed here. I_4 in our case actually refers to I_5 from reference [14].

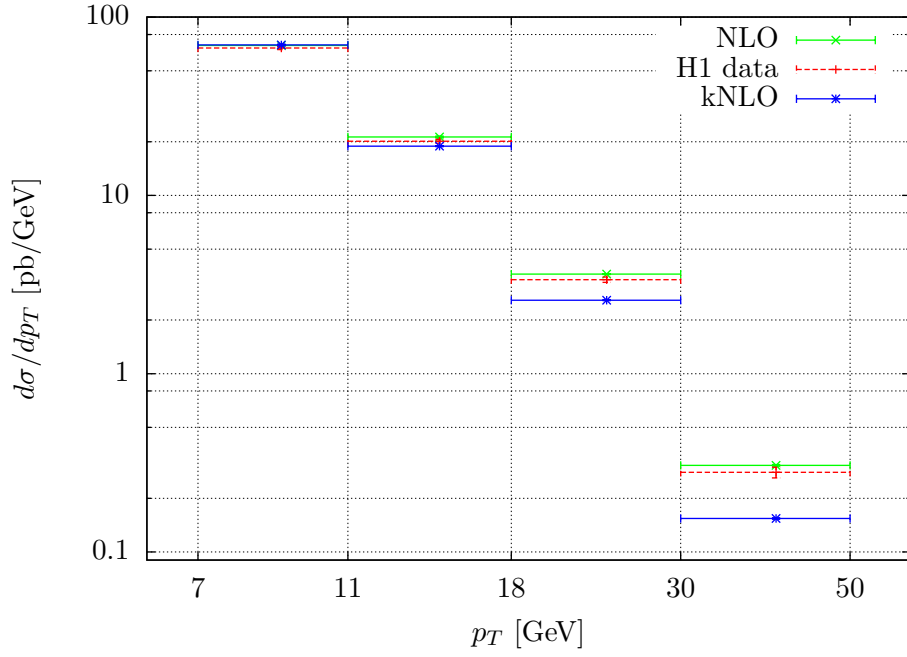
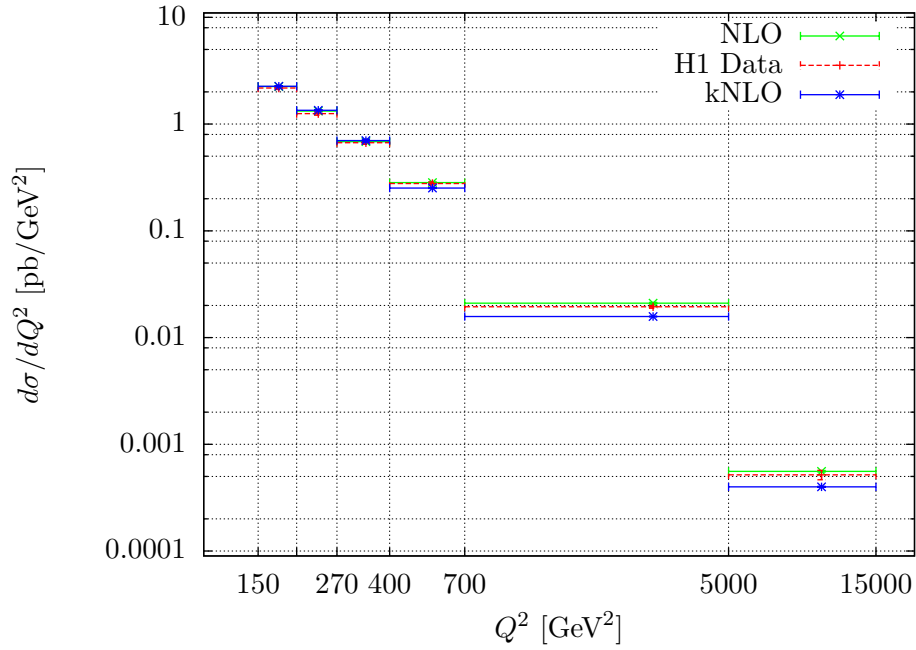
(a) $d\sigma/dp_T$ -distribution(b) $d\sigma/dQ^2$ -distribution

Figure 4.1.: kNLO results compared to experimental data and full NLO results.

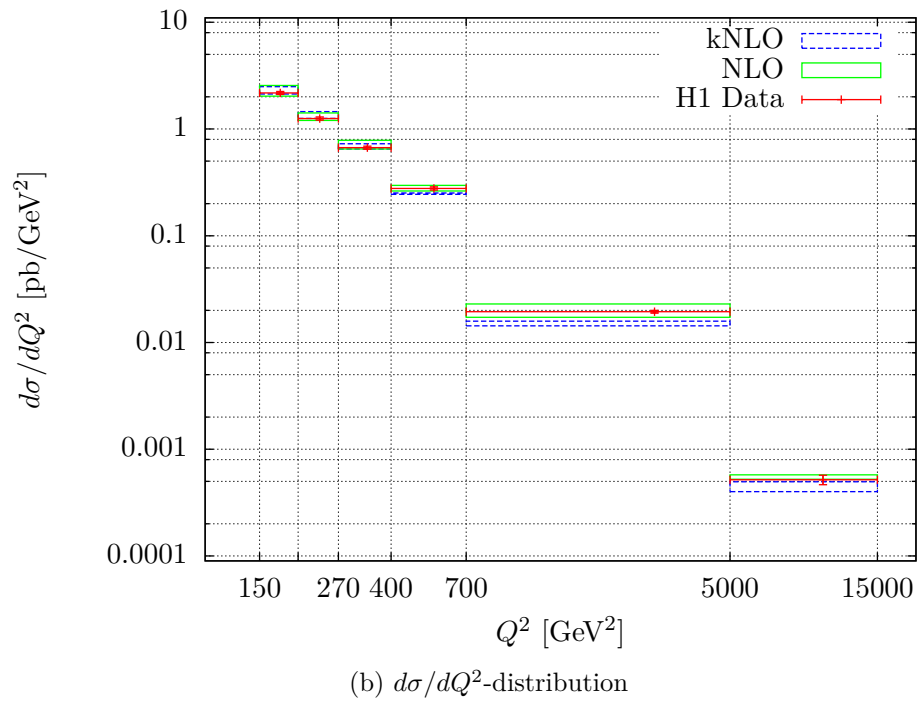
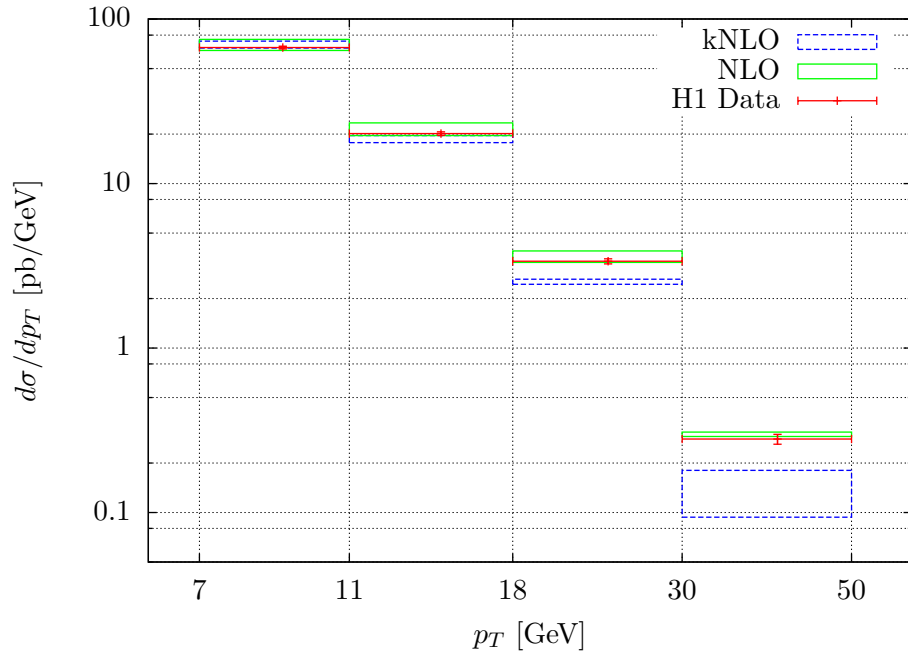


Figure 4.2.: kNLO results with error bands obtained by variation of μ_R and μ_F by a factor of 1/2 and 2.

approximation and the NLO results nearly coincide. For higher transverse momentum the kNLO results are drastically below the NLO results and the experimental data. A similar behavior can be established in the Q^2 -distribution. However, the differences in the high- Q^2 bins are not as big.

We finally check how the kNLO approximation reacts under the variation of the renormalization and the factorization scale μ_R and μ_F by a factor of 1/2 and 2, as was done before in the reproduction of the H1 analysis. The results are depicted in figure 4.2. Overall we see that the error bars of the kNLO approximation are smaller than the NLO errors, what is not that surprising since we neglect terms containing both scales in the approximation. Exceptions are the highest bins in the p_T - and the Q^2 -distributions. Interestingly, the scale dependence increases by an order of magnitude in the highest p_T -bin, though the resulting huge error bar still does not reach the data point.

4.4. NNLO contributions

Having calculated the coefficients c_1 , c_2 and c_3 being present in the NNLO master formula 4.44 in the previous section, we can implement the NNLO contributions into the program JetViP. Of course, they have to be added to the full NLO calculation and not to the kNLO approximation. The corresponding terms could most easily be added to the NLO initial-state corrections on the proton side, since for them the z -integration was already there. Technical details regarding the implementation are given in the appendix in chapter E. Here, we will focus on the physical aspects and the results.

As was already mentioned in section 4.2, we had to neglect the two-loop quantities

$$2\text{Re}\Gamma_S^{\prime(2)} - \sum_i \nu_{fi}^{(2)}, \quad (4.58)$$

stemming from initial-state partons, and

$$\sum_j \left(B_j^{\prime(2)} + \nu_j^{(2)} \right), \quad (4.59)$$

stemming from final-state partons, because an appropriate expression for them could not be found. Since previous work [45] already lacked the knowledge of those two-loop terms, yet obtained reasonable results, we are pretty sure that we do not neglect crucial contributions of the NNLO master formula.⁴ The coefficient c_1 , c_2 and c_3 were implemented as they were predicted by Kidonakis and as they are depicted in the left column of table D.1, i.e., including the terms which could not be identified in the NLO corrections (written in blue), because that was just a side-effect of phase space slicing.

After implementation of the NNLO master formula we unluckily had to observe that we produced results differing to the experimental data by 2 to 3 orders of magnitude. After verifying that no mistake was done implementing the terms, we began to analyze if we could find individual terms producing that error. In reference [45] the same problem emerged and was fixed by discarding all terms including the δ -function. Led by this

⁴*Crucial* here refers to the NNLO contributions grouped in the rest R that is not predicted by the threshold resummation approach and neglected in our approach.

observation and after some time of trial and error, we could spot the troublemaker. In the NNLO master formula we have the term

$$\hat{\sigma}'^{(2)} = \dots + \left\{ \frac{1}{2} c_1^2 + \dots \right\} \delta(1-z). \quad (4.60)$$

It produces way to big contributions for the quark-initiated partonic processes. To be more precise, it is the scale-independent part $T_1(\gamma^* q \rightarrow qg)$ that provokes them at this place in the formula, even though in the case of the gluon-initiated process $\gamma^* g \rightarrow q\bar{q}$ everything works fine. We could not find another solution to this problem rather than just ignore the problematic contribution and calculate for the quark-initiated process just

$$\hat{\sigma}'^{(2)}(\gamma^* q \rightarrow qg) = \dots + \left\{ \frac{1}{2} c_1^{\mu^2} + \dots \right\} \delta(1-z). \quad (4.61)$$

Of course, this is quite unsatisfactory, but by this substitution we could gain reasonable results, with corrections to the NLO calculation of the expected size. We will describe them in detail in the following section.

4.4.1. Results

We will compare our NNLO results to the same experimental data of the H1 collaboration [1] that we already analyzed by means of our NLO calculation. In figure 4.3 we see the central NNLO and NLO predictions together with the experimental data differentially in p_T and Q^2 .⁵ We generally see that the NNLO contributions reduce the cross section predictions of the NLO calculation in the complete observed phase space regime, which is a good first impression, since we saw in subsection 3.5.3 that the NLO prediction seems to slightly overestimate the cross section. We therefore find an improvement in the description of the p_T -differential data in figure 4.3a, except in the lowest bin, where the NNLO result lies below the data point. In the Q^2 -distribution we see similar accuracy between NLO and NNLO. A small tendency becomes visible that the difference between NNLO and NLO increases for high Q^2 .

In the next step we investigate the scale-dependence of the NNLO predictions using the usual method of varying both scales μ_R and μ_F by a factor of 1/2 and 2. The results are shown in figure 4.4. All experimental data points lie inside of the resulting error bars. In the p_T -distribution we have to observe that the error bars of the NNLO calculation are bigger than the ones of the NLO calculation. This contradicts our expectation. The results depend on the scales, because we truncate the perturbative expansion of the partonic hard-scattering cross section at a finite order. By scale-variation we hope to get an estimation of the missing higher-order contributions, so we hope to reduce the scale-dependence by including contributions of the next higher order of perturbation theory. In our approach this argumentation is not completely valid, since we do not have the full NNLO corrections. Yet we expected to reduce the scale-dependence, because the contributions we implemented were obtained from a resummation formalism, where specific terms of the perturbative expansion are summed to all orders. However, this is

⁵With *central* results we refer to the scale choice $\mu_F^2 = Q^2$ and $\mu_R^2 = Q^2 + p_T^2$ and the MSTW2008 PDF set with fixed $\alpha_s(M_Z) = 0.118$.

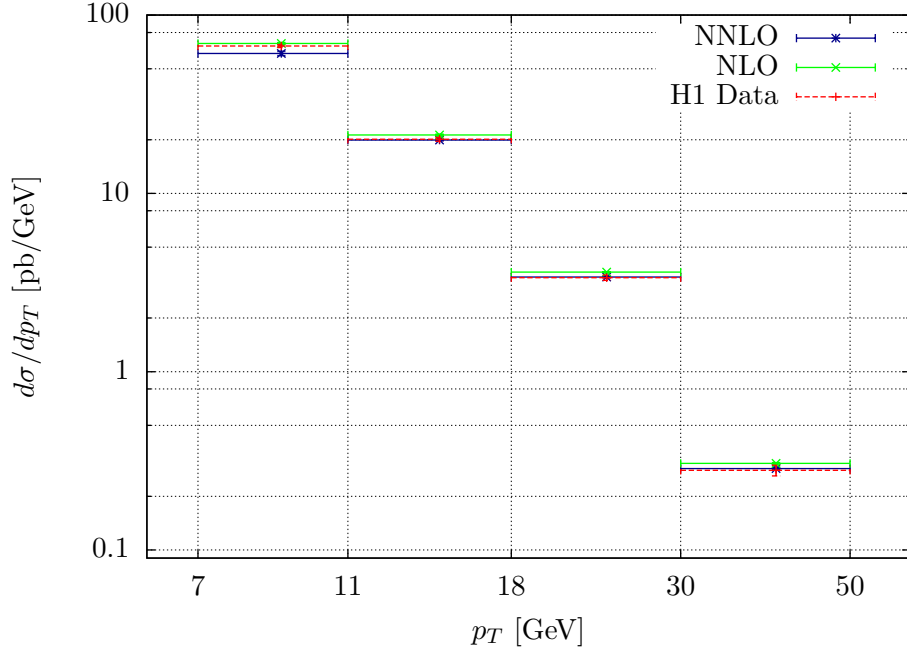
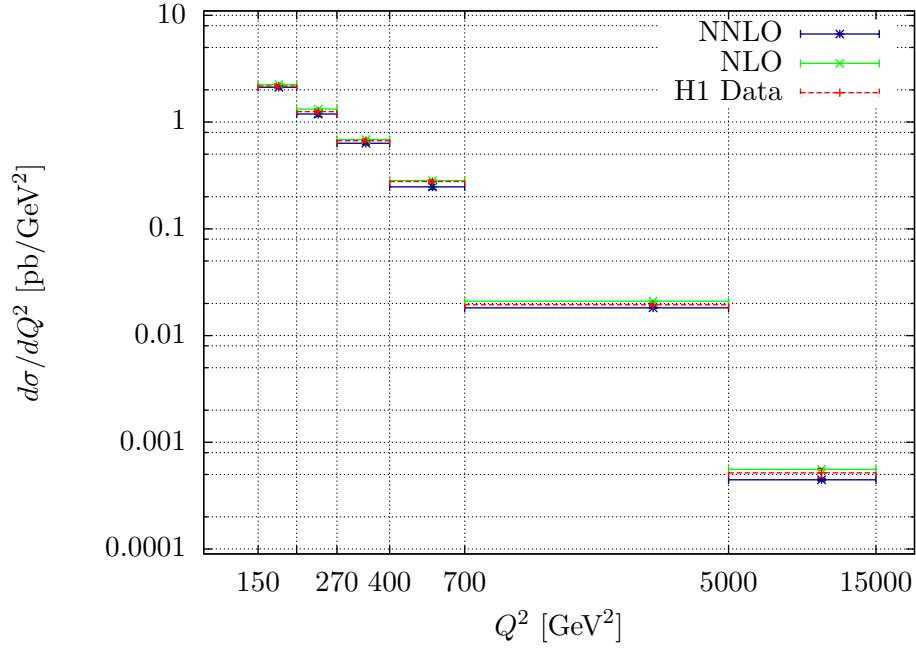
(a) $d\sigma/dp_T$ -distribution(b) $d\sigma/dQ^2$ -distribution

Figure 4.3.: NNLO results compared to NLO and H1 data.

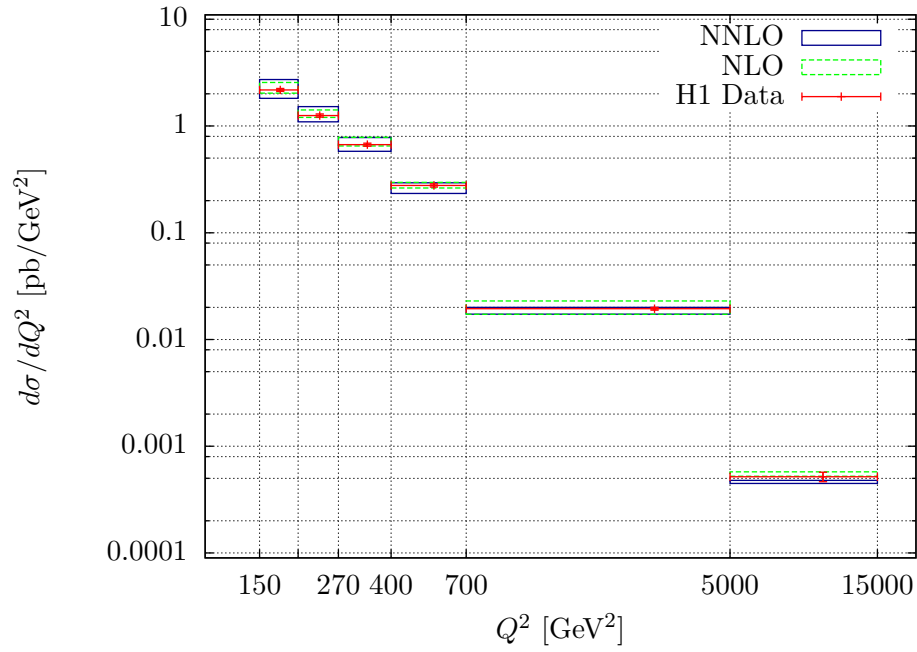
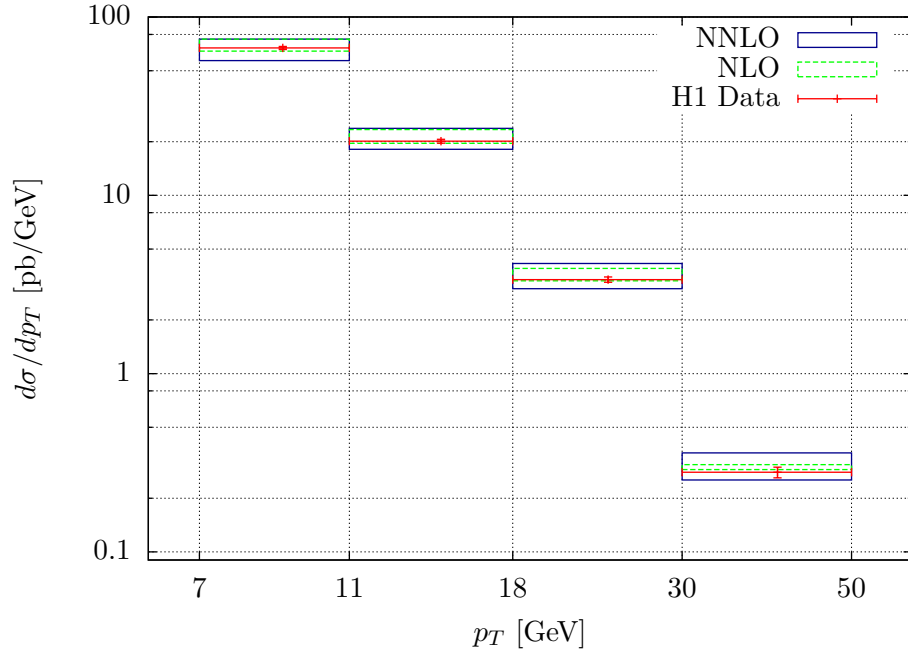


Figure 4.4.: NNLO results with error bands obtained by variation of μ_R and μ_F by a factor of 1/2 and 2 compared to NLO and H1 data.

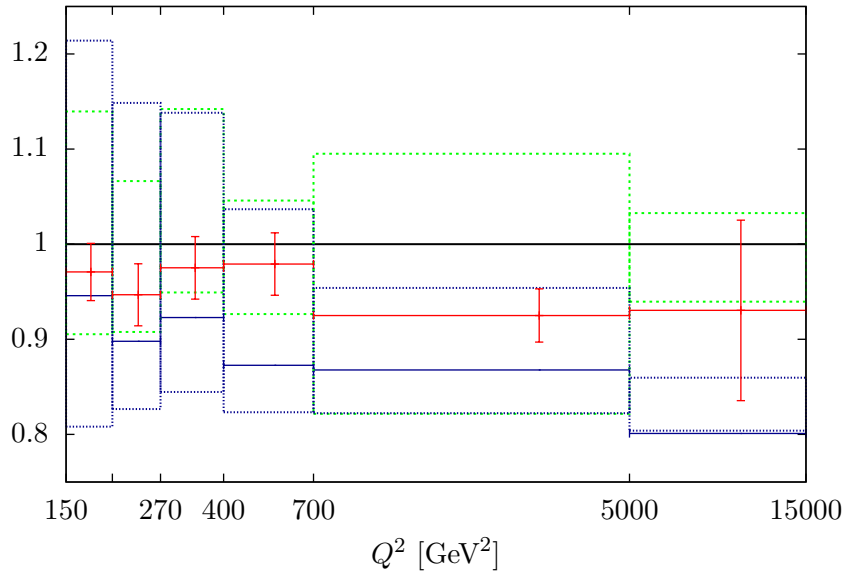
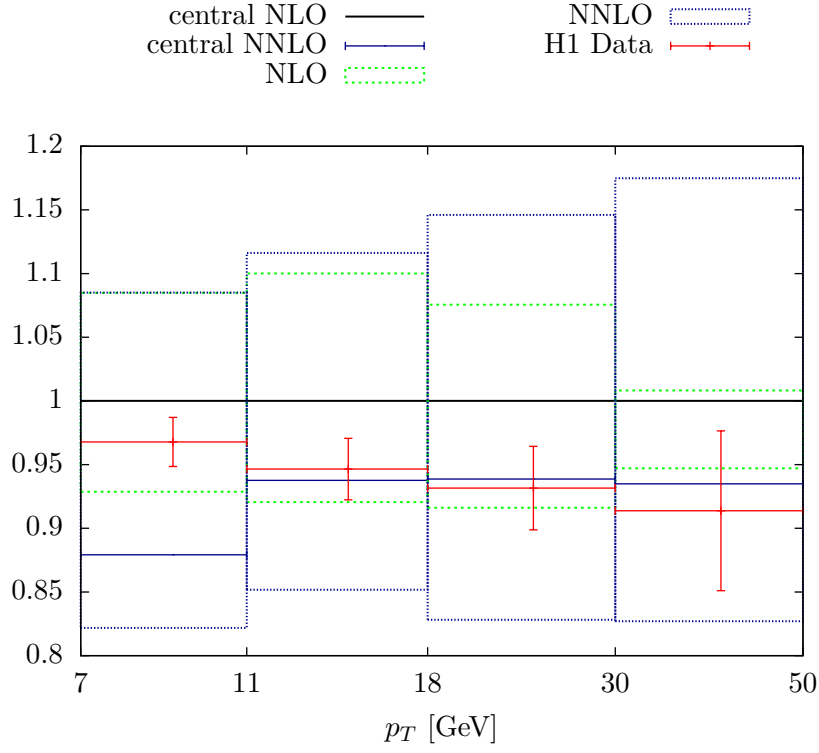


Figure 4.5.: NNLO results for the differential cross section normalized to central NLO. The error bands are due to scale variation.

not guaranteed, and unfortunately we find an increasing scale-dependence in the given p_T -regime. The finding of the Q^2 -distribution is different at least in the highest two Q^2 -bins, where the scale-dependence actually is reduced in NNLO. Nevertheless, for lower Q^2 we confirm that scale-dependence is enhanced by the extended NNLO calculation.

For better visibility figure 4.5 shows the results normalized in each bin to the central NLO value. The fact that the scale-dependence is actually reduced for high Q^2 was additionally checked by evaluating the predictions for even higher Q^2 , for which we of course were missing experimental data to compare with. A corresponding plot can be found in the appendix in figure F.1.

4.4.2. Determination of the strong coupling constant

The theoretical cross section predictions are functions depending on the strong coupling constant, given in turn at a certain renormalization scale. The running coupling has to be fixed at a random scale, which normally corresponds to the mass of the Z boson M_Z . By regarding $\alpha_s(M_Z)$ as a global fit parameter of the cross section predictions, we can find a best-fit $\alpha_s(M_Z)$ in relation to the experimental data. Technically, we use the MSTW2008 proton PDF sets with fixed $\alpha_s(M_Z)$. These sets contain 22 different members for $\alpha_s(M_Z)$ in the range from 0.110 to 0.130 in NLO and from 0.107 to 0.127 in NNLO. The calculations were done with each member and the reduced χ_{red}^2 was calculated to investigate the goodness of the predictions.

However, the determination of $\alpha_s(M_Z)$ is seriously affected by the experimental and theoretical uncertainties. On the theoretical side, in particular, one should include the scale uncertainty. Unfortunately, we had to discover in the previous section that the NNLO contributions increase the scale uncertainty in the observed phase space, quite contrary to expectations. This means that also the error of the $\alpha_s(M_Z)$ -determination would increase, when the NNLO contributions are included. To avoid this, we separately analyzed the dependence on the factorization scale μ_F and the renormalization scale μ_R . In appendix F the results are plotted in figure F.2 for the variation of μ_F and in figure F.3 for μ_R , respectively. Comparing both distribution, one can see that the increase of the scale uncertainty of the NNLO calculation with respect to the NLO calculation is caused by the dependence on μ_F , while the dependence on μ_R is similar. Nevertheless, a detailed analysis showed that even if we just vary μ_R and keep μ_F fixed, the resulting error in the determination of $\alpha_s(M_Z)$ still would not be reduced. To demonstrate this, we plot the reduced χ_{red}^2 against $\alpha_s(M_Z)$ for different values of μ_R in figures F.4 and F.5 for the NLO calculation and in figures F.6 and F.7 for the NNLO calculation. μ_R is varied around the central value by the prefactors 0.50, 0.75, 1.00, 1.50 and 2.00. μ_F is fixed to its central value. One can see that the minima of χ_{red}^2 move to the right with increasing μ_R by approximately equal distances comparing the NLO and NNLO results. This, and the fact that the minima of some plots did not even lie in the given range of $\alpha_s(M_Z)$, we decided to determine an $\alpha_s(M_Z)$ -value without including an error representing the scale uncertainties.

Thus, with the central scales we find at NLO

$$\alpha_s^{NLO}(M_Z) = 0.1151_{-0.0016}^{+0.0016}. \quad (4.62)$$

Including the NNLO contributions we find

$$\alpha_s^{NNLO}(M_Z) = 0.1221^{+0.0017}_{-0.0018}. \quad (4.63)$$

The errors are determined by the values for $\alpha_s(M_Z)$, where χ_{red}^2 increases about 1 unit with respect to its minimum. $\alpha_s(M_Z)$ is significantly shifted to higher values when NNLO accuracy is taken into account. Comparing both results to the world average value of [10]

$$\alpha_s^{WA}(M_Z) = 0.1184 \pm 0.0007, \quad (4.64)$$

we see that neither the NLO $\alpha_s(M_Z)$ -value nor the NNLO $\alpha_s(M_Z)$ -value lies within the error band of the world average value. We finally compare our results to the one of the H1 collaboration [1]. Based on a fit to their NLO calculation, they determined the strong coupling constant to be

$$\alpha_s^{H1}(M_Z) = 0.1185 \pm 0.0017, \quad (4.65)$$

using absolute double-differential inclusive jet, dijet and trijet cross section data as functions of Q^2 and p_T . A more precised value was obtained from normalized jet cross sections, yielding

$$\alpha_s^{H1_n}(M_Z) = 0.1165 \pm 0.0008. \quad (4.66)$$

Important to note is that the given uncertainties in equations 4.65 and 4.66 are just the experimental uncertainties, including statistical and systematic uncertainties. Surprisingly, our NLO result from equation 4.62 coincides only with the one from the H1 collaboration, where normalized data was used, even though we employed absolute data. The value of the H1 collaboration obtained by using absolute cross section data lies in between our NLO result from equation 4.62 and our NNLO result from equation 4.63.

5. Conclusion and outlook

The aim of this thesis was to calculate the inclusive jet production cross section in neutral-current deep inelastic scattering experiments to approximate NNLO, using the theory of quantum chromodynamics for describing the hadronic interaction. The basic features of this theory were presented, and by means of renormalization and factorization properties it was shown, why a perturbative approach is effective for calculating scattering processes including hadrons. Particularly, the running of the strong coupling constant guaranteed the usefulness of perturbation theory at high energies. In fact, the quark-parton model was justified in the field theoretical context. The cancellation of mass singularities lead to the need of resumming to all orders contributions otherwise spoiling the perturbative expansion at partonic threshold. By the re-expansion of the resummed partonic cross section Kidonakis could derive master formulas, predicting NLO and NNLO contributions to any partonic cross section [2]. These master formulas were evaluated and incorporated into the Fortran program JetViP to extend the calculation to NNLO accuracy.

Before that, the program was modified to reproduce the NLO analysis of the H1 collaboration of inclusive jet cross section data, measured double differentially in the virtuality of the exchanged photon and the jet transverse momentum at the HERA collider in Hamburg. For that purpose, several changes to the code had to be made. The kinematical conditions were adopted properly, what amongst other things meant to include the geometric properties of the H1 detector by cuts on the leptonic and the jet phase space. Apart from that, the technical parameters of the underlying NLO calculation had to be defined just in the same way, like, for instance, the renormalization and the factorization scale. Also the right proton parton distribution function and the correct jet algorithm had to be used. The phase space slicing cut parameter was chosen to achieve the best numerical stability. In the end, the output of the program had to be multiplied by correction factors to allow for electroweak corrections and hadronization effects in the final state. It was found excellent agreement between the H1 analysis and our full NLO calculation. Remarkably, our results exhibit a quite smaller scale uncertainty in the high transverse momentum regime.

Having adjusted the NLO calculation to the experimental environment, the NNLO contributions could be implemented. The first step towards this was to compare the coefficients appearing in the NLO master formula to the full NLO calculation. All terms predicted by the resummation approach should be present in the NLO virtual and real corrections. Regarding the scale-dependent terms total agreement was found. All predicted terms were identified analytically. Some scale-independent terms, in contrast, could not be find. They all stem from summations over final-state partons in the formulas of Kidonakis. We think that they are not present in the full NLO calculation, because phase space slicing is used there, producing terms depending on the cut param-

eter instead, which of course cannot be comprised in the NLO master formula. Other terms differed by a factor of 2, caused by this factor in the term $2\text{Re}(\Gamma_S^{(1)})$ contributing to the coefficient c_2 . This problem already arrived in previous work on jet photoproduction [51]. Nevertheless, up to the problems mentioned above, there was otherwise good agreement, and using the coefficients of the master formulas as predicted by Kidonakis in the NNLO master formula provided us with an extension of our calculation to approximate NNLO accuracy. A single term in the part proportional to the delta function in the NNLO master formula had to be discarded though, as it produced way too big contributions.

It turned out that the cross section was significantly reduced in comparison to the NLO results. Regarding the cross section differential in the transverse momentum, this gave rise to a better description of the experimental data. In contradiction to our expectation, the scale-dependence was not diminished by taking into account the higher-order contributions. By a global fit to the data the strong coupling constant at the mass of the Z boson was determined with NLO and NNLO accuracy. Consequently to the observation that the theoretical cross section prediction was reduced by the NNLO contributions, the final value of the coupling constant was shifted towards higher values in comparison to our NLO result. The scale uncertainty was not included in the determination of the coupling constant, because the accuracy would not been enhanced by the NNLO contributions.

There are some ways by which one might be able to improve the current results. For example, it could be worthwhile to compare the predictions of Kidonakis to the NLO corrections of other groups that in best case scenario were calculated without making use of phase space slicing. It would be interesting to see, if terms of the resummation approach that did not coincide with our NLO calculation, will be present there. Also the effect of the already mentioned discarded term could be studied alternatively by means of a second set of virtual corrections, on which that term depends predominantly. As long as the full NNLO calculation to jet production in deep inelastic scattering is still missing, another possibility to improve the results could be to additionally implement a master formula for NNNLO soft and virtual corrections in hard scattering processes near threshold, published by Kidonakis [52]. In our case, since the NNLO contributions already extended the running time of the Fortran program by a factor of 5 to 10, it will be necessary to speed up the event generation before adding once more terms, to obtain results in a reasonable amount of time, for instance, within a master's project. Of course, the NNNLO contributions are in principle to reduce the scale uncertainty, since the over-all correction to the cross section will be even smaller than the NNLO corrections.

A. Conventions

All formulas in this thesis are given in natural units, i.e.,

$$\hbar = c = 1. \quad (\text{A.1})$$

Thus we have

$$[\text{length}] = [\text{time}] \quad (\text{A.2})$$

and

$$[\text{energy}] = [\text{mass}]. \quad (\text{A.3})$$

Finally, both dimensions are inverse

$$[\text{length}] = [\text{mass}]^{-1}. \quad (\text{A.4})$$

We make use of the Einstein summation convention. Each time an index appears twice, its summation is implied.

The gamma function is defined by

$$\Gamma(t) = \int_0^\infty x^{t-1} e^{-x} dx, \quad (\text{A.5})$$

being identical to the factorial function

$$\Gamma(n) = (n-1)!, \quad (\text{A.6})$$

for all positive integers n . The beta function is defined by

$$B(x, y) = \int_0^1 t^{x-1} (1-t)^{y-1} dt \quad \text{for} \quad \text{Re}(x), \text{Re}(y) > 0. \quad (\text{A.7})$$

If x and y are positive integers, the beta function is connected to the gamma function by

$$B(x, y) = \frac{\Gamma(x)\Gamma(y)}{\Gamma(x+y)}. \quad (\text{A.8})$$

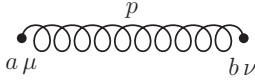
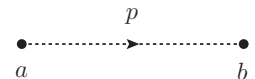
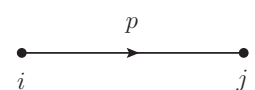
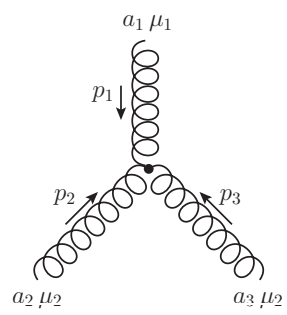
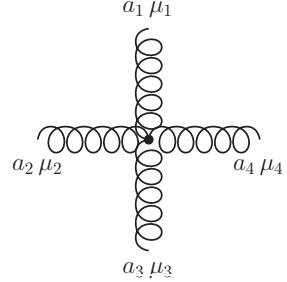
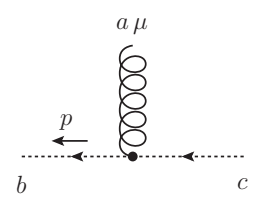
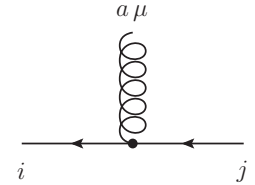
The fourvector γ^μ has as entries the Dirac matrices. The defining property of that 4×4 matrices is the *Clifford algebra*

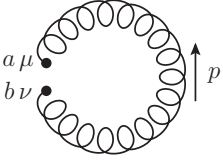
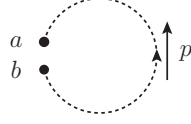
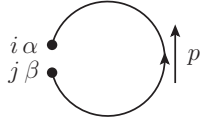
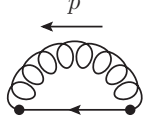
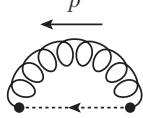
$$\gamma^\mu \gamma^\nu + \gamma^\nu \gamma^\mu = 2g^{\mu\nu} \mathbb{1}_4, \quad (\text{A.9})$$

where $g^{\mu\nu}$ is the usual metric tensor and $\mathbb{1}_4$ is the four dimensional identity matrix. A scalar product in Minkowski space of any fourvector p^μ with γ_μ is shortened by using the *slash notation*

$$p \cdot \gamma = p^\mu \gamma_\mu = \not{p}. \quad (\text{A.10})$$

B. Feynman rules for QCD

Gluon propagator		$\frac{\delta_{ab}}{p^2} d_{\mu\nu}$
Ghost propagator		$\frac{-\delta_{ab}}{p^2}$
Quark propagator		$\delta_{ij} \frac{\not{p} + m}{p^2 - m^2}$
3-gluon vertex		$-ig f^{a_1 a_2 a_3} V_{\mu_1 \mu_2 \mu_3}(p_1, p_2, p_3)$
4-gluon vertex		$-g^2 W_{\mu_1 \mu_2 \mu_3 \mu_4}^{a_1 a_2 a_3 a_4}$
Gluon-ghost vertex		$-ig f^{abc} p_\mu$
Gluon-quark vertex		$g \gamma_\mu T_{ij}^a$

Gluon loop		$\int \frac{d^4 p}{(2\pi)^4 i} \delta^{ab} g^{\mu\nu}$
Ghost loop		$-\int \frac{d^4 p}{(2\pi)^4 i} \delta^{ab}$
Quark loop		$-\int \frac{d^4 p}{(2\pi)^4 i} \delta^{ab}$
Gluon-quark loop		$\int \frac{d^4 p}{(2\pi)^4 i}$
Gluon-ghost loop		$\int \frac{d^4 p}{(2\pi)^4 i}$

The QCD Feynman rules are taken from [5].

For the quark propagator the tensor

$$d_{\mu\nu} = g_{\mu\nu} - (1 - \xi) \frac{p_\mu p_\nu}{p^2} \quad (\text{B.1})$$

was defined. For the 3-gluon vertex the function

$$V_{\mu_1 \mu_2 \mu_3}(p_1, p_2, p_3) \equiv \left((p_1 - p_2)_{\mu_3} g_{\mu_1 \mu_2} + (p_2 - p_3)_{\mu_1} g_{\mu_2 \mu_3} + (p_3 - p_1)_{\mu_2} g_{\mu_3 \mu_1} \right) \quad (\text{B.2})$$

and for the 4-gluon vertex the function

$$W_{\mu_1 \mu_2 \mu_3 \mu_4}^{a_1 a_2 a_3 a_4} \equiv \left((f^{13,24} - f^{14,32}) g_{\mu_1 \mu_2} g_{\mu_3 \mu_4} + (f^{12,34} - f^{14,23}) g_{\mu_1 \mu_3} g_{\mu_2 \mu_4} \right. \\ \left. + (f^{13,42} - f^{12,34}) g_{\mu_1 \mu_4} g_{\mu_3 \mu_2} \right) \quad (\text{B.3})$$

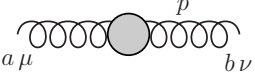
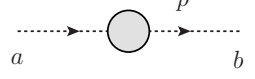
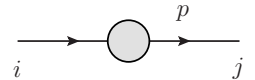
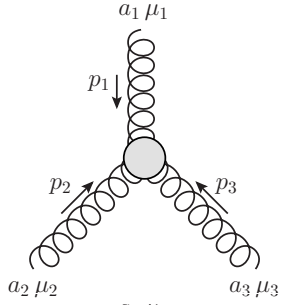
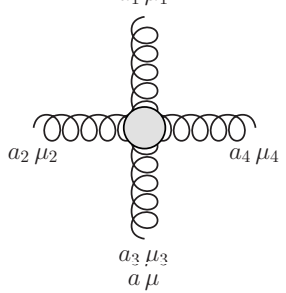
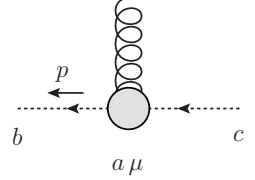
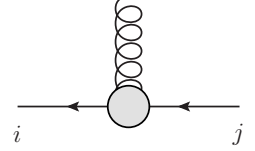
with

$$f^{ij,kl} = f^{a_i a_j a} f^{a_k a_l a} \quad (\text{B.4})$$

were defined. If the following gluon-structures appear, a symmetry factor has to be inserted:

$$\begin{array}{c} \text{Diagram 1: A circle of eight gluon loops with two external lines.} \end{array} \rightarrow \frac{1}{2!} \quad \left| \quad \begin{array}{c} \text{Diagram 2: A circle of four gluon loops with two external lines.} \end{array} \rightarrow \frac{1}{2!} \quad \left| \quad \begin{array}{c} \text{Diagram 3: A circle of six gluon loops with two external lines.} \end{array} \rightarrow \frac{1}{3!}$$

The additional Feynman-rules from the counter terms in the renormalized Lagrangian (here indicated by a grey dot) are the following [5]:

	$(Z_3 - 1)\delta_{ab} (p_\mu p_\nu - p^2 g_{\mu\nu})$
	$(\tilde{Z}_3 - 1)\delta_{ab} p^2$
	$[(Z_2 - 1)\not{p} - (Z_2 Z_m - 1)m_r] \delta_{ij}$
	$(Z_1 - 1)(-ig)g_r f^{a_1 a_2 a_3} V_{\mu_1 \mu_2 \mu_3}(p_1, p_2, p_3)$
	$(Z_4 - 1)(-1)g_r^2 W_{\mu_1 \mu_2 \mu_3 \mu_4}^{a_1 a_2 a_3 a_4}$
	$(\tilde{Z}_1 - 1)(-i)g_r f^{abc} p_\mu$
	$(Z_{1F} - 1)g_r T_{ij}^a \gamma_\mu$

C. Hadronic ep cross section

In the one-photon-exchange approximation neglecting the electron mass the inclusive electron-proton cross section can be written as [29]

$$d\sigma = \frac{(4\pi\alpha)^2}{Q^4} \frac{4\pi M}{4(k \cdot p)} L_{\mu\nu} W^{\mu\nu} \frac{d^3k'}{2E'(2\pi)^3}, \quad (\text{C.1})$$

where α is the electromagnetic coupling constant, Q^2 the virtuality of the exchanged photon, M and p the proton mass and its momentum and k and k' the momentum of the incoming and outgoing electron respectively. The energy of the electron is E before and E' after the collision. The lepton tensor $L_{\mu\nu}$ can be determined by the Feynman rules for QED to be

$$L^{\mu\nu} = \frac{1}{2} \sum_{s,s'} (\bar{u}(k', s') \gamma^\mu u(k, s)) (\bar{u}(k', s') \gamma^\nu u(k, s))^*. \quad (\text{C.2})$$

Here s and s' denote the spin of the electron. The summation over the spins is present, because we sum over initial state electron spins and average over final state electron spins. Using

$$(\bar{u}_1 \gamma^\mu u_2)^* = (\bar{u}_1 \gamma^\mu u_2)^\dagger = \bar{u}_2 \gamma^\mu u_1, \quad (\text{C.3})$$

the completeness relation for the Dirac spinors

$$\sum_s u(p, s) \bar{u}(p, s) = \not{p} + m \quad (\text{C.4})$$

and usual trace algebra of Dirac matrices we find

$$L^{\mu\nu} = 2(k'^\mu k^\nu + k^\mu k'^\nu + \frac{q^2}{2} g^{\mu\nu}). \quad (\text{C.5})$$

It is useful to note that

$$\bar{u}(k', s') \gamma^\mu u(k, s) \sim \langle k', s' | \hat{j}_{em}^\mu(e) | k, s \rangle, \quad (\text{C.6})$$

where $\hat{j}_{em}^\mu(e)$ is the electromagnetic current operator for the electron. Current conservation tells us that

$$\partial_\mu \hat{j}_{em}^\mu(e) = 0. \quad (\text{C.7})$$

providing the condition

$$q_\mu (\bar{u}(k', s') \gamma^\mu u(k, s)) = 0 \quad (\text{C.8})$$

in momentum space. Therefore we can write

$$q_\mu L^{\mu\nu} = q_\nu L^{\mu\nu} = 0. \quad (\text{C.9})$$

We do not want to make any assumptions on the inner structure of the proton. Hence, we express the hadron tensor $W^{\mu\nu}$ with the help of structure functions. The question is how many of those functions we need, or rather, what the tensor structure of the hadron tensor is, since the structure functions are scalar functions multiplied to any tensor that $W^{\mu\nu}$ is made of. To answer that question, we use the information we got. Before the scattering we have a proton P with momentum p and after scattering we have any hadronic state X with momentum $p' = p + q$. The hadron couples to the electron electromagnetically. Hence, we can define $W^{\mu\nu}$ accordingly to $L^{\mu\nu}$ by an electromagnetic current. We write

$$e^2 W^{\mu\nu} \sim \sum_{r,r'} \sum_X \langle p, r | \hat{j}_{em}^\mu(P) | X, p' \rangle \langle X, p' | \hat{j}_{em}^\nu(P) | p, r \rangle. \quad (\text{C.10})$$

r and r' are the proton spins before and after scattering and $\hat{j}_{em}^\mu(P)$ is the electromagnetic current operator for the proton. Since $W^{\mu\nu}$ is built out of this current, it should follow the current conservation law in the same manner as $L^{\mu\nu}$ does. We deduce

$$q_\mu W^{\mu\nu} = q_\nu W^{\mu\nu} = 0. \quad (\text{C.11})$$

Using the fourvectors playing a role in the process, one can only find two possible combinations to construct a Lorentz and parity invariant tensor of rank two.¹ The combinations are

$$\left[p^\mu - \frac{(p \cdot q)}{q^2} q^\mu \right] \cdot \left[p^\nu - \frac{(p \cdot q)}{q^2} q^\nu \right] \quad \text{and} \quad -g^{\mu\nu} + \frac{q^\mu q^\nu}{q^2}. \quad (\text{C.12})$$

We then can parametrize $W^{\mu\nu}$ by

$$W^{\mu\nu} = \frac{1}{M^2} W_2(Q^2, \nu) \left[p^\mu - \frac{(p \cdot q)}{q^2} q^\mu \right] \left[p^\nu - \frac{(p \cdot q)}{q^2} q^\nu \right] + W_1(Q^2, \nu) \left[-g^{\mu\nu} + \frac{q^\mu q^\nu}{q^2} \right]. \quad (\text{C.13})$$

We now have expressions for both tensors. To carry out the contraction we use C.9 to get

$$L_{\mu\nu} W^{\mu\nu} = \frac{1}{M^2} W_2 L_{\mu\nu} p^\mu p^\nu + W_1 L_{\mu\nu} (-g^{\mu\nu}). \quad (\text{C.14})$$

Inserting C.5 gives

$$L_{\mu\nu} W^{\mu\nu} = \frac{2}{M^2} W_2 \left((k' \cdot p)(k \cdot p) + (k \cdot p)(k' \cdot p) + \frac{q^2}{2} (p^2) \right) - 2W_1 \left((k' \cdot k) + (k \cdot k') + 2q^2 \right) \quad (\text{C.15})$$

$$= \frac{4}{M^2} W_2 (k \cdot p)(k' \cdot p) + W_2 \frac{q^2 p^2}{M^2} - 4W_1 (k \cdot k') - 4W_1 q^2. \quad (\text{C.16})$$

¹QED and QCD conserve parity. We do not take into account weak processes with W - and Z -boson exchange. In this case, parity invariance is violated, which admits a third possible combination, what makes it necessary to introduce a third structure function.

From momentum conservation at the $e\gamma^*$ -vertex we get

$$(k - k')^2 = q^2 = -2(k \cdot k'), \quad (\text{C.17})$$

so the result simplifies to

$$L_{\mu\nu}W^{\mu\nu} = \frac{4}{M^2}W_2(k \cdot p)(k' \cdot p) - 2W_2\frac{(k \cdot k')p^2}{M^2} + 4W_1(k \cdot k'). \quad (\text{C.18})$$

To calculate further we go into the rest frame of the incoming proton, where the momenta are

$$p = (M, 0, 0, 0), \quad k = (E, 0, 0, E), \quad k' = (E', k'_x, k'_y, E' \cos \theta), \quad (\text{C.19})$$

θ being the polar angle of the outgoing electron. The scalar products are then

$$p^2 = M^2, \quad k \cdot p = EM, \quad k' \cdot p = E'M, \quad k \cdot k' = EE'(1 - \cos \theta). \quad (\text{C.20})$$

Inserting these expressions leads to

$$\begin{aligned} L_{\mu\nu}W^{\mu\nu} &= 4W_2EE' - 2W_2EE'(1 - \cos \theta) + 4W_1EE'(1 - \cos \theta) \\ &= 2W_2EE'(1 + \cos \theta) + 4W_1EE'(1 - \cos \theta) \\ &= 4EE' \left[W_2 \cos^2 \left(\frac{\theta}{2} \right) + 2W_1 \sin^2 \left(\frac{\theta}{2} \right) \right]. \end{aligned} \quad (\text{C.21})$$

Finally, we put the above expressions into C.1 to get the inclusive cross section in the proton rest frame.

$$\begin{aligned} d\sigma &= \frac{(4\pi\alpha)^2}{16E^2E'^2 \sin^4 \left(\frac{\theta}{2} \right)} \frac{4\pi M}{4EM} 4EE' \left[W_2 \cos^2 \left(\frac{\theta}{2} \right) + 2W_1 \sin^2 \left(\frac{\theta}{2} \right) \right] \frac{d^3k'}{2E'(2\pi)^3} \\ &= \frac{\alpha^2}{4E^2E'^2 \sin^4 \left(\frac{\theta}{2} \right)} \left[W_2 \cos^2 \left(\frac{\theta}{2} \right) + 2W_1 \sin^2 \left(\frac{\theta}{2} \right) \right] d^3k' \\ &= \frac{\alpha^2}{4E^2 \sin^4 \left(\frac{\theta}{2} \right)} \left[W_2 \cos^2 \left(\frac{\theta}{2} \right) + 2W_1 \sin^2 \left(\frac{\theta}{2} \right) \right] dE' d\Omega \end{aligned} \quad (\text{C.22})$$

To obtain formula 3.6 we have to express the phase space integration in terms of Q^2 and ν . Therefore, we express the differential solid angle by

$$d\Omega = 2\pi d(\cos \theta), \quad (\text{C.23})$$

and use the relations

$$Q^2 = 2(k \cdot k') = 2EE'(1 - \cos \theta), \quad \nu = \frac{p \cdot q}{M} = q^0 = E - E'. \quad (\text{C.24})$$

The determinant of the Jacobian matrix corresponding to the variable transformation $(\cos \theta, E') \rightarrow (Q^2, \nu)$ is

$$\begin{vmatrix} \frac{\partial Q^2}{\partial \cos \theta} & \frac{\partial Q^2}{\partial E'} \\ \frac{\partial \nu}{\partial \cos \theta} & \frac{\partial \nu}{\partial E'} \end{vmatrix} = \begin{vmatrix} -2EE' & 2k(1 - \cos \theta) \\ 0 & -1 \end{vmatrix} = 2EE', \quad (\text{C.25})$$

so we find

$$dE' d\Omega = \frac{\pi}{EE'} dQ^2 d\nu. \quad (\text{C.26})$$

Inserting the latter expressions leads to the final result

$$\frac{d\sigma}{dQ^2 d\nu} = \frac{\pi\alpha^2}{4E^2 \sin^4\left(\frac{\theta}{2}\right)} \frac{1}{EE'} \left[W_2(Q^2, \nu) \cos^2\left(\frac{\theta}{2}\right) + 2W_1(Q^2, \nu) \sin^2\left(\frac{\theta}{2}\right) \right]. \quad (\text{C.27})$$

D. NNLO coefficients

In table D.1 we state the coefficients c_i appearing in the NLO and NNLO master formulas from equation 4.35 and 4.44 for the two contributing partonic processes. In the left column the coefficients are given as they are predicted by Kidonakis and the threshold formalism, with s being replaced by M^2 , as was motivated in section 4.3. In the right column we show the corresponding coefficients that could be taken from the NLO virtual and real NLO corrections implemented in the code of JetViP. If they conform with the Kidonakis prediction, they are written in green. For c_2 we see a discrepancy by a factor of $1/2$ marked in red. It arises because of the 2 in the term $c_2 = 2\text{Re}(\Gamma_S^{(1)}) + \dots$, which is present in the Kidonakis prediction of that coefficient. In the first column we see terms that could not be identified in the code. They are written in purple. They all come from final-state contributions, i.e., the summation over all final-state partons j . The terms in c_2 arise through the expression $c_2 = -\sum_j B_j^{(1)} + \dots$. The missing terms in c_3 stem from the expression $c_3 = -\sum_j C_{Fj} + \dots$. They are not present in the code, because there the cancellation of mass singularities is carried out with phase space slicing, what instead of giving rise to the above mentioned contributions, produces logarithms containing the phase space slicing cut parameter (see subsection 2.3.1). Obviously, there are no equivalent cut-parameter-depending expressions predicted by threshold resummation.

Table D.1.: Coefficients predicted by the threshold formalism compared to the coefficients that can actually be found in the code of JetViP.

	KIDONAKIS ($s \rightarrow M^2$)	JETVIP ($M^2 = Q^2$)
c_1^μ	$\gamma q \rightarrow qg$	$-\frac{3}{4}C_F \ln\left(\frac{\mu_F^2}{M^2}\right) + \frac{\beta_0}{4} \ln\left(\frac{\mu_R^2}{M^2}\right)$
	$\gamma g \rightarrow q\bar{q}$	$-\frac{\beta_0}{4} \ln\left(\frac{\mu_F^2}{M^2}\right) + \frac{\beta_0}{4} \ln\left(\frac{\mu_R^2}{M^2}\right)$
c_2	$\gamma q \rightarrow qg$	$2C_F \ln\left(\frac{-u}{M^2}\right) + N_C \ln\left(\frac{t}{u}\right) - C_F \ln\left(\frac{\mu_F^2}{M^2}\right) - \frac{3}{4}C_F - \frac{\beta_0}{4}$
	$\gamma g \rightarrow q\bar{q}$	$N_C \ln\left(\frac{tu}{M^4}\right) - N_C \ln\left(\frac{\mu_F^2}{M^2}\right) - \frac{3}{2}C_F$
c_3	$\gamma q \rightarrow qg$	$2C_F$
	$\gamma g \rightarrow q\bar{q}$	$2N_C$

E. Details on the implementation

In listing E.1 you can see the steering file of the program that was modified giving access to the newly implemented calculation methods kNLO and NNLO. For this purpose the flags `iknlo`, `iknnlo` and `ikdelta` were added to the already existing flags `iborn`, `itwo` and `ithree`. Table E.1 shows how to set the flags to get the desired method.¹ `ikdelta = 1` switches on the NNLO contributions proportional to the δ -function. In the final version it is not really necessary anymore that they can be reached separately, but it was helpful to fix bugs in the code. Another modification was made concerning the proton PDF selection. We implemented the LHAPDF interface to the code. The desired PDF has to be selected by its name directly in the code, while the member of the PDF set can be chosen in the steering file in line 34. Actually, that is the only important line in the PDF paragraph of the steering file after the change to LHAPDF, and since for DIS the resolved photon contributions are not relevant. In the lines 47 and 48 we added the option to set a prefactor, by which the central scale choice is multiplied. A bit confusing is that the definition of the scale in line 44 only sets the form of the renormalization scale μ_R , and the factorization scale μ_F can only be changed in the code. This could be modified easily, but we had no need to this, because we did not change the scales besides the prefactors.

The NNLO contributions could be implemented most easily by adding them to the initial-state corrections on the proton-side, where the z -integration was already present. The NNLO terms and the initial-state corrections contain plus distributions of the form

$$\int dz [f(z)]_+ g(z) = \int_{z_{min}}^1 dz f(z) g(z) - g(1) \int_0^1 dz f(z), \quad (\text{E.1})$$

Technically, in the code the corrections are divided into three terms

$$I - I^p + I^d. \quad (\text{E.2})$$

Table E.1.: Correct setting of flags for the different calculation methods.

	LO	NLO	kNLO	NNLO
<code>iborn</code>	1	1	1	1
<code>itwo</code>	0	1	1	1
<code>ithree</code>	0	1	1	1
<code>iknlo</code>	0	0	1	0
<code>iknnlo</code>	0	0	0	1
<code>ikdelta</code>	0	0	0	1

¹We just describe the modifications, since the unmodified pieces are well described in the manual of JetViP [35, 37].

Listing E.1: Modified steering file

```

1  '=====',
2  'CONTRIBUTION',
3  '=====',
4  1      iproc   [1=ep; 2=ee]
5  2      isdr    [1=D; 2=SR; 3=SR*; 4=DR]
6  1      iborn   [2->2 Born]
7  1      itwo    [2->2 singular contributions (for NLO)]
8  1      ithree  [2->3 contribution]
9  0      iknlo   [Kidonakis NLO contribution]
10 1      iknnlo  [Kidonakis NNLO contribution]
11 1      ikdelta [Kidonakis NNLO delta-contr.]
12 0      isplit  [gamma->qq term]
13 0      iqcut   [yqi_min in 2->3 matrices? 1=yes; 0=no]
14 '=====',
15 'INITIAL STATE',
16 '=====',
17 27.6d0    Ea      [energy on side a (ep,ee: lepton)]
18 920.d0    Eb      [energy on side b (ep: proton; ee: lepton)]
19 '-----Lepton a-----',
20 0          iwwa   [Weizs.-Will.: -1,0=ln(Q2mx/Q2mn); 1=ln(thmax/me)]
21 180.d0    thmax  [max angle]
22 '-----Lepton b (only relevant for the ee-case)-----',
23 4.d0      P2max   [P2=virtuality of real photon]
24 0          iwwb   [which Weizs.-Will.: 0=ln(P2mx/P2mn); 1=ln(thmax/me)]
25 180.d0    thebmx [max angle for Weizs.-Will]
26 '=====',
27 'SUBPROCESS',
28 '=====',
29 5.d0      Nf      [Number of active flavours]
30 0.2000d0  lambda  [Lambda_QCD (has to match Nf)]
31 2          ialphas [QCD coupling: 1=one-loop; 2=two-loop; 3=PDFLIB]
32 1.d-4     y-cut   [phase-space-slicing parameter]
33 '-----PDFs for the resolved contributions-----',
34 9          PDF member of MS1W
35 1          idisga  [DISg -> MSbar for photon a]
36 1          ipdftyp [PDF for y*(res): 1=SaS;2=GRS;3=DG;4=PDFLIB]
37 1          igroupa (Param. for SaS or PDFLIB -> see manual)
38 0          iseta   ( )
39 0
40 0          idisgb  [DISg -> MSbar for photon b]
41 4          igroupb [authors of PDF on side b: y(res) or prot]
42 46         isetb   [Set-No]
43 '-----Scales-----',
44 0.d0      a       [Scale: mu^2=a+b*Q^2+c*pt^2]
45 0.5d0     b
46 0.5d0     c
47 1.0d0     scvarR   [Scale: mu_R=scvarR*mu_R]
48 1.0d0     scvarF   [Scale: mu_F=scvarF*mu_F]
49 '=====',
50 'PHASE SPACE INTEGRATION',
51 '=====',
52 150.d0     Q2min   [0.d0 selects photoproduction]
53 15000.d0   Q2max
54 0.2d0      ymin    [min y]
55 0.7d0      ymax    [max y]
56 7.d0       ptmin   [ptmin for parton in hadr cms; =Etjet_min/2]
57 '=====',
58 'VEGAS and OUTPUT',
59 '=====',
60 100000000  ipoin   [no of events produced in phase space above]
61 20         itt      [no of iterations]
62 ''        jfileout [Filename]

```

I contains everything that depends on z , but from the appearing plus distribution it just contains the first integral. The second integrals of all plus distributions are packed in I^p . I^d includes all terms that either do not depend on the integration variable z , or whose z -integration was carried out analytically before entering the code. Consequently, I^d is not integrated over z numerically. For the NNLO contributions that applies to the terms being proportional to $\delta(1-z)$. Yet, because of the choice of the boundaries in equation E.1, some counter terms had to be included additionally if a plus distribution is present. The reason is that the first and the second integration have different lower integration boundaries. The numerical integration is performed from z_{min} to 1 for both terms, i.e.,

$$\int_{z_{min}}^1 dz \{f(z)g(z) - f(z)g(1)\}, \quad (\text{E.3})$$

so we have to compensate for the missing part from $0 < z < z_{min}$ of the second term in equation E.1, by solving the integral

$$I^{CT} = g(1) \int_0^{z_{min}} dz f(z) \quad (\text{E.4})$$

analytically and supplementarily subtracting it for every appearing plus distribution,

$$[f(z)]_+ g(z) = \int_{z_{min}}^1 dz \{f(z)g(z) - f(z)g(1)\} - I^{IC}. \quad (\text{E.5})$$

I^{CT} are the counter terms that are put into I^d .

For the NNLO and kNLO contributions we needed counter terms for functions of the form

$$f(z) = \mathcal{D}_l(z) = \frac{\ln^l(1-z)}{1-z}, \quad (\text{E.6})$$

where $l = 0, 1, 2, 3$ and $0 \leq z \leq 1$. We find by integration by substitution

$$\begin{aligned} \int_0^{z_{min}} dz \mathcal{D}_l(z) &= \int_0^{z_{min}} dz \frac{\ln^l(1-z)}{1-z} = \int_{u(z_{min})}^{u(0)} du \frac{\ln^l(u)}{u} \\ &= \int_{v(u(z_{min}))}^{v(u(0))} (u dv) \frac{v^l}{u} = \int_{v(u(z_{min}))}^{v(u(0))} dv v^l \\ &= \left[\frac{1}{l+1} v^{l+1} \right]_{v(u(z_{min}))}^{v(u(0))} = -\frac{1}{l+1} \ln^{l+1}(1-z_{min}). \end{aligned} \quad (\text{E.7})$$

F. Further plots

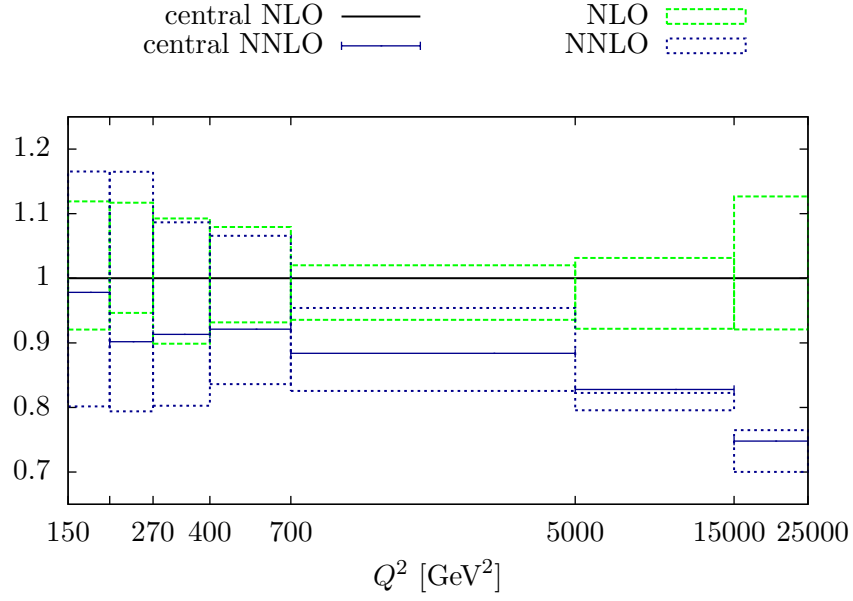


Figure F.1.: Results for the differential cross section $d\sigma/dQ^2$ normalized to central NLO for Q^2 -values even higher than those being observed by the H1 collaboration [1]. The error bands are due to scale variation. The plot confirms the observation that NNLO contributions reduce the scale uncertainty for high Q^2 . Because of bigger statistical errors of the integration routine due to the drastically falling scaling behavior of the cross section with increasing Q^2 , the absolute value of the data should not be taken too seriously, but the tendency mentioned above is clearly present.

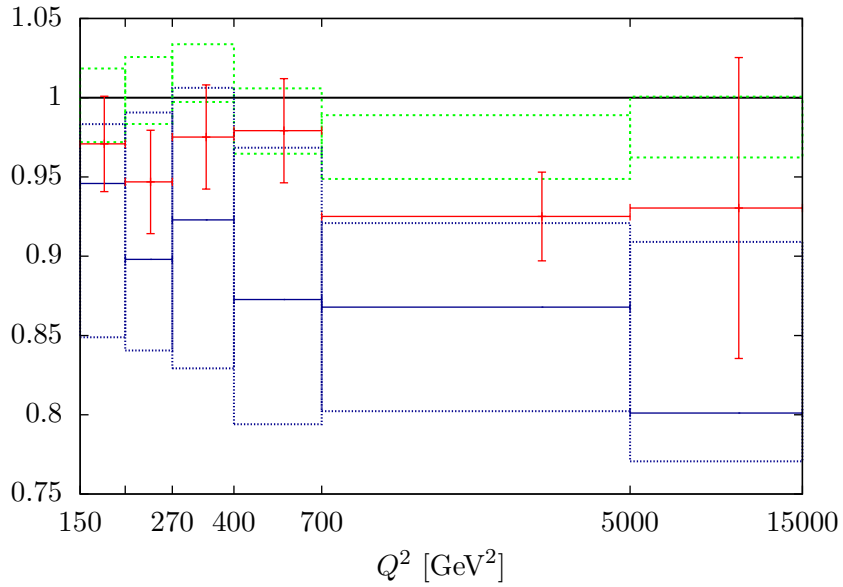
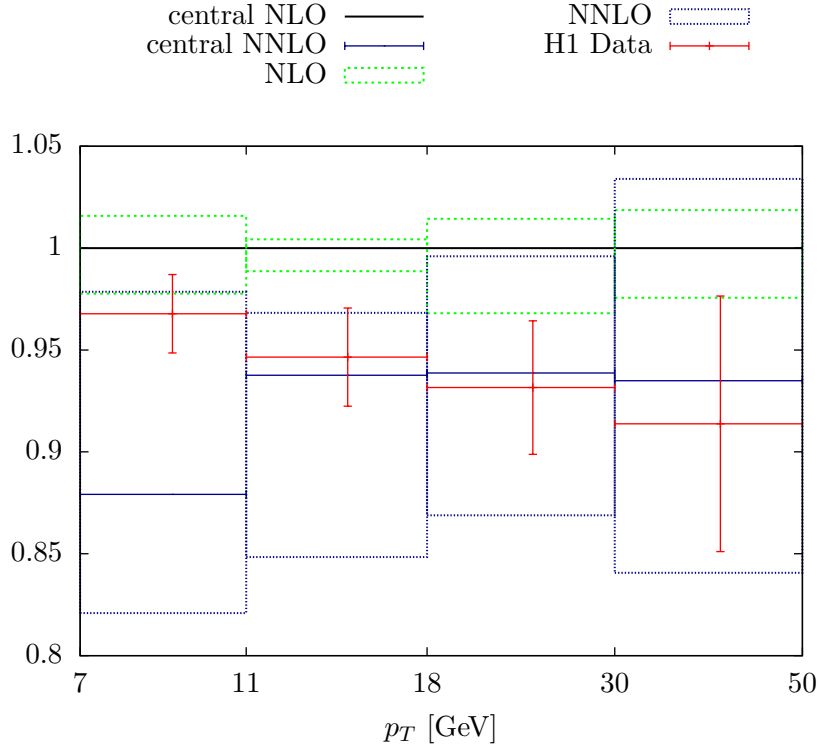


Figure F.2.: NNLO and NLO results with error bands obtained by variation of just μ_F by a factor of 1/2 and 2 compared to H1 data.

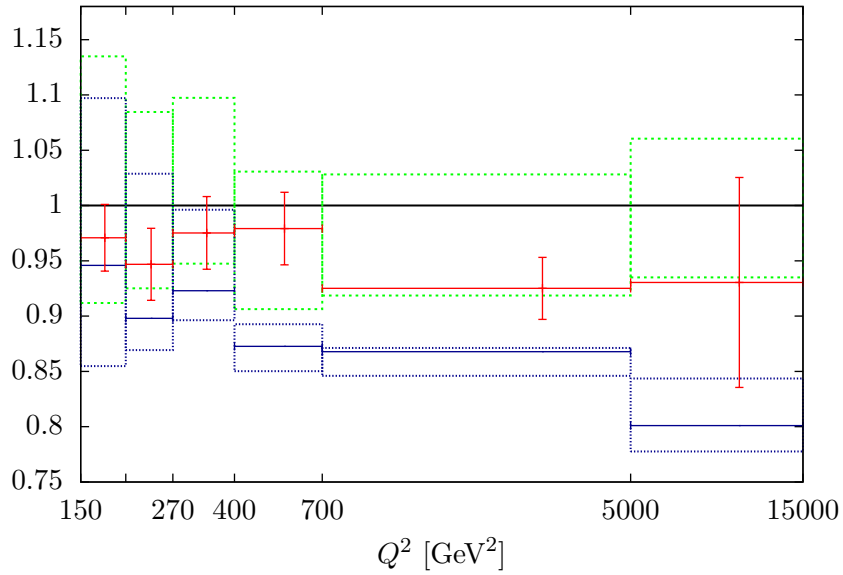
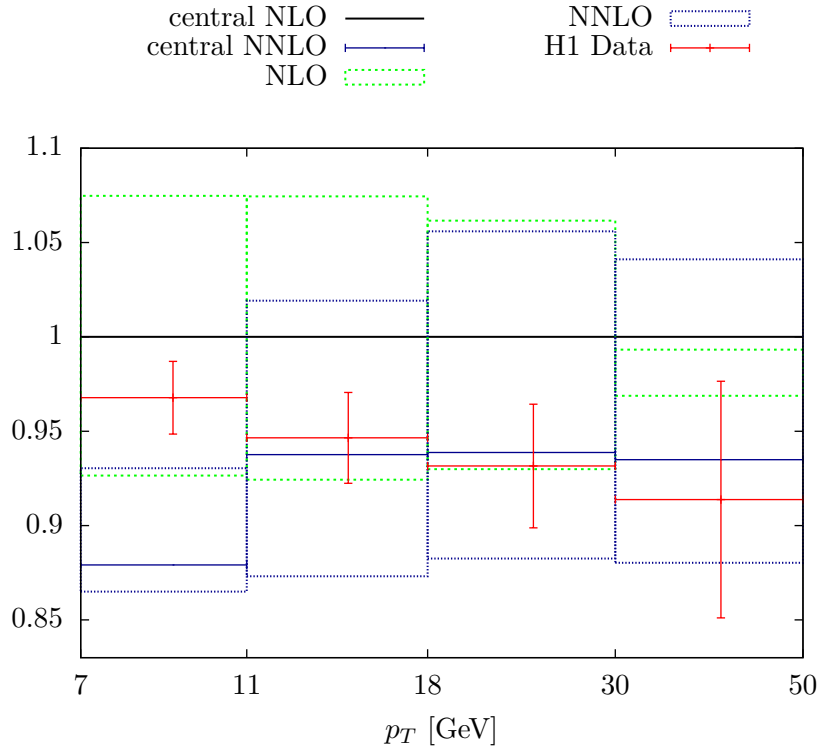


Figure F.3.: NNLO and NLO results with error bands obtained by variation of just μ_R by a factor of 1/2 and 2 compared to H1 data.

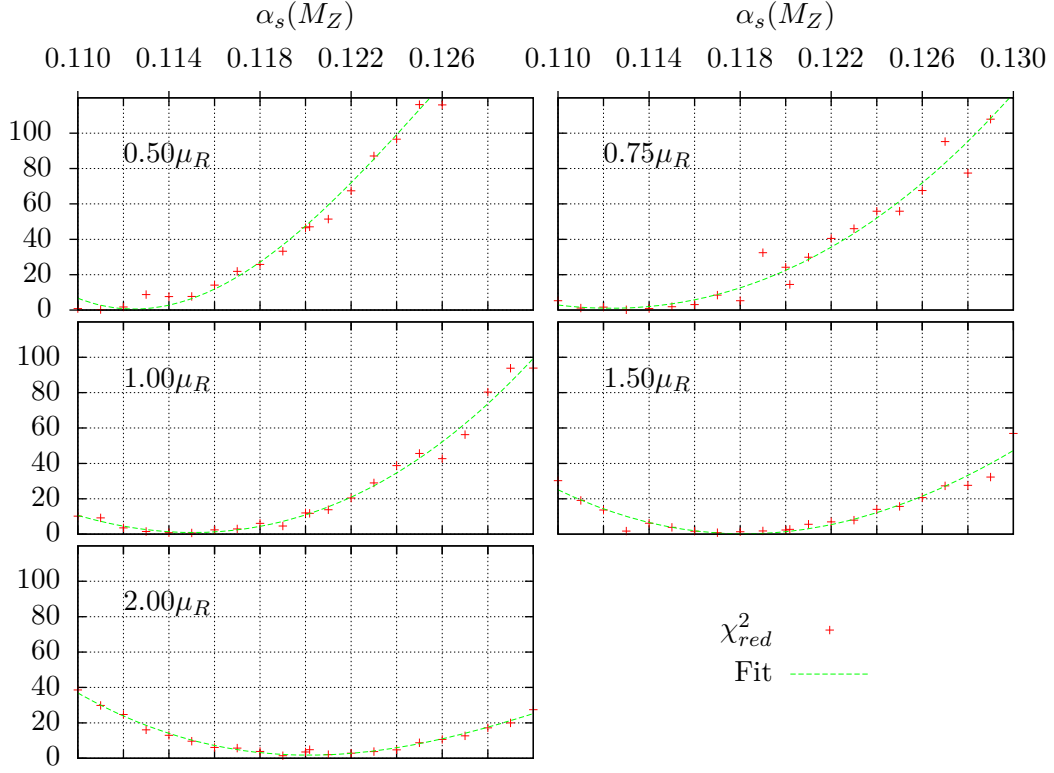


Figure F.4.: It is shown χ_{red}^2 of the theoretical NLO predictions for the p_T -distribution, plotted as a function of $\alpha_s(M_Z)$, whose values could be run through by separately evaluating the NLO calculation with each member of the fixed- α_s NLO PDF set of the MSTW group [44]. Each plot shows the data for different choices of the renormalization scale μ_R . The central value $\mu_R = \sqrt{p_T^2 + Q^2}$ is varied by the prefactor depicted in the corresponding plot.

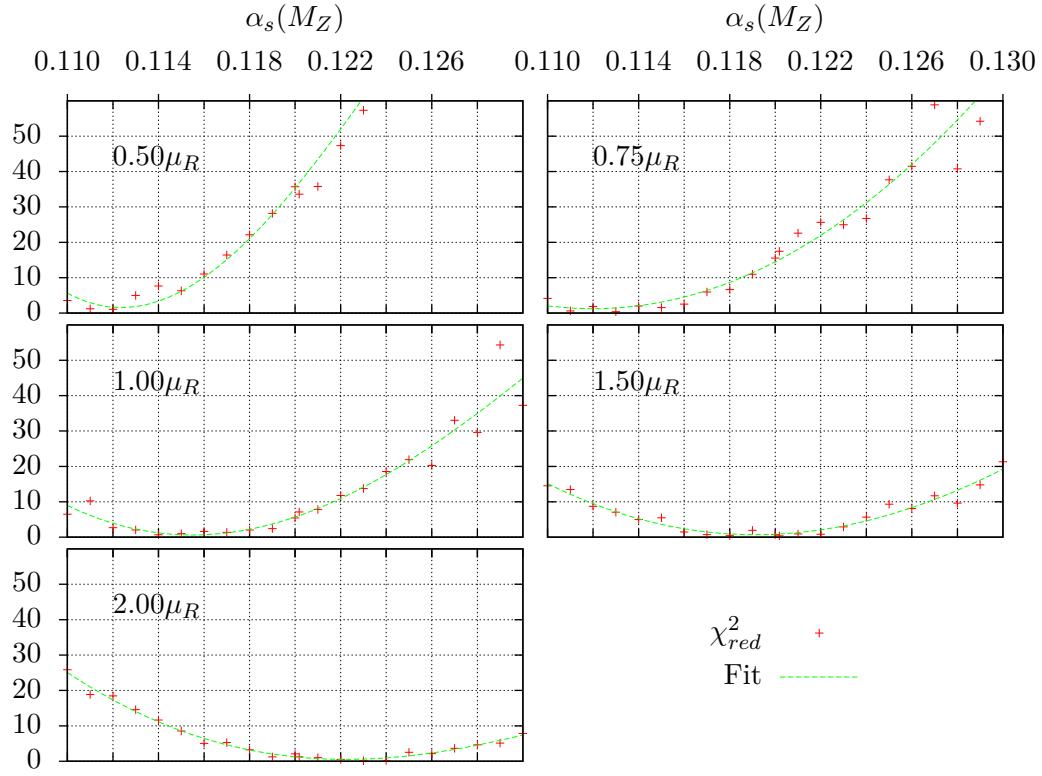


Figure F.5.: It is shown χ^2_{red} of the theoretical NLO predictions for the Q^2 -distribution, plotted as a function of $\alpha_s(M_Z)$, and for different choices of the renormalization scale μ_R .

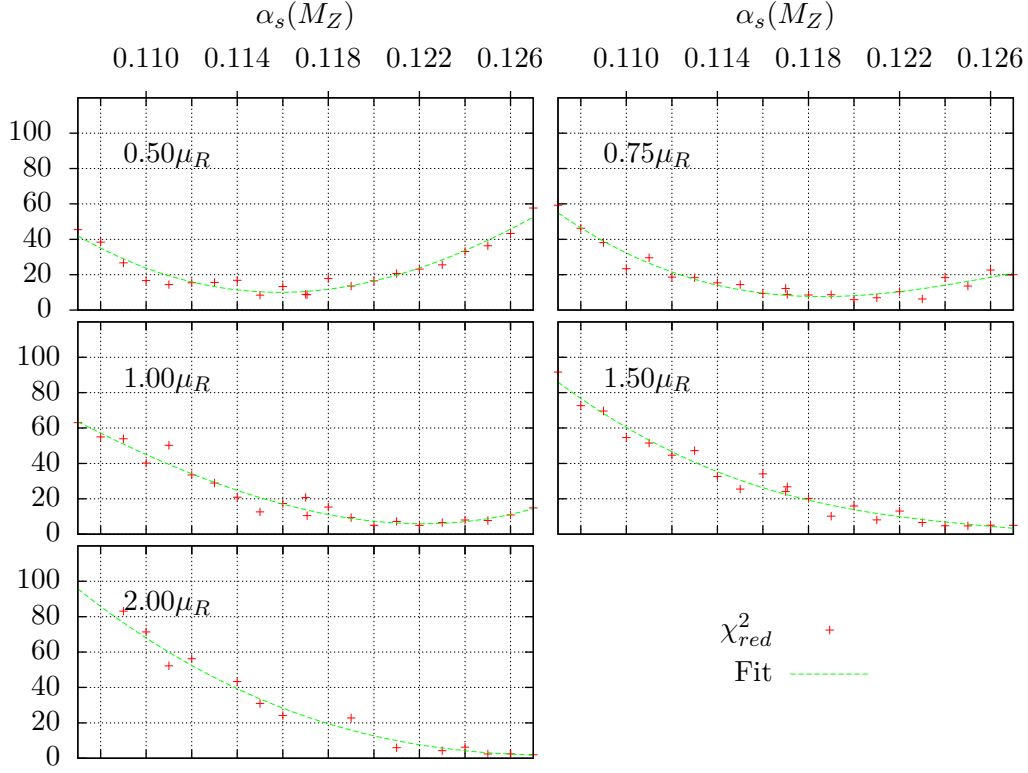


Figure F.6.: It is shown χ_{red}^2 of the theoretical NNLO predictions for the p_T -distribution, plotted as a function of $\alpha_s(M_Z)$, and for different choices of the renormalization scale μ_R . Comparing to the NLO results depicted in figure F.4, χ_{red}^2 takes its minimum at higher values of $\alpha_s(M_Z)$. Additionally, one can see higher statistical fluctuations due to the Monte-Carlo integration.

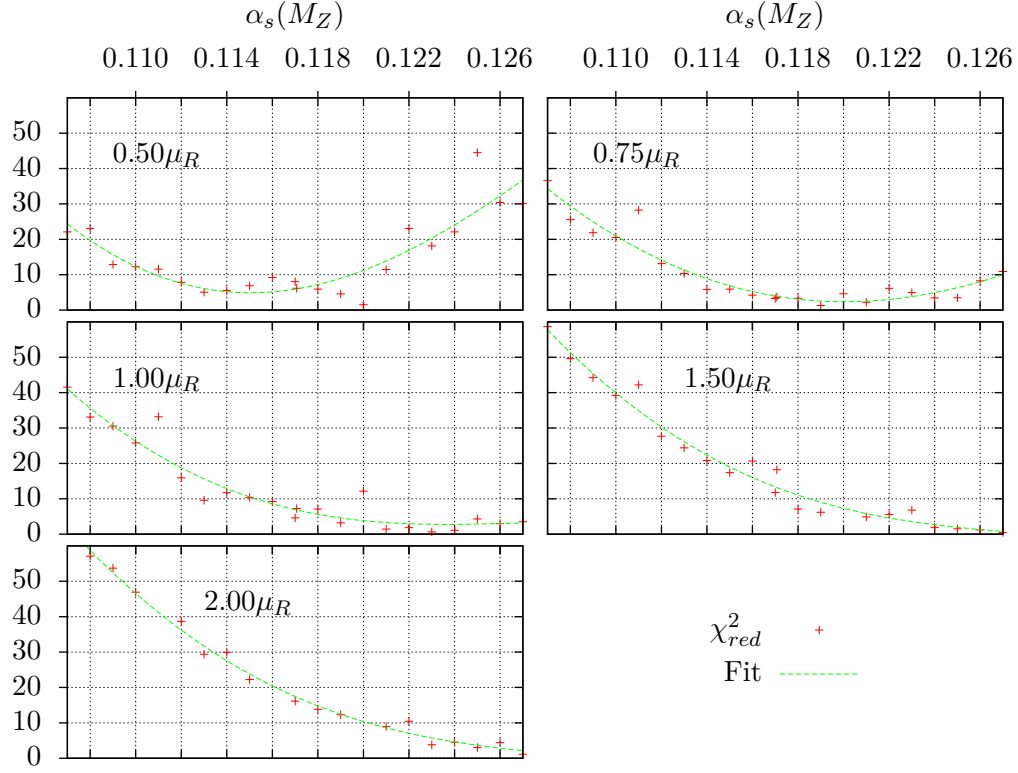


Figure F.7.: It is shown χ_{red}^2 of the theoretical NNLO predictions for the Q^2 -distribution, plotted as a function of $\alpha_s(M_Z)$, and for different choices of the renormalization scale μ_R . Comparing to the NLO results depicted in figure F.5, χ_{red}^2 takes its minimum at higher values of $\alpha_s(M_Z)$. Additionally, one can see higher statistical fluctuations due to the Monte-Carlo integration.

References

- [1] D. A. Britzger, “Regularized Unfolding of Jet Cross Sections in Deep-Inelastic ep Scattering at HERA and Determination of the Strong Coupling Constant,”.
- [2] N. Kidonakis, “A Unified approach to NNLO soft and virtual corrections in electroweak, Higgs, QCD, and SUSY processes,” *Int.J.Mod.Phys.* **A19** (2004) 1793–1821, [arXiv:hep-ph/0303186](#) [hep-ph].
- [3] M. Gell-Mann, “The Eightfold Way: A Theory of strong interaction symmetry,”.
- [4] W. A. Bardeen, H. Fritzsch, and M. Gell-Mann, “Light cone current algebra, π^0 decay, and $e^+ e^-$ annihilation,” [arXiv:hep-ph/0211388](#) [hep-ph].
- [5] T. Muta, *Foundations of Quantum Chromodynamics*. World Scientific Publishing Co Pte Ltd, 1987.
- [6] E. Laenen, “Resummation.” Slides of talk given at the Theory Meeting, Nikhef, Amsterdam, Sept. 14, 2007.
http://www.nikhef.nl/pub/theory/center-talks/ericlaenen_14-9-07.pdf.
- [7] M. Klasen, *Theoretical Review of Hard Photoproduction*. 2001.
<http://books.google.de/books?id=vLk-PgAACAAJ>.
- [8] G. ’t Hooft and M. Veltman, “Regularization and renormalization of gauge fields,” *Nuclear Physics B* **44** no. 1, (1972) 189 – 213.
<http://www.sciencedirect.com/science/article/pii/0550321372902799>.
- [9] T. van Ritbergen, J. Vermaseren, and S. Larin, “The Four loop beta function in quantum chromodynamics,” *Phys.Lett.* **B400** (1997) 379–384,
[arXiv:hep-ph/9701390](#) [hep-ph].
- [10] **Particle Data Group** Collaboration, S. Bethke, G. Dissertori, and G. P. Salam, “Review of Particle Physics,” *Phys. Rev. D* **86** (Jul, 2012) 010001.
<http://link.aps.org/doi/10.1103/PhysRevD.86.010001>.
- [11] F. Bloch and A. Nordsieck, “Note on the radiation field of the electron,” *Phys. Rev.* **52** (Jul, 1937) 54–59. <http://link.aps.org/doi/10.1103/PhysRev.52.54>.
- [12] T. Kinoshita, “Mass singularities of Feynman amplitudes,” *J.Math.Phys.* **3** (1962) 650–677.
- [13] T. Lee and M. Nauenberg, “Degenerate systems and mass singularities,” *Phys. Rev.* **133** (Mar, 1964) B1549–B1562.
<http://link.aps.org/doi/10.1103/PhysRev.133.B1549>.

- [14] B. Potter, *Inclusive Single- and Dijet Rates in Next-to-Leading Order QCD for γ^*p and $\gamma^*\gamma$ Collisions*. PhD thesis, Institute for Theoretical Physics, University of Hamburg, 1997.
- [15] M. Furman, “Study of a non-leading {QCD} correction to hadron calorimeter reactions,” *Nuclear Physics B* **197** no. 3, (1982) 413 – 445.
<http://www.sciencedirect.com/science/article/pii/0550321382904527>.
- [16] M. Bonvini, “Resummation of soft and hard gluon radiation in perturbative QCD,” [arXiv:1212.0480](https://arxiv.org/abs/1212.0480) [hep-ph].
- [17] H. Baer, J. Ohnemus, and J. Owens, “Next-to-leading-logarithm calculation of jet photoproduction,” *Phys. Rev. D* **40** (Nov, 1989) 2844–2855.
<http://link.aps.org/doi/10.1103/PhysRevD.40.2844>.
- [18] S. Catani and M. Seymour, “A General algorithm for calculating jet cross-sections in NLO QCD,” *Nucl.Phys.* **B485** (1997) 291–419, [arXiv:hep-ph/9605323](https://arxiv.org/abs/hep-ph/9605323) [hep-ph].
- [19] Z. Kunszt and D. Soper, “Calculation of jet cross sections in hadron collisions at order α_s^3 ,” *Phys. Rev. D* **46** (Jul, 1992) 192–221.
<http://link.aps.org/doi/10.1103/PhysRevD.46.192>.
- [20] J. C. Collins, D. E. Soper, and G. F. Sterman, “Factorization of Hard Processes in QCD,” *Adv.Ser.Direct.High Energy Phys.* **5** (1988) 1–91,
[arXiv:hep-ph/0409313](https://arxiv.org/abs/hep-ph/0409313) [hep-ph].
- [21] G. S. et al., “Handbook of perturbative QCD,” *Rev. Mod. Phys.* **67** (Jan, 1995) 157–248. <http://link.aps.org/doi/10.1103/RevModPhys.67.157>.
- [22] G. F. Sterman, “Approaching the final state in perturbative QCD,” *Int.J.Mod.Phys.* **A18** (2003) 4329–4342, [arXiv:hep-ph/0301243](https://arxiv.org/abs/hep-ph/0301243) [hep-ph].
- [23] N. Kidonakis, G. Oderda, and G. F. Sterman, “Threshold resummation for dijet cross-sections,” *Nucl.Phys.* **B525** (1998) 299–332, [arXiv:hep-ph/9801268](https://arxiv.org/abs/hep-ph/9801268) [hep-ph].
- [24] V. Gribov and L. Lipatov, “Deep inelastic e p scattering in perturbation theory,” *Sov.J.Nucl.Phys.* **15** (1972) 438–450.
- [25] G. Altarelli and G. Parisi, “Asymptotic freedom in parton language,” *Nuclear Physics B* **126** no. 2, (1977) 298 – 318.
<http://www.sciencedirect.com/science/article/pii/0550321377903844>.
- [26] Y. L. Dokshitzer, “Calculation of the Structure Functions for Deep Inelastic Scattering and e+ e- Annihilation by Perturbation Theory in Quantum Chromodynamics,” *Sov.Phys.JETP* **46** (1977) 641–653.

- [27] E. Laenen, “QCD Resummation (Large x).” Slides of talk given at the INT workshop on Gluon and Quark Sea at High Energies, Seattle, 2010.
http://www.int.washington.edu/talks/WorkShops/int_10_3/People/Laenen_E/Laenen.pdf.
- [28] V. Sudakov, “Vertex parts at very high-energies in quantum electrodynamics,” *Sov.Phys.JETP* **3** (1956) 65–71.
- [29] I. J. R. Aitchison and A. J. G. Hey, *Gauge Theories in Particle Physics*. IOP Publishing Ltd, 1989.
- [30] J. Bjorken, “Asymptotic sum rules at infinite momentum,” *Phys. Rev.* **179** (Mar, 1969) 1547–1553. <http://link.aps.org/doi/10.1103/PhysRev.179.1547>.
- [31] E. Bloom, D. Coward, H. DeStaebler, J. Drees, G. Miller, L. Mo, R. Taylor, M. Breidenbach, J. Friedman, G. Hartmann, and H. Kendall, “High-energy inelastic $e - p$ scattering at 6° and 10° ,” *Phys. Rev. Lett.* **23** (Oct, 1969) 930–934.
<http://link.aps.org/doi/10.1103/PhysRevLett.23.930>.
- [32] R. P. Feynman, *Photon-Hadron Interactions*. W. A. Benjamin, Inc., 1972.
- [33] C. Callan and D. Gross, “High-energy electroproduction and the constitution of the electric current,” *Phys. Rev. Lett.* **22** (Jan, 1969) 156–159.
<http://link.aps.org/doi/10.1103/PhysRevLett.22.156>.
- [34] M. Peskin and D. Schroeder, *An Introduction to Quantum Field Theory*. Advanced book classics. Addison-Wesley Publishing Company, 1995.
<http://books.google.de/books?id=i35LALN0GosC>.
- [35] B. Potter, “JetViP 2.1: The hbook version,” *Comput.Phys.Commun.* **133** (2000) 105–118, [arXiv:hep-ph/9911221](https://arxiv.org/abs/hep-ph/9911221) [hep-ph].
- [36] M. Klasen, G. Kramer, and B. Potter, “Inclusive jet production with virtual photons in next-to-leading order QCD,” *Eur.Phys.J.* **C1** (1998) 261–270, [arXiv:hep-ph/9703302](https://arxiv.org/abs/hep-ph/9703302) [hep-ph].
- [37] B. Potter, “Jet production in deep inelastic electron photon scattering at e^+e^- colliders in next-to-leading order QCD,” *Nucl.Phys.* **B540** (1999) 382–404, [arXiv:hep-ph/9805436](https://arxiv.org/abs/hep-ph/9805436) [hep-ph].
- [38] G. P. Lepage, “A new algorithm for adaptive multidimensional integration,” *Journal of Computational Physics* **27** no. 2, (1978) 192 – 203.
<http://www.sciencedirect.com/science/article/pii/0021999178900049>.
- [39] H. Plathow-Besch, “Pdffib: a library of all available parton density functions of the nucleon, the pion and the photon and the corresponding α_s calculations,” *Computer Physics Communications* **75** no. 3, (1993) 396 – 416.
<http://www.sciencedirect.com/science/article/pii/001046559390051D>.

- [40] M. Whalley, D. Bourilkov, and R. Group, “The Les Houches accord PDFs (LHAPDF) and LHAGLUE,” [arXiv:hep-ph/0508110](#) [hep-ph].
- [41] S. Catani, Y. Dokshitzer, and B. Webber, “The kt-clustering algorithm for jets in deep inelastic scattering and hadron collisions,” *Physics Letters B* **285** no. 3, (1992) 291 – 299.
<http://www.sciencedirect.com/science/article/pii/037026939291467N>.
- [42] G. Sterman and S. Weinberg, “Jets from quantum chromodynamics,” *Phys. Rev. Lett.* **39** (Dec, 1977) 1436–1439.
<http://link.aps.org/doi/10.1103/PhysRevLett.39.1436>.
- [43] T. Sjostrand, S. Mrenna, and P. Z. Skands, “PYTHIA 6.4 Physics and Manual,” *JHEP* **0605** (2006) 026, [arXiv:hep-ph/0603175](#) [hep-ph].
- [44] A. Martin, W. Stirling, R. Thorne, and G. Watt, “Uncertainties on α_s in global PDF analyses and implications for predicted hadronic cross sections,” *The European Physical Journal C* **64** no. 4, (2009) 653–680.
<http://dx.doi.org/10.1140/epjc/s10052-009-1164-2>.
- [45] M. Klasen, G. Kramer, and M. Michael, “Next-to-next-to-leading order contributions to jet photoproduction and determination of α_s ,” *Phys.Rev.* **D89** no. 7, (2014) 074032, [arXiv:1310.1724](#) [hep-ph].
- [46] G. Sterman, “Summation of large corrections to short-distance hadronic cross sections,” *Nuclear Physics B* **281** no. 1–2, (1987) 310–364.
<http://www.sciencedirect.com/science/article/pii/0550321387902586>.
- [47] N. Kidonakis, “QCD resummation and heavy quark cross-sections,” [arXiv:hep-ph/9606474](#) [hep-ph].
- [48] N. Kidonakis and G. F. Sterman, “Resummation for QCD hard scattering,” *Nucl.Phys.* **B505** (1997) 321–348, [arXiv:hep-ph/9705234](#) [hep-ph].
- [49] N. Kidonakis, “Resummation for heavy quark and jet cross-sections,” *Int.J.Mod.Phys.* **A15** (2000) 1245–1296, [arXiv:hep-ph/9902484](#) [hep-ph].
- [50] T. Kucs, “QCD resummation techniques,” [arXiv:hep-ph/0403023](#) [hep-ph].
- [51] M. Michael, “NNLO Contributions to Jet Photoproduction,” Master’s thesis, Westfälische Wilhelms-Universität Münster, Germany, 2013.
- [52] N. Kidonakis, “Next-to-next-to-next-to-leading-order soft-gluon corrections in hard-scattering processes near threshold,” *Phys.Rev.* **D73** (2006) 034001, [arXiv:hep-ph/0509079](#) [hep-ph].

Danksagung

Ich möchte abschließen mit einer Liste erlesener Personen, denen ich meine Dankbarkeit aussprechen möchte:

Ich danke Prof. Dr. Michael Klasen für die Möglichkeit, an einem spannenden Projekt zu arbeiten, für die freundliche Aufnahme in die Arbeitsgruppe und für die Zeit, die er sich für die Betreuung meiner Arbeit genommen hat.

Der gesamten Arbeitsgruppe danke ich für die Hilfsbereitschaft und die spannende und humorvolle Art, den Alltag zu gestalten.

Insbesondere gilt mein Dank meinem Bürokollegen Florian, seiner Majestät dem König, für die Hilfe bei physikalischen und technischen Problemen.

Ich danke Prof. Dr. Gernot Münster, dessen Humor mich von der Physik 1 und diverser anderer interessanter Vorlesungen, über die Betreuung meiner Bachelorarbeit und letztlich durch die Übernahme der Zweitkorrektur dieser Masterarbeit mein gesamtes Studium begleitet hat.

Meinem guten Freund Matthias Hüls sei gedankt für das ausführliche und gewissenhafte Korrekturlesen meiner Arbeit.

Zu guter Letzt möchte ich meinen Eltern Dorothea und Bernd danken für die aufopferungsvolle Hilfe bei den vielen Dingen im Leben, die nichts mit Physik zu tun haben, und für die finanzielle Unterstützung, die mir das Studium ermöglicht hat.

Eidesstattliche Erklärung

Hiermit versichere ich, dass die vorliegende Arbeit mit dem Titel

NNLO Contributions to Jet Production in Deep Inelastic Scattering

selbstständig verfasst worden ist, dass keine anderen Quellen und Hilfsmittel als die angegebenen benutzt worden sind und dass die Stellen der Arbeit, die anderen Werken - auch elektronischen Medien - dem Wortlaut oder Sinn nach entnommen wurden, auf jeden Fall unter Angabe der Quelle als Entlehnung kenntlich gemacht worden sind.

Münster, den 5. Juli 2015

Ich erkläre mich mit einem Abgleich der Arbeit mit anderen Texten zwecks Auffindung von Übereinstimmungen sowie mit einer zu diesem Zweck vorzunehmenden Speicherung der Arbeit in eine Datenbank einverstanden.

Münster, den 5. Juli 2015